Thesis entitled

AN INVESTIGATION OF THE PROPERTIES OF LOW DENSITY POTASSIUM CHLORIDE LAYERS AS SECONDARY ELECTRON EMITTERS AND CHARGE STORAGE LAYERS

by

MICHAEL EMANUEL ROSENBLOOM, B.SC.

Presented for the degree of
Doctor of Philosophy in the
University of London

Physics Department,
Imperial College,
London, S.W.7.

July 1965

Abstract

Following a short discussion on the methods of image intensification in general, and by transmitted secondary electron emission in particular, the preparation and testing of a new form of dynode is described. Finely divided potassium chloride, prepared by evaporation in argon, was used as the secondary emitter. The dynode possessed high electrical resistivity and was able to support electric fields which caused electron gains in the region of 50.

The current gain of the dynodes was investigated in a demountable tube, and sealed off image intensifiers using these dynodes were produced. Apart from the high secondary emission of these dynodes, these intensifiers did not show promise; the resolution was poor, sustained emission was observed, and the image was marred by localised breakdown. The electron gain fluctuated when the primary current was interrupted for a short time.

Measurements of the equilibrium surface potential showed that it depended on the energy of the primary electrons and on the potential of a mesh near the exit surface of the dynode. The electron gain was a nearly exponential function of the surface potential.

The dynodes were investigated as targets for television camera tubes; a tube was produced which showed charge gains of up to 30, was free from lag, and had a target capacity of 500pf.

This tube was used to investigate the dynamic behaviour of the dynodes in intensifiers. The surface potential rose and then fell to an equilibrium value; it also fell when the primary current was interrupted. The complicated behaviour of the dynodes was shown to be associated with the electric fields necessary for enhanced electron gain.

Acknowledgements

The author would like to thank Professor J. D. McGee for the facilities afforded him at Imperial College. He would like to thank Dr. W. L. Wilcock, who supervised the work described, for his continued interest and his much needed critiscism and encouragement. Various people assisted with the preparation of apparatus, in particular the author would like to mention Messrs. B. Weekley and P. Smith. The author would like to express his thanks to Messrs. R. Filby and S. Mende and Dr. N. D. Twiddy in collaboration with whom the work described in Chapter 7 was performed.

The author was supported for three years by a maintenance grant from N.R.D.C. He would also like to thank the L.C.C. for part-time employment which enabled him to carry on his work after the expiry of this grant.

He would like to thank Miss P. Anson for her assistance in the preparation of the diagrams and Miss S. M. Weston for her patience whilst typing this thesis.

Most of all, the author would like to thank his wife for her encouragement and forebearance both during the period of research and later while the thesis was being written.

CONTENTS

CHAPTER 1

Introduction and Survey

1.1 Introduction

During the last few years image intensifiers have been developed in various forms and are now of use in many branches of science. In medicine, x-ray image intensifiers[1] have reduced the radiation dose necessary for fluoroscopic examination; they have also removed the necessity for dark adaption on the part of the operators who no longer have to work in total darkness to see the feeble illumination from x-ray excited phosphors. The use of image intensifiers in astronomy has brought about an effective increase in film speeds and may bring about a reduction in the threshold brightness of stars which can be photographed. In nuclear physics the use of particle detectors with high time and spatial resolution has been made possible by the use of image intensifiers. Other fields in which image intensifiers have been of use include electron microscopy[2], high field ion emission[3], and x-ray diffraction[4]. The image intensifier increases the effective sensitivity of the eye at low light levels[5] and has reduced the light level at which cine and television cameras can be used[6].

It is a consequence of the quantum nature of light, that a maximum signal to noise ratio is inherent in a light signal of given intensity and duration incident on a given area. No amount of amplification can increase this signal to noise ratio, whilst it can all too easily be degraded by a detector which fails to respond to all the incident photons and adds noise.

The comprehension of a picture involves its dissection into a large number of small elements and the evaluation of the relative light intensities within these elements. Suppose a picture element receives photons at an average rate of $\bar{n}$ per second, and that the incident photons are counted by some means for a time t. Because of the random emission of photons, counting will in general reveal a number different to $\bar{n}t$. The probability of counting a given number of photons will be given by a Poissonion distribution with a mean value and mean square fluctuation of $\bar{n}t$[7,8,9]. The maximum signal to noise ratio will be given by

$$S/N = \frac{\bar{n}t}{(\bar{n}t)^{\frac{1}{2}}} = (\bar{n}t)^{\frac{1}{2}}$$

It follows that an increase in either $\bar{n}$ or t leads to an increase in the signal to noise ratio. The counting of photons over a finite time is known as integration;

because no measurement of the rate of arrival of photons can be made without the passage of a finite time, integration forms an essential part of any image evaluation process. The period of integration can vary over wide limits. In photography it can vary from micro-seconds to hours. The integration period of the human eye is in the region of 0.2 sec[10], that of a studio television camera is 0.04 sec. Integration over an extended period is frequently used to increase the signal to noise ratio of weak or low contrast images, see for example sections 1.3 and 7.1.

If the signal to noise ratio in the incident image is to be maintained, each photon must be recorded by the detector. In many instances a fraction σ of the incident photons will each elicit a response from the detector corresponding to one incident photon, while the remaining $1 - \sigma$ will elicit no response at all. An example of such a detector is a photo-emissive layer with a quantum efficiency of σ. It is easy to show that the maximum signal to noise ratio at the output is reduced from $\sqrt{\bar{n}t}$ to $\sqrt{\sigma\bar{n}t}$.

Further degradation in the signal to noise ratio may be occasioned by spurious signals produced by the detector, and by multiplication processes which are subject to

statistical fluctuations

It is of interest to consider the detection of barely distinguishable features within an image. Suppose N photons are detected within a small area of an image, where it would have been expected to detect $\bar{N}$ photons had the region around and including the area considered been uniformly illuminated. Is the fact that N is different to $\bar{N}$ the result of a feature within the image, or is it the result of a statistical fluctuation? The only statement which can be made is that if

$N \sim \bar{N} \geq k(\overline{\Delta^2 N})^{\frac{1}{2}}$ where $\overline{\Delta^2 N}$ is the mean square fluctuation of N, there is a 'degree of certainty' that the change in photon density is the result of a feature within the image. The value of k will vary with the 'degree of certainty' required. Experimental values of k are in the region of five,[8] although mathematical analysis indicates lower values, barely in excess of unity.[9] N varies with the area of the picture element and it can be seen that the resolution within the image is a function of the integrated light flux as well as the properties of the light detector.

1.2 Quantum Efficiency

The ratio $\frac{\text{number of countable output events}}{\text{number of incident photons}}$ is defined as the responsive quantum efficiency of a detector[9]. Within limits, it is a useful concept, but in many circumstances it is ambiguous and does not always give a real indication of the usefulness of a detector. For example, although a detector has a high responsive quantum efficiency, it may also be very noisy, and present less information about a given light signal than a detector which has a lower responsive quantum efficiency but adds very little noise. A more satisfactory criterion of the usefulness of a detector is given by the equivalent or detective quantum efficiency[8,9] which is defined as $\left(\frac{\text{signal to noise ratio at output of detector}}{\text{signal to noise ratio at input of detector}}\right)^2$. When every photo-electron from the cathode of an image tube is detected with equal weight, and no spurious electrons appear to be detected, the responsive and detective quantum efficiences are equal. In all practical image tubes, the responsive quantum efficiency is greater than the detective quantum efficiency.

A striking example of the difference between the two definitions of quantum efficiency is given by considering

a television camera, which may employ a photo-cathode with a responsive quantum efficiency approaching 20%. At low light levels the detective quantum efficiency may drop astronomically as the signals produced by incident photons cannot be distinguished from those produced randomly within the camera and associated amplifiers.

A large part of the usefulness of image intensifiers lies in their use of photocathodes of high responsive quantum efficiency. The quantum efficiency of a photocathode can reach values around 20% under optimum conditions,[11] and image tubes can be designed with detective quantum efficiencies of this order. This value compares favourably with 1% to 5% for the dark adapted eye[8,9,10] and 0.1% to 1% for the photographic emulsion[12].

Two uses of image intensifiers in nuclear physics and astronomy which illustrate the different demands made on image intensifiers will be discussed briefly.

1.3 The Detection of Very Weak Star Images

The use of an unaided photographic emulsion for the detection of weak star images against the sky background is first considered. Suppose that on the area of emulsion occupied by a star image, n_b photons per second arrive from

the sky background, and that an additional n_s photons per second arrive from a star. Suppose also that the area of emulsion considered contains N_μ statistically effective silver halide grains. The maximum signal to noise ratio in the developed photograph will be obtained if the emulsion is exposed for a time t until nearly all the grains have been rendered developable by the sky background. Under these conditions the noise represented by fog can be neglected. The star can be recognised if

$$\sigma_p n_s t \geq k(\sigma_p n_b t)^{\frac{1}{2}}, \quad \text{where} \quad t \simeq \frac{N_\mu}{\sigma_p n_b}$$

k is the coefficient of certainty, and σ_p is the quantum sensitivity of the emulsion. Substitution gives the condition that a star can be recognised as

$$n_s \geq \frac{k n_b}{N_\mu^{\frac{1}{2}}}$$

It can be seen that the threshold magnitude of detectable stars is partly determined by the number of grains per unit area of the storage capacity of the emulsion. For practical reasons, an upper limit exists for the storage capacity of the emulsion[13]. If the number of grains of a given size is increased, the additional grains overlap and no advantage is gained. The use of finer grained plates is prevented by the decreased film speed and the onset of reciprocity

failure[14] before the threshold of finer plates is excelled.

Wilcock and Baum have considered the use of an image intensifier to intensify the image before it is projected on the emulsion[15]. They showed that it is possible to obtain an effective increase in film speed without an appreciable increase in the threshold brightness of detectable stars, if the number of grains rendered developable by individual photo-electrons leaving the cathode of the tube is much less than one. On the other hand, if each photo-electron renders g grains developable, where $g \geq 1$, the further increase in film speed is obtained at the cost of an increase by a factor $(2g + 1)^{\frac{1}{2}}$, of the threshold brightness of detectable stars. This increase in threshold brightness arises from fluctuations in the light gain of the tube, and the reduction in the effective storage capacity of the emulsion as g grains are used to record a single photo-electron. It should now be possible to decrease the threshold brightness of detectable stars by the use of a finer grained emulsion. This possibility arises because the gain of an intensifier could be adjusted so that the effective speed of the finer emulsion is increased and reciprocity failure is avoided, but the storage capacity is not wasted by the 'over-recording' of photo-electrons.

It is important in this application of image intensifiers that the tube background should be low. A high background would add spurious signals and cause premature saturation of the emulsion.

1.4 The Use of Image Intensifiers in Nuclear Physics

Scintillation chambers[16,17] and Cerenkov detectors[17,18] provide the possibility of particle detection with both high time and high spatial resolution. Because only a small number of photons is associated with the track or the ring produced by a high energy particle incident on these two detectors, image intensifiers are required to provide a record of as large a fraction as possible of these photons.* To do this the cathode of the image intensifier must have a high quantum sensitivity, a large fraction of the emitted photo-electrons must produce an output pulse, and the light gain of the intensifier must be sufficient to ensure that each light flash from the output phosphor produces a photographic record. Because the position of arrival of the photons provides the information required about the particles, the intensity fluctuations of the output pulses are of secondary importance. Furthermore, the tube is pulsed to be sensitive for only short periods, and the

* If fibre scintillation chambers are used, this requirement is slightly less exacting although image intensifiers are still required.

presence of background, whilst undesirable, is less important than it would be in astronomical applications where comparitively long exposures are made. Considerable advances have been made with 'gated' tubes which are arranged to be sensitive for only a short time[19]. The particle detectors described are continuously exposed to particle fluxes, and when it has been decided by auxilliary counter equipment that an event of interest has occurred, the tube is made sensitive by the application of a high voltage pulse to suitable tube electrodes.

1.5 Practical Image Intensifiers

Although various forms of image intensifier have been developed, the great majority use a photo-cathode to convert the incident optical image into an electron image. It is in the subsequent treatment of the electron image that the various forms differ.

1.6 Image Intensifiers Using Electronography

The most direct method of image intensification is that developed by Lallemande[20] where the photo-electrons are accelerated and focussed on to an electron sensitive emulsion in the same vacuum chamber. The electrons are accelerated to about 25Kv and are each able to produce at least one developable grain. The electron sensitive emulsion is very

fine grained and free from fog. Although the technique yields extremely good results, it is difficult to use and the life time of the photo-cathodes is limited by the demountable nature of the system and by attack by vapours from the emulsion.

The technique has been modified by Hiltner et al[21] who separated the cathode and emulsion by a foil thin enough to allow the passage of fast electrons, but able to prevent the passage of the vapours responsible for the deterioration of the cathode. It is certain that whatever the success of this technique, its use is complicated by the need for continuous pumping and air-vacuum locks.

The Lenard window tube[22,23,24], developed by McGee and Wheeler, shows promise of retaining the advantages of Lallemande's technique and the simplicity of use inherent in a 'sealed off' tube. It consists of an evacuated tube with a photo-cathode at one end and a thin mica window at the other. The mica window, although able to withstand atmospheric pressure, is thin enough to allow the passage of fast electrons. The emergent electrons are able to cause the production of a developable image in an electronographic emulsion pressed against the mica window. The images produced show resolutions in the region of 801p/mm[24]. but the usable area of the photo-cathode is limited by the

small size of mica windows able to withstand atmospheric pressure.

1.7 Tubes with Phosphor Outputs

A different method of utilising the photo-electrons is to focus the electron image onto a phosphor screen in the same vacuum envelope as the photo-cathode. The electrons are accelerated and strike the screen with an energy of 10 to 20 Kv; the electron image is converted into an optical image which can be viewed directly or photographed. The light gain of such a tube has been derived theoretically by Mandel[25]. Typical values are in the range 30 to 90, depending on the photo-cathode, the phosphor, the spectral composition of the incident light, and the spectral response of the final detector.

It is difficult to design an optical system which will transfer more than about 20% of the phosphor output on to a photographic emulsion. The effective light gain of the tube is reduced by this fraction to a value which is usually of very little practical use. It is possible to dispense with the optical system by settling the phosphor screen on to a thin mica window against which a photographic emulsion is pressed[26]; scattering within the mica reduces the resolution of the tube to a value in the range of 20 lp/mm.

1.8 Cascaded Image Intensifier

The gain of several phosphor output tubes can be utilised by cascading them. If the phosphor and photo-cathode of successive intensifiers are formed on opposite sides of a thin membrane, almost complete optical coupling can be obtained with very little image degradation due to light spreading within the membrane. An intensifier giving very high light gains can be made by incorporating several such phosphor photo-cathode sandwiches within one vacuum envelope.[1]

1.9 Tubes Employing Secondary Electron Emission

Several methods have been developed whereby the photocurrent is multiplied by several stages of secondary electron emission, the electron image being preserved in succeeding generations of electrons.

1.10 Multipactor

In the Multipactor[27] the photo-electrons are returned to the photo-cathode by a combination of alternating electric fields with sufficient energy to liberate secondary electrons. The latter are returned as many times as is necessary to give the desired electron gain after which they are accelerated on to a phosphor. Although the tube gives high

electron gains, it is complicated in operation, requires strong magnetic fields for focussing, and can only be used in applications where its short sensitive period is not a disadvantage.

1.11 Channelled Image Intensifier

In the channelled image intensifier[28,29,30,31], the electron image is focussed onto an array of parallel electron multipliers. Each multiplier multiplies the current from a small area of the image, and within this area no attempt is made to retain the image focus. The output from the array of electron multipliers is finally accelerated and focussed onto a phosphor. Several forms of this intensifier have been developed, the most promising of which is that of Wiley and Hendee[31]. Very fine tubes of glass coated internally with a resistive coating serve as the individual multipliers. A potential, typically 1,000 to 2,000 volts is applied along the tubes, and the electrons focussed on the inside of the tube give rise to a cascade of secondaries along the inside of each tube. The resolution of the intensifier is limited by the discrete nature of the multiplier array. At present resolutions of 2 lp/mm have been reported, although it is possible that resolutions of 20lp/mm might eventually be achieved.

The advantage of this intensifier is its small size and the fact that no auxilliary focussing equipment is necessary.

1.12 Transmitted Secondary Electron Emission Image Intensifier

Electron multiplication by transmitted secondary electron emission was first proposed before the war. Its successful application is based on the observation by Sternglass and Wachtel that if a thin layer of a suitable insulator was used as a secondary electron emitter, electron gains of up to eight could be obtained from a single dynode.[32,33] Of the materials tried, potassium chloride appeared the most promising, and it was established that 90% of the emergent electrons had energies below 6 volts and were suitable for refocussing on to succeeding stages. At the same time it was estimated that an upper time limit for the production of secondaries was 10^{-10} sec. Since these observations, several laboratories[34,35,36] have produced successful intensifiers using transmitted secondary emission from potassium chloride, and several practical intensifiers are now available commercially.

A description of the intensifier developed by Wilcock, Emberson and Weekley at Imperial College follows.[36,38] A series of dynodes is held normal to the axis of an evacuated tube,

figure 1.1. Electrons from a photo-cathode at one end of the tube are accelerated and focussed on to the first dynode. Each electron releases secondary electrons from the far side of the dynode which are focussed on to another dynode. This process is continued down the length of the tube and the electrons from the last dynode are accelerated and focussed on to a phosphor at the far end of the tube.

Each dynode (figure 1.2) consists of three layers; the first is an anodically prepared layer of Al_2O_3 which is 500 Å thick and strong enough to support the dynode. A 200 Å layer of aluminium is vacuum deposited on the support membrane and provides electrical conduction to the dynode. The secondary emitter is a 500 Å layer of potassium chloride vacuum deposited on the aluminium layer. The incident primary electrons penetrate the Al_2O_3 and Al layers and form secondary electrons in the potassium chloride layer, which are emitted from its far side. The electron gain of a typical dynode and the electron and photon gains of a typical five dynode tube are shown in figure 1.3.

A particular advantage of the T.S.E.M.* image intensifier is the speed with which secondary emission occurs. Recent measurements by Blattner et al[37] have confirmed the early estimate by Sternglass and Wachtel of the speed of emission.

* Transmitted Secondary Electron Multiplication.

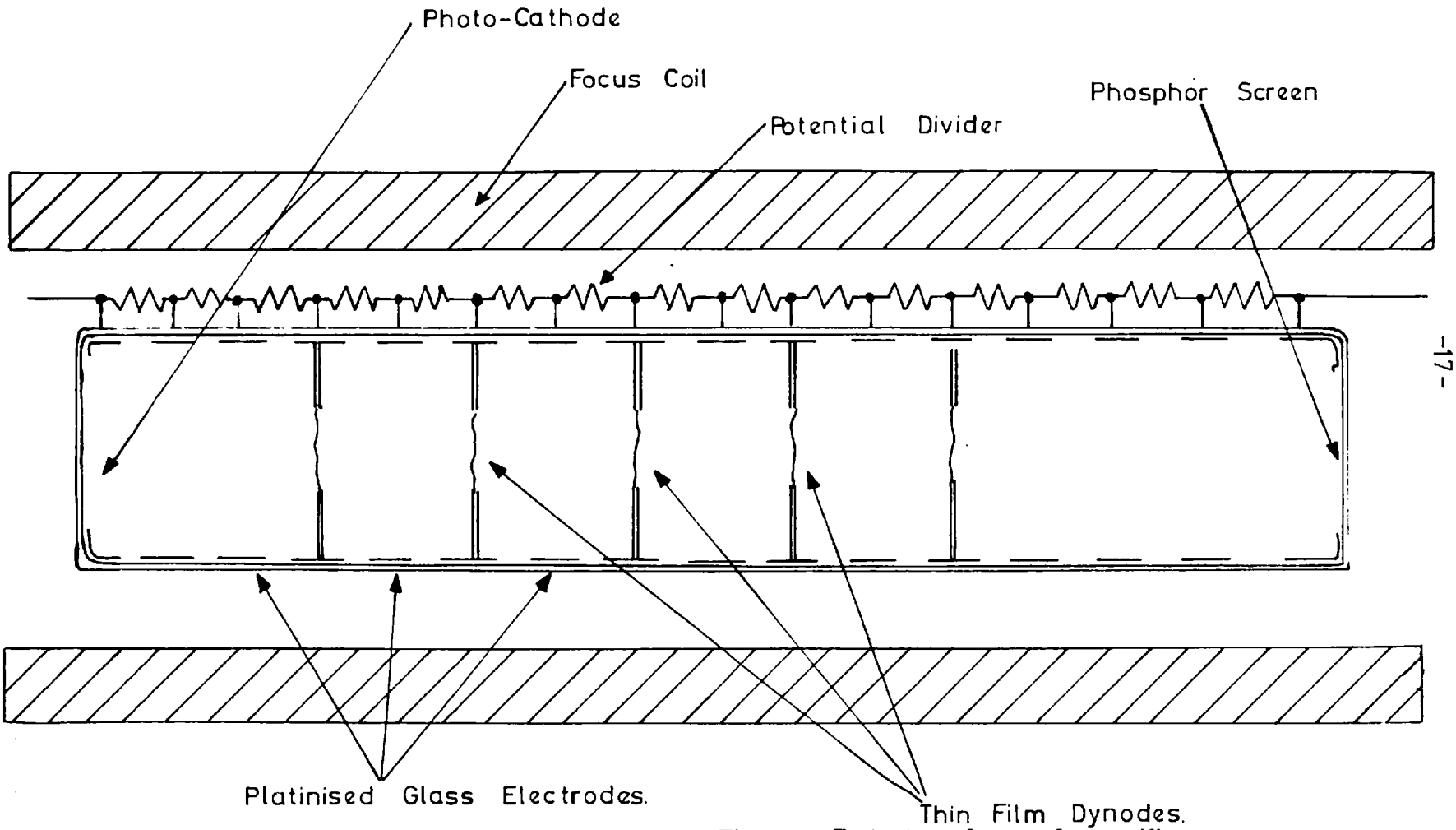

Fig. 1.1 Five Dynode Transmitted Secondary Electron Emission Image Intensifier

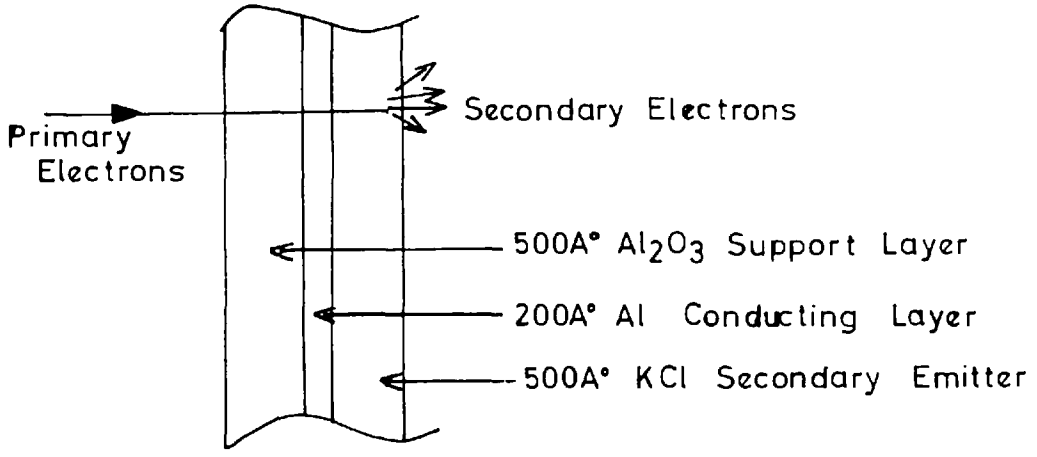

Fig.I.2. Section Through Transmitted Secondary Emission Dynode

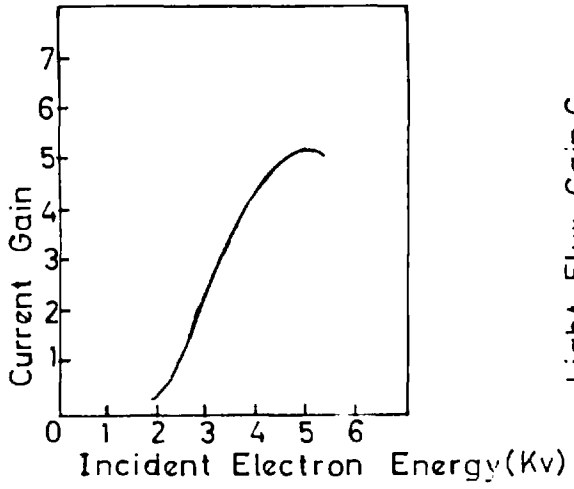

Fig.I-3 Current Gain of Typical Dynode as a Function of Energy.

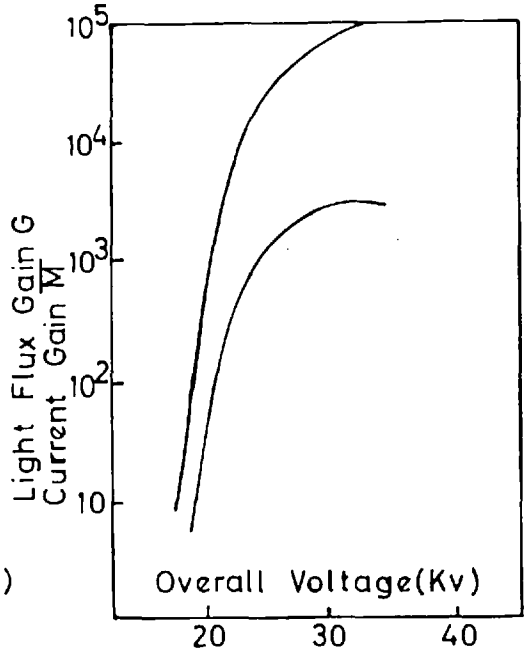

Fig.I-4 Variation with Overall Voltage of Light Gain and Current Gain of Five Dynode Tube

Blattner, using a travelling wave tube, found that secondary emission from a dynode similar to that just described took less than 2×10^{-10} sec.

Spatial resolutions approaching 40lp/mm have been obtained in commercially available tubes, with five dynodes[35] and it appears possible that the resolution could be increased to values approaching 50lp/mm by the use of finer output phosphors and closer dynode spacing.

1.13 Contrast Degradation by Penetrating Primary Electrons

A fault, peculiar to T.S.E.M. intensifiers is that of contrast degradation resulting from the penetration of primary electrons through the dynode. Not all the electrons emitted from the dynode have a low energy; a substantial fraction have energies above 50 eV, many of the latter being primary electrons etc, which have penetrated the dynode. As a result of their large forward velocities, these electrons are unable to satisfy the same focussing conditions as the slow electrons which comprise the greater part of the secondary electron current. The optimum tube focus is obtained when the latter are focussed and consequently the fast electrons arrive out of focus at the next focal plane. The result is a light induced background and a degradation of the image contrast.

1.14 Variation In Intensity of Output Pulses

As a result of the discrete nature of the photo-electron current, the output from a focussed tube will be localised flashes of light which can be seen or photographed when the light gain of the tube is high. Inspection of photographs of these output scintillation reveals a large variation in their intensity. This variation has been investigated by coupling a photo-multiplier to the output phosphor.[38,39] After suitable shaping, the pulses obtained from the photomultiplier were passed to a pulse height discriminator and pulse counter. The integral pulse height distributions were found to obey different laws according to the origins of the electrons causing the pulses. An exponential variation of pulse heights was obtained for output pulses produced by photoelectrons. When the cathode was in darkness, pulses due to dark emission were still recorded. For small pulses, the same variation in frequency with pulse amplitude was obtained as for photo-electrons. A greater fraction of larger pulses was obtained for dark emission than was the case for photo-emission. This variation of the frequency distributions was explained by the fact that the photo-current consisted only of singly emitted electrons whilst the dark current

contained groups of electrons. The source of these electron groups has not been satisfactorily identified. A connection with positive ions formed from residual gas in the tube has been established by Catchpole[1], who suggests that high field emission is also involved. Catchpole's findings are at variance with those of Wilcock et al[39].

1.15 Pulse Efficiency of T.S.E.M. Intensifiers

The pulse efficiency of an image intensifier can be defined as the fraction of photo-electrons which produce an output light pulse at the phosphor. The pulse efficiency of typical 5 dynode T.S.E.M. image intensifiers is 50%[40]. Low pulse efficiency seems to be a fault peculiar to T.S.E.M. intensifiers; the pulse efficiencies of cascade intensifiers can be as high as 85%[41]. It can be shown that the failure of a photo-electron to produce an output pulse in a multi-dynode tube is to a large extent due to its failure to produce any secondary electrons from the first dynode.[39]. It is unlikely that the failure of electrons to produce secondaries from succeeding dynodes leads to a complete loss of information, although an increase in the statistical fluctuation of the light gain will result. The non-detection of photo-electrons is equivalent to a reduction in the quantum sensitivity of the

photo-cathode, and can lead to a reduction in the usefulness of the tube. Low pulse efficiency could mean the difference between success and failure in the use of the photography of Cerenkov radiation as a means of single particle detection in nuclear physics.[41]

1.16 Image Intensification Using Low Density Deposits of Potassium Chloride

A modification of the dynode structure has been described by Goetze.[42,43] The vacuum deposited layer of potassium chloride was replaced by a low density deposit of potassium chloride which was formed by evaporation in an argon atmosphere. These dynodes gave electron gains in the region of 50 and could be prepared in such a manner as to give stable operation. The following explanation was advanced for the observed high gains. When the dynode was bombarded by high velocity electrons, the emission of secondary electrons from the low density deposit caused the formation of positive charge near the exit surface. Because of the very good insulating properties of the potassium chloride layer, the charge accumulated and a potential gradient was developed across the layer. Secondary electrons formed within the layer were accelerated, and owing to their greatly increased free path in the low

density deposit, were able to acquire sufficient energy to reduce the probability of their being recaptured. A greater fraction of the secondaries produced within the layer were able to escape and the dynodes exhibited large electron gains.

The potential across the dynode, and the electron gain, were controlled by the potential of a mesh near the exit surface of the dynode. Typical potentials applied to the mesh were in the region of 100 to 300 volts, and high gains were obtained for primary voltages in the range 4 to 10 Kv. The performance claimed for these dynodes was impressive, and it was decided that the investigation of intensifiers using these dynodes should be started at Imperial College. The following advantages were hoped to arise from the use of these dynodes: because only two dynodes would be needed to achieve electron multiplications of 2,000 to 3,000, tube construction would be simplified. The reduction in the number of dynodes would lead to a reduction in overall operating voltages. The considerable increase in electron gain of a single dynode must lead to a reduction in the effect of the penetrating primaries. It was hoped also that improved multiplication statistics and pulse efficiencies might result.

Immediate disadvantages of tubes using low density dynodes might have included the following. A finite time would be required to charge the dynode; it was, however, reported that once they were charged, the dynodes retained their charge and responded quickly to incident primary electrons. Also the presence of a mesh might lead to a reduction in the resolution of the tube as a result of the low potential gradient between the dynode and the mesh; Goetze claimed that resolutions of 24 lp/mm had been achieved.

1.17 Enhanced Secondary Emission

Various reports have been made of experiments where special surface treatments have yielded secondary emission ratios in excess of those normally exhibited by insulators.[44,45] These surfaces were usually prepared by the oxidation and sometimes cesiation of suitable metals, such as magnesium and barium, and the increased yield was believed to result from positive charges on the surfaces.

Malter[46] obtained yields of up to 1,000 from surfaces prepared by the cesiation and subsequent oxidation of anodic layers of Al_2O_3. He found that the yield from such a target varied with a power of the collector voltage and a

power of the primary current density. The high yields took time to build up, were unstable and once initiated by a primary current could continue for hours after the primary current ceased. Similar results were reported by Piore[47] from barium borate surfaces treated in the same way as Malter treated his Al_2O_3 surfaces. Koller and Johnson[48], and Mahl[49] made a study of the instability of the Malter emission by dusting a phosphor on the emitting surface, and by focussing the emitted electrons on to a phosphor. They showed that the emission was not uniform but came from various discrete emitting points. They also found that enhanced photo-emission from the same surface could be initiated by light from a tungsten filament in the same vacuum chamber. Nelson[50] demonstrated that the high gain was associated with a positive charge on the surface of the emitter. He also showed that a minimum bombarding voltage existed for the enhanced emission to occur; at this voltage the normal secondary emission from the surface was very nearly unity. The insulating films were very thin, in the order of 2,000 Å, and the high secondary emission ratios were attributed to field emission. Malters work contrasts strongly with that of Jacobs[51] on freshly prepared magnesium oxide. Jacobs obtained electron gains in the region of 100, but found that the decay times

were short, being of the order of 15 - 40μ sec. The yield varied exponentially with collector voltage and was independent of the incident current density and primary energy. He demonstrated the charge build up on the surface by pulse techniques. He likened the mechanism causing enhanced secondary emission to the Townsend avalanche occurring in a gas discharge, where electrons accelerated by an electric field are able to release secondary electrons which in their turn release yet more secondary electrons. He attributed the possibility of this mechanism to the porosity and poor conductivity of his layers, which were approximately 1μ m thick. Surfaces which were prepared so as to be more conducting would only exhibit electron gains in the region 4 - 5.

Yields of up to 80 had been obtained by Aranovitch[52] form surfaces prepared by evaporating magnesium through an atmosphere of dry oxygen. Some time delays were observed but the secondary emission responded fast enough to follow a 40 Kc/s modulation of the primary current. Yields of up to 10,000 were obtained but these definitely exhibited Malter effect.

Malter and Gunterschulz also found that increased secondary emission took place from surfaces coated with fine dusts of suitable insulators which included Al_2O_3,

willemite, SiO_2, and MgO. This effect was explained by the presence of positive charges which caused high field emission.

Serebrov and Fridrikhov[54] obtained enhanced secondary emission from vacuum deposited layers (5,000 Å) of NaCl. They controlled the surface potential of the layer by flooding the surface with low energy electrons (several hundred volts) and collecting the secondary electrons with an adjacent mesh; the surface potential followed the potential of the control mesh. On applying energetic electrons (several kilovolts) to the surface in short pulses, increases in electron yield by a factor of five were obtained; these enhanced yields were shown to result from the potential gradient within the NaCl layer.

All the results so far described have been on reflection secondary emission. The first results on enhanced transmission secondary emission were published by Butkevitch and Butslov[55], who made observations on films of MgO deposited on 3,000 Å layers of Al. The gains reported by these workers did not exceed 8, but the variation of the gain with the collector potential suggested that field enhanced emission was taking place. Krasovsky[56] obtained gains of up to 36 on such emitters processed in cesium. Results showing a strong similarity to those

published by Goetzc were reported by Yasnopol'ski, Malysheva and Karelina[57] who investigated the transmission secondary emission of deposits of magnesia, prepared by igniting magnesium in air, on 300 Å films of Aluminium supported on fine meshes. Yasnopol'ski et al. worked with two distinct forms of magnesia, the original porous deposit and a compressed form prepared by treatment in the vapour of volatile liquids. The compressed form showed a maximum gains of up to 12, which reached a saturation value for a collector voltage of only 30 volts. With some uncompressed samples, a monotonic increase in the secondary emission ratio was observed as the collector voltage was increased, and stable gains in the region of 50 were obtained. When a critical collector voltage was increased, a spontaneous increase in the secondary emission current was observed and self maintaining emission set in. Under these conditions, the secondary emission ratio reached values approaching 10^4. It was concluded that the yield from the compressed layers was the normal unenhanced transmission yield, and that the high yields observed in the uncompressed layers, were the result of current amplification under the influence of electric fields within the layers.

CHAPTER 2

The Preparation and Some Properties of the Low Density Potassium Chloride Dynodes

2.1 Preparation of Supporting Film

The aluminium oxide support films were made by anodising household aluminium foil on one side only[58]. The electrolyte was acid ammonium tartrate (pH 5.5) and the voltage applied was chosen so that the resulting film was 500 Å thick. After the foil was anodised, it was dissolved in acid, leaving a self-supporting membrane of aluminium oxide. Before it was anodised, the foil had been glued to Tufnol rings which supported the oxide films after the aluminium was dissolved. The oxide films were rinsed and allowed to dry.

When the films were dry, they were mounted on soda glass rings on which two contacts had been produced by firing in platinum paint. A gap was left between these contacts so that the electrical conduction between them and the aluminium backing could be checked later. The rings were coated with 0.1% potassium silicate solution and gently applied to the film by means of a vertically operating rack and pinion mechanism. When the potassium silicate solution had dried, the films were cut out with a razor blade or a paint

brush slightly damped with potassium silicate solution. Some of the aluminium oxide was scraped away over the platinum paint to ensure electrical contact to the conducting layer which was subsequently deposited.

The films were then baked to 420°C. Because of the differing thermal expansions of the soda glass rings and the oxide films, the films were stretched beyond their elastic limit. When they cooled the films became slack and wrinkled. This 'wrinkling' was originally carried out to avoid the breaking of dynodes using bulk density KCl when the tubes were baked in the degassing schedule prior to 'seal off'. It was found[38] that owing to a structural change which took place in the KCl layer on heating, tensile stresses were set up which caused dynodes supported by taut Al_2O_3 films to break as they cooled. If an anular area at the edge of the dynode was shielded from KCl, and the dynodes were supported by wrinkled films, the stresses were absorbed by taking up the slack in the wrinkled films without causing the rupture of the dynode.

It was later found that the dynodes using low density potassium chloride were far less strained and that no shadowing of the deposit was necessary to prevent breaking. There was however, always a substantial chance that a film would break on first being baked. It was a matter of chance

whether a particular film would survive the first bake, although uncoated films which had survived one bake very rarely broke on successive baking. Because wrinkled films were inherently less likely to break on baking, they were used to support the dynodes. The dynodes were, however, completely coated with potassium chloride.

2.2 The Preparation of the Conducting Layer

After the support films had been prepared, the conducting layer was formed by the vacuum deposition of aluminium. The evaporation was carried out in the demountable system illustrated in figure 2.1. A metal frame supported a horizontal plated on which the films were laid. The films were fitted into recesses over holes in the plate which also carried a small glass monitor plate at its centre. The thickness of the deposit on the films was monitored by observing the optical transmission of the monitor plate which received a deposit of aluminium whose thickness was proportional to that deposited on the films. The optical transmission was measured by shining a beam of light through the monitor plate; the beam of light was focussed on to a photo-voltaic cell connected to a galvanometer. The thickness of the deposit on the films was 200 Å; this was the minimum necessary to ensure a continuous

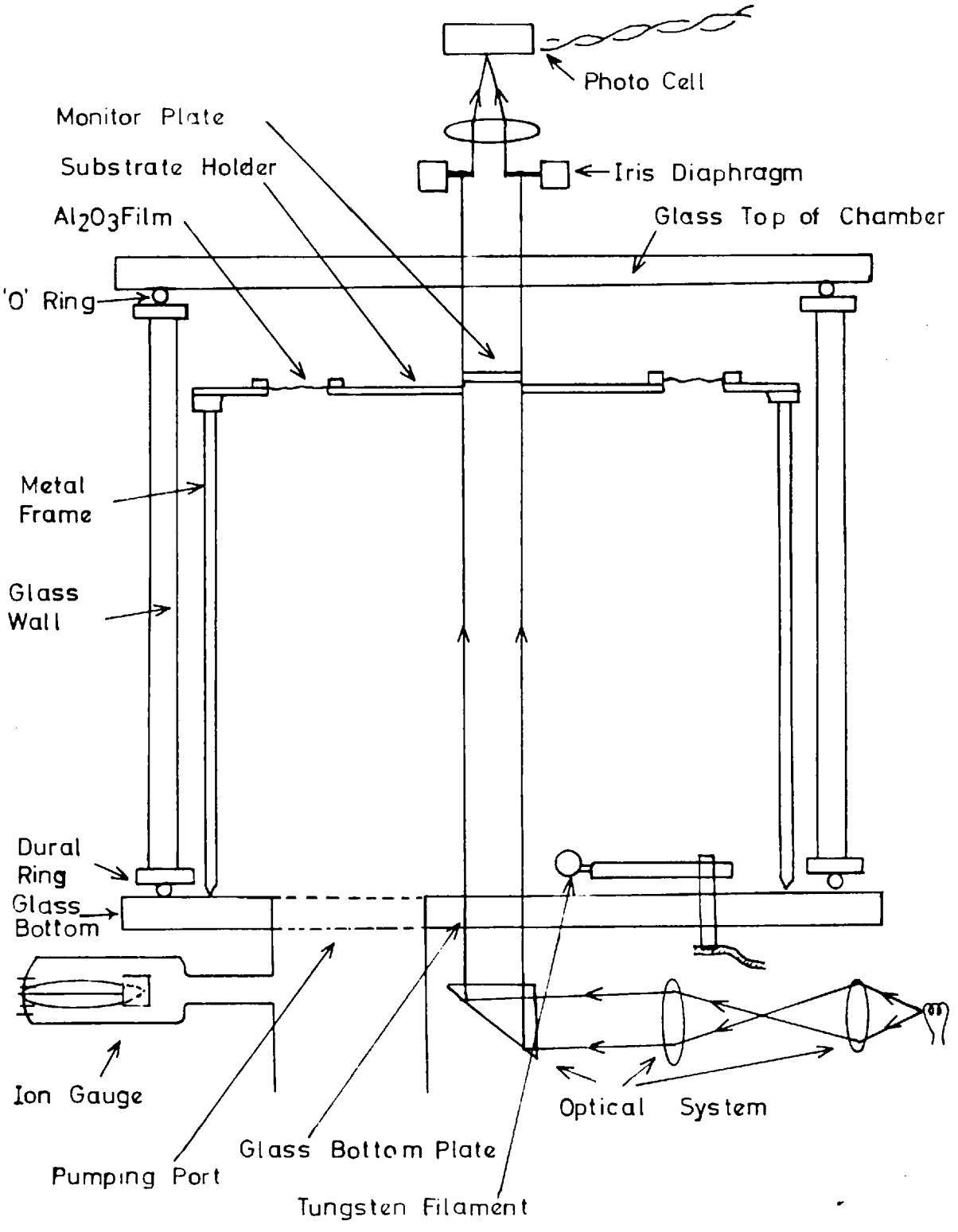

Fig. 2.1. Evaporation of Aluminium.

deposit after baking[38].

2.3 The Preparation of the Low Density Potassium Chloride Deposit

The chamber used for the evaporation of the aluminium coating was also used for the deposition of the low density potassium chloride. The potassium chloride was evaporated from an open molybdenum boat mounted 2 inches from the centre of the substrate assembly. The boat was heated directly by the passage of an electric current. Before it was loaded with potassium chloride, the boat was cleaned and degassed by heating it in vacuum. Finely ground Analar grade potassium chloride was placed in the boat, moistened with distilled water, and allowed to dry forming a compact crystalline mass. Because spitting often occurred on first heating a fresh charge of potassium chloride, the loaded boat was heated in vacuum to evaporation temperature before a film was placed in the chamber.

Before it was admitted to the chamber, the argon was dried by passing it through a battery of drying towers; these contained silica gel and a mixture of silica gel and phosphorus pentoxide. The argon was finally passed through a cold finger immersed in liquid oxygen before being admitted to the chamber by means of a needle valve. In early

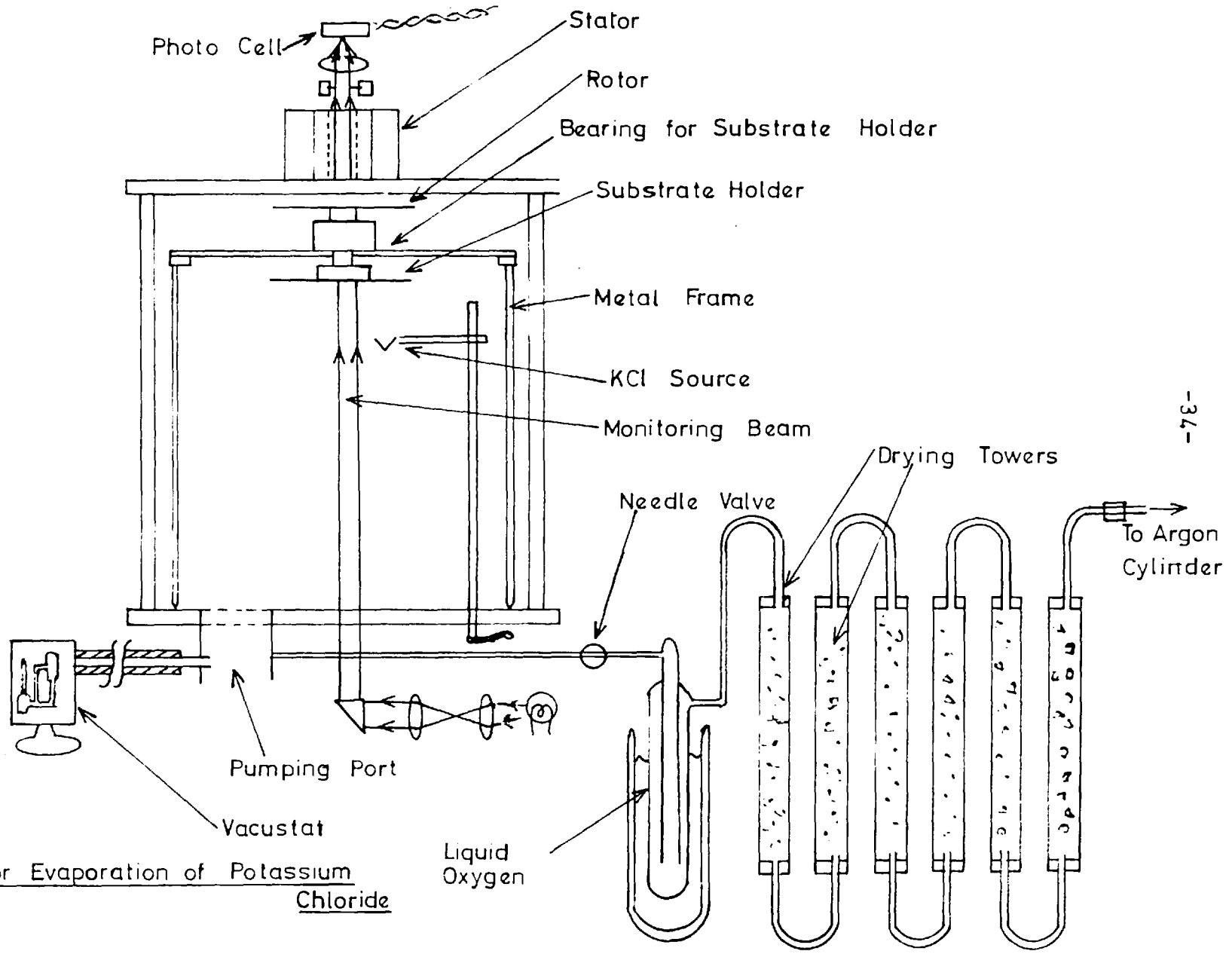

Fig. 2.2 Plant for Evaporation of Potassium Chloride

experiments the pressure in the chamber was adjusted by balancing the inflow of the argon and the effective pumping speed of the system. Later, however, the chamber was filled to the desired pressure and isolated. No change in the properties of the dynodes was found to result from this change in technique. The pressure, which was always 2 torr during an evaporation was measured by means of an Edwards 'Vacustat'. Before argon was finally admitted for the evaporation of the potassium chloride, the chamber was alternately exhausted and flushed with argon several times.

The first evaporations gave very uneven deposits of KCl. The uneveness of the deposits and the presence of streaky deposits on the wall of the chamber showed that gas currents were playing an important part in the evaporation process. To reduce the effect of these currents and to obtain a more uniform deposit, the films were continuously rotated during the evaporation by means of a simple induction motor whose construction is illustrated in figure 2.4. The motor and bearings were within the chamber, and the field coils rested outside the chamber on the glass top plate. The stator consisted of four relay driving coils, screwed into a soft iron ring.

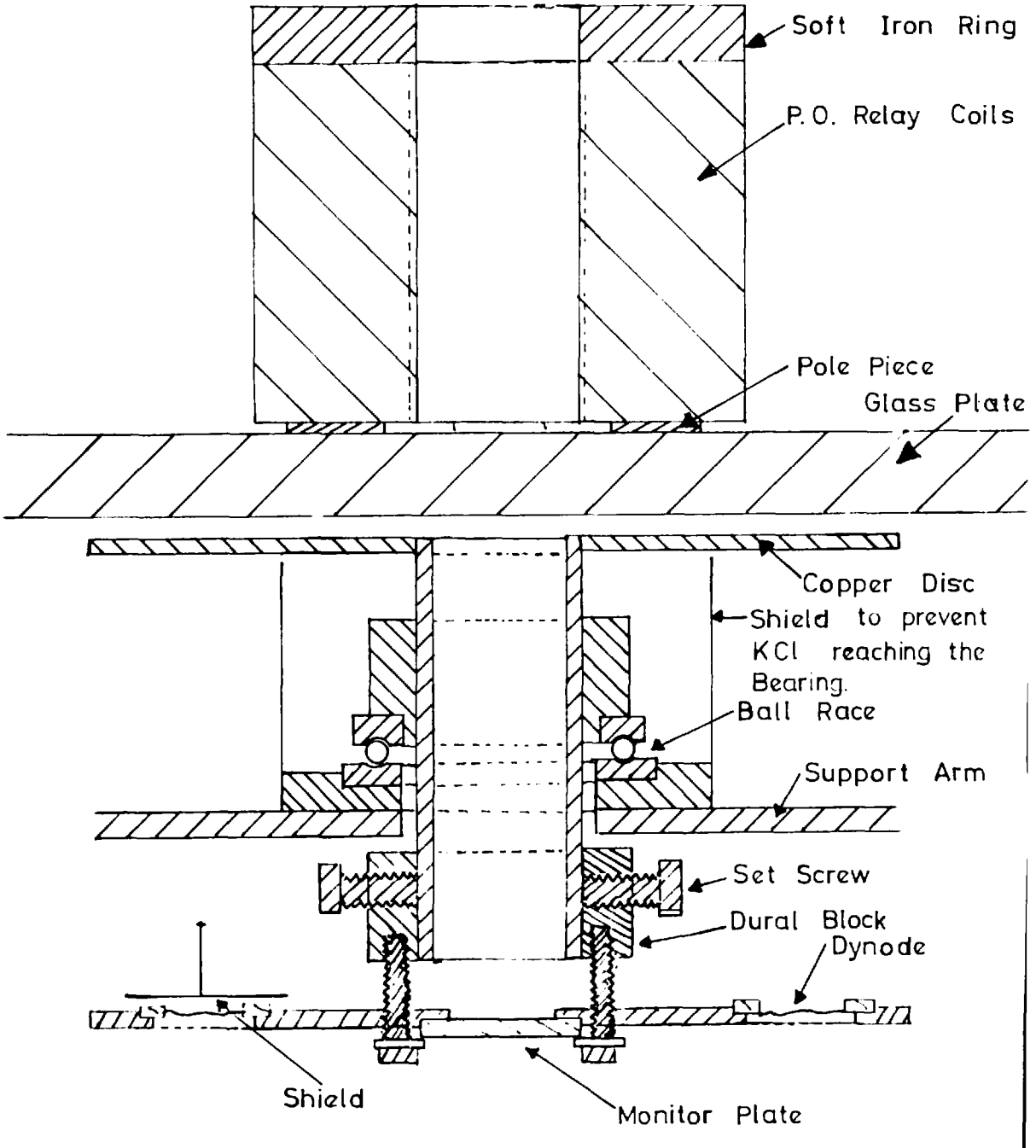

Fig.2.3. Rotating Substrate Holder

Fig. 2.4 Chamber set up for Evaporation of Potassium Chloride

Opposing coils were connected in pairs, one pair being fed through a $\frac{1}{2}\mu F$ condenser, which introduced a 90^{o} phase lag. It is easy to show[59] that this arrangement produced a 50 c/s rotating magnetic field.

The rotor was a copper disc soldered to a brass tube. The rotating field induced eddy currents in the copper disc, the interaction of these with the rotating field produced a torque which caused the rotor to rotate. The rotor ran on a ball race which was supported by three horizontal members. The latter rested on a frame-work and could be lifted quickly and placed, still supporting the substrate assembly, in a dessicator. A shield prevented the potassium chloride particles reaching and jamming the motor bearings. The speed of the motor was controlled by varying the supply voltage by means of a variable transformer. Because later work showed the desirability of evaporating several films at the same time, a modified film holder was built in which four dynodes rested in recesses in a stainless steel plate. The dynodes were covered on their upper surfaces by shields to prevent KCl particles settling on the wrong surface of the

dynode. The thickness of the dynodes was monitored by the optical transmission of a glass monitor plate in the centre of the plate on which the dynodes rested. The rotating sustrate holder was constructed to allow the monitoring beam to pass through its axis.

The dynodes produced using the rotary substrate holder were found to be satisfactorily uniform in thickness.

2.4 Appearance of the Dynodes

The freshly prepared dynodes retained the mirror-like appearance of the aluminium layer, except that the reflecting surface assumed a milky texture. In thicker dynodes this milky appearance was more dense, and the films assumed a white colour. When viewed at large angles to the normal the potassium chloride deposit was seen to have a yellow tint which resulted from the scattering of light by the fine particles of which it was composed.

2.5 Attack by Water Vapour

When they were exposed to moist air, the dynodes assumed a more solid appearance, becoming matt reflectors, and sometimes showing considerable crazing. When the dynodes were examined under a microscope, a crystalline structure could be resolved only in dynodes which had been

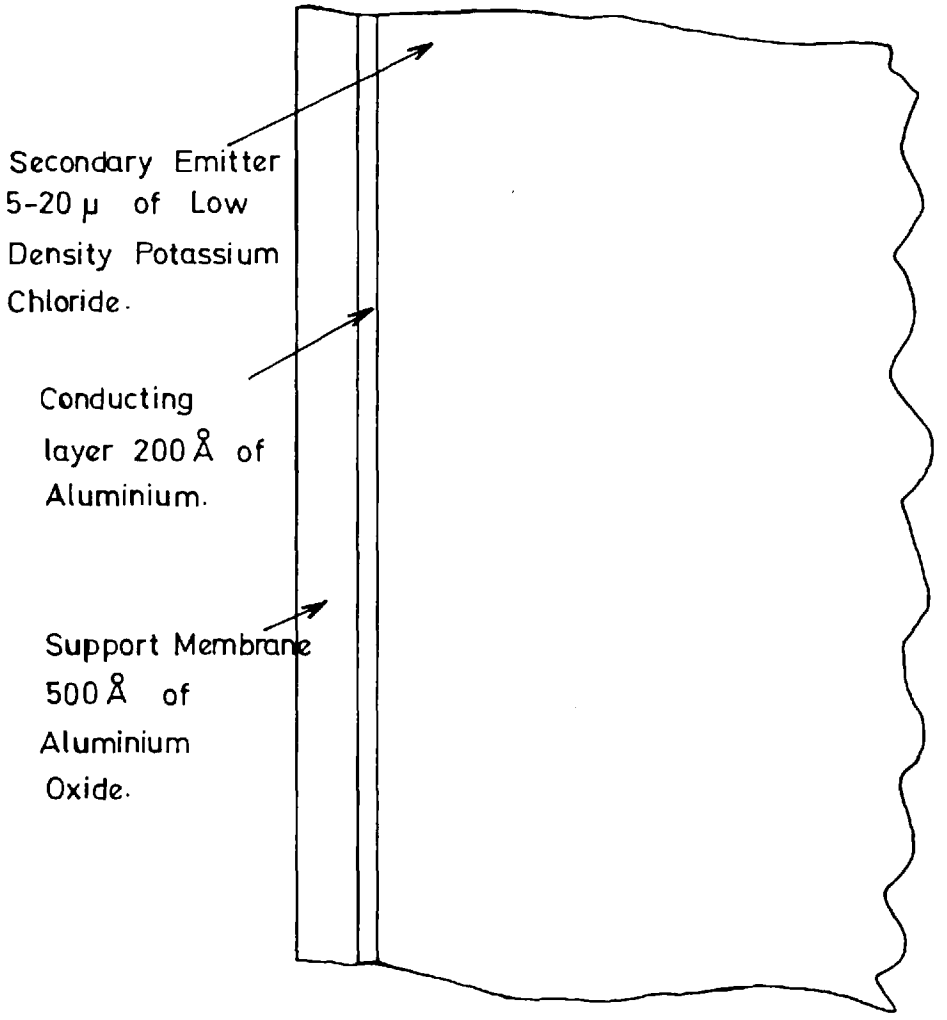

Fig. 2.5. Section through Low Density Potassium Chloride Dynode. (Not to scale)

exposed to moist air. Microscopic examination was hindered by the fact that it was essential to avoid moistening the dynodes which appeared extremely susceptible to attack by water vapour. The susceptibility of the dynodes to attack by water vapour arose as a result of the high solubility of potassium chloride in water, and the small crystal size and consequent high surface energy of the low density deposit . The condensation of water on the deposit provided an opportunity for the structure to recrystallise and lower the surface energy by the formation of larger crystals.

2.6 The Thickness of the Potassium Chloride Deposit

Attempts to measure the thickness by a depth microscope were unsuccessful because it was difficult to recognise surface features with certainty.

Tolansky has described a technique[61] whereby silver was deposited over the edge of a layer whose thickness was to be measured; by placing an optical flat above the silvered step, interference fringes were obtained from which the thickness of the layer could be deduced. Because the potassium chloride layer was very rough, it was not possible to evaporate a reflecting metal layer directly on to it, and a modification of Tolansky's technique was

developed. The low density deposit was evaporated on to an aluminised glass plate and a transparent film draped across the surface of the deposit. A collimated beam of green light from a filtered mercury lamp was directed downwards onto the film by means of a glass slip held at 45° to the beam, and the film was observed with a microscope. Interference fringes of constant thickness were obtained between the transparent film and the aluminised surface on which the potassium chloride was deposited. Counting the fringes over the region of varying thickness at the edge of the deposit enabled its thickness to be estimated. Because the semi-transparent layer of KCl was between the two reflecting surfaces, the method gave the optical thickness of the deposit. However, the refractive index of such a low density deposit must have been very nearly unity, and the geometrical and optical thicknesses very nearly equal.

At first, aluminium oxide was used for the draping films, however, it was not sufficiently pliable and tended to hang between high spots without actually touching much of the potassium chloride deposit. As an alternative, collodion films prepared by dropping filming solution onto water were tried. Although these films were more pliable than the aluminium oxide films, good results were only

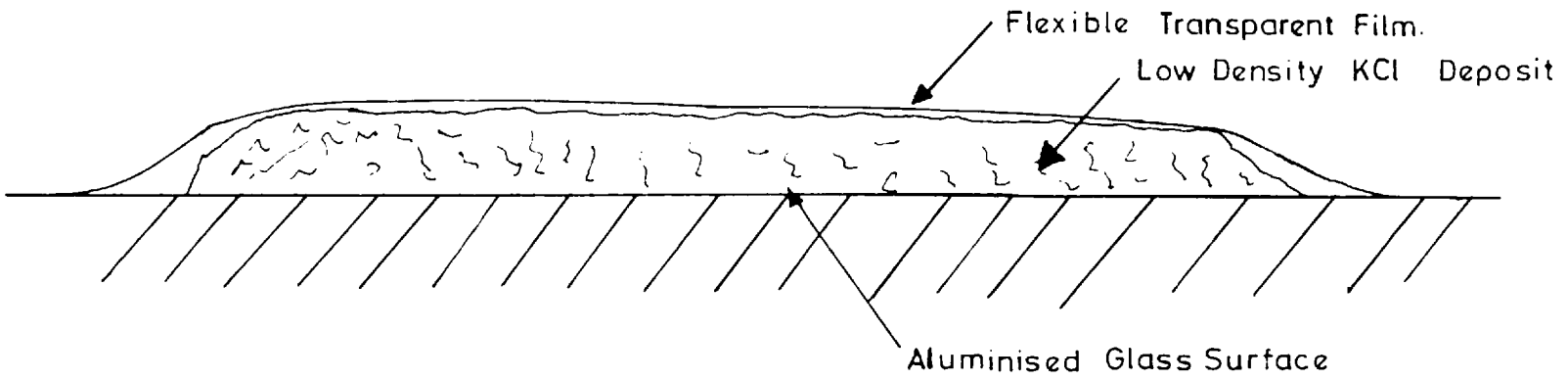

Fig. 2. 6. Interferometric Thickness Measurement

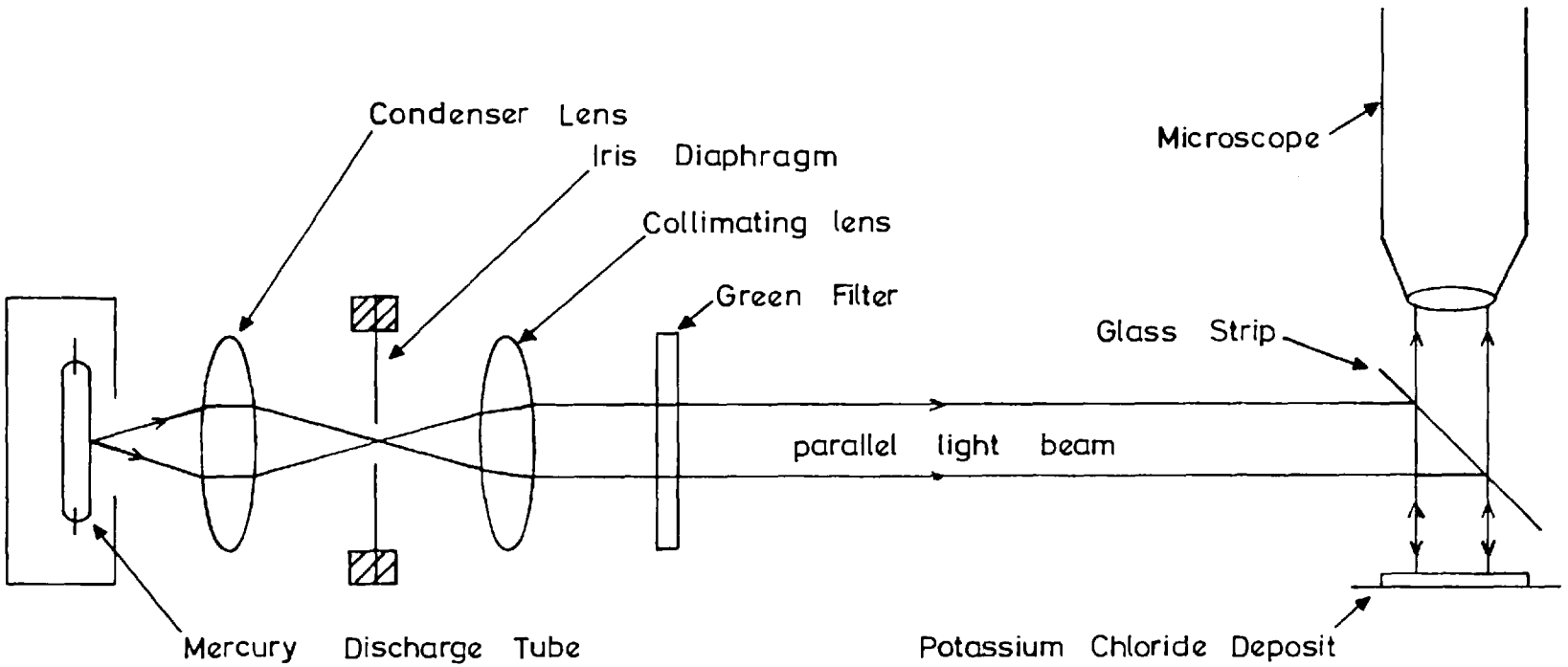

Fig. 2.7. Optical System for Measuring the Thickness of the Potassium Chloride by an Interferometric Technique

obtained when the collodion films were exposed to acetone vapour after they had been draped across the potassium chloride. The acetone vapour softened the collodion film which sagged and came into contact with the deposit. The photograph in fig. 2.8 shows some fringes obtained after this treatment. The plateau where the collodion film touched the potassium chloride is clearly visible; the treatment was not, however, completely successful in this case and it can be seen that the film was still suspended in places without touching the potassium chloride.

Although the method was capable of yielding measurements of high precision, it took a considerable time to perform and it was felt that there was danger of attack by water vapour. For this reason it was abandoned in favour of a quicker method of measurement. It is probable however, that the technique just described might be of use for estimating the thickness of deposits too rough to allow the evaporation of a layer of metal on their surface, but which are not attacked by water vapour.

The method finally adopted was to view a transverse section of a dynode in a microscope. The potassium chloride did not adhere strongly to the aluminium oxide layer, and it was found that on breaking the dynode, the support membrane curled back on itself, leaving the potassium

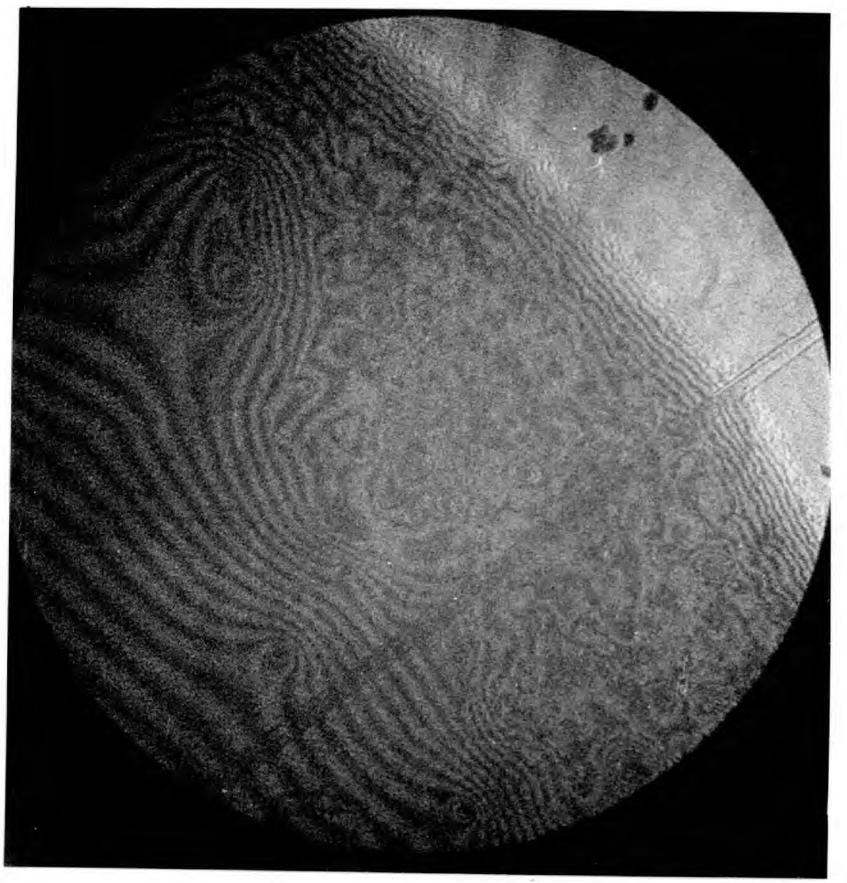

Fig. 2.8 Interferometric Measurement of Film Thickness

chloride as free standing flakes which could be manouvered into position and viewed end on. The unbroken dynode was placed under a stereo microscope and punctured by means of a fine glass rod. When a flake was found to be in the right position, the dynode was transferred to a high magnification monocular microscope. Consistent measurements of thickness were obtained, using a calibrated eyepiece.

It was essential to work fast and keep the films in a dessicator as much as possible to avoid attack by water vapour.

2.7 Estimation of the Mass of the Potassium Chloride

A conductrimetric technique was developed to enable the mass of the potassium chloride deposit to be determined. A conduction cell was designed so that it would enable measurements of a total mass of 25 μgm. of KCl to be made with reasonable accuracy. This minimum sensitivity was chosen so that the measurements could be made on solid KCl dynodes. It was known from Goetze's published figures that the low density dynodes would have a greater total mass, and that the accuracy obtained in measurements of bulk density dynodes would be exceeded.

The cell was in the form of a glass U-tube.

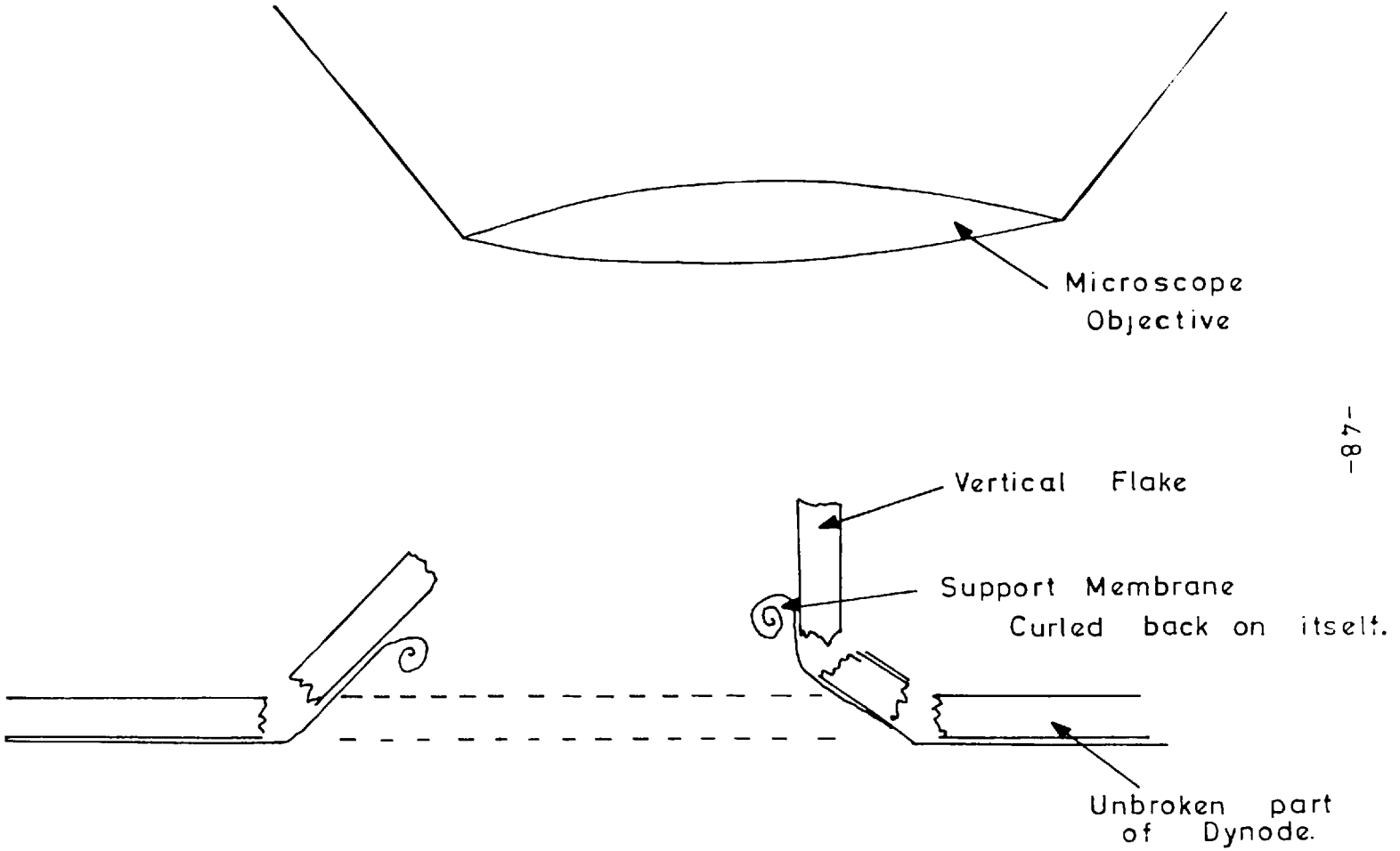

Fig. 2. 9. Microscopic Measurement of Dynode Thickness

Its volume was 1cc. and its dimensions were such that filling with a solution of 25 μ gm. of potassium chloride per cc. gave a resistance of 1 megohm. Two electrodes were made by firing platinum paint into the tops of the tube. These extended over a region enclosing a volume of a fraction of a cc.with the result that liquid in this region did not contribute to the conductance of the cell. The fact that the resistance was not affected by slight variations in the filling of the cell, ensured that, provided the cell was filled to a minimum level, the measurement was essentially that of concentration. A slight spillage or failure to pick up all the sample would not introduce an error so long as the correct volume of liquid had been used to make up the solution.

The resistance of the cell was measured directly with an Avo-meter. In order to prevent polarization by the internal batteries of the Avo-meter, the connections between the cell and the Avo-meter were periodically reversed by means of the circuit shown in figure 2.10. This circuit consisted of a pair of high speed relays wired to cause reversal when the their driving coils were simultaneously energised. The relays were driven by a small power transistor which amplified the output of a multivibrator. The latter generated a square wave with a fundamental

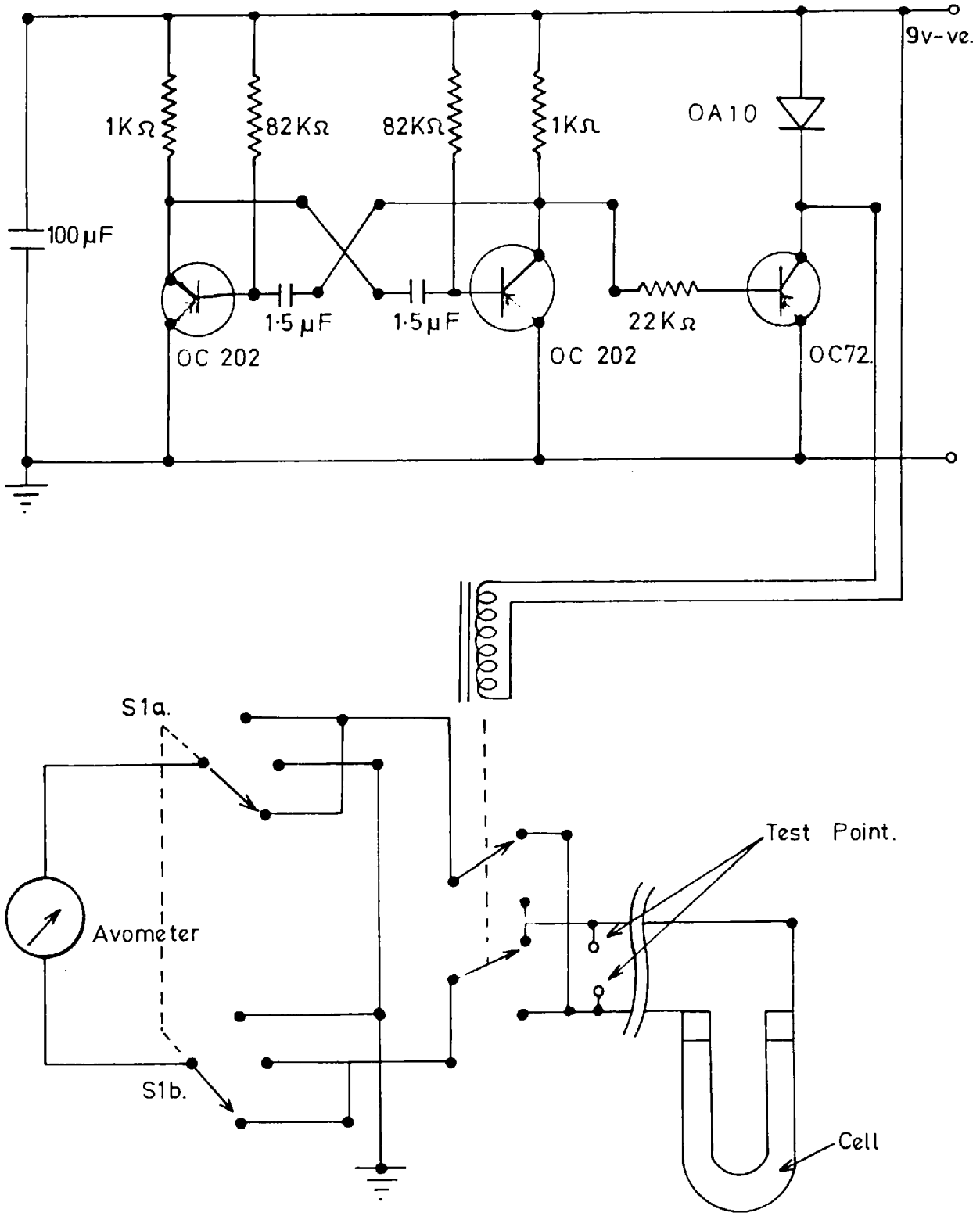

Fig. 2.10. Circuit of Resistance Unit

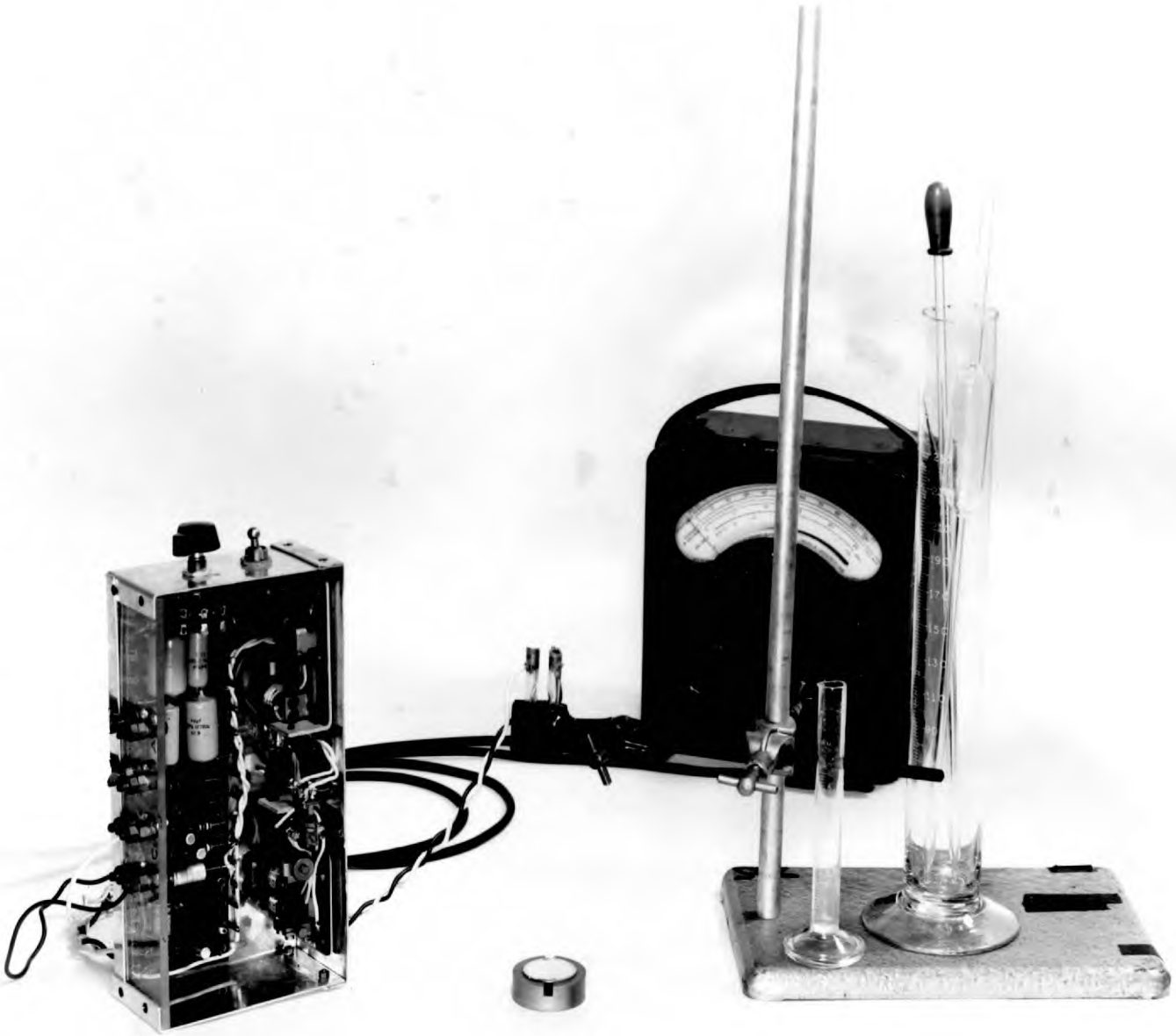

Fig. 2.11 Apparatus for the Determination of the Mass of KCl in Dynodes

frequency of about 15 c/s and unity mark-space ratio. It was important to achieve unity mark-space ratio (the ratio of the time 'on' to the time 'off'), in order to avoid a net D.C. bias being applied to the cell. A switch S1 was provided to allow the output from each relay to be displayed on a double beam oscilloscope, in order that the relay contacts might be adjusted.

The unit proved simple and reliable in operation, and enabled steady readings to be obtained. Although no leakage resistance was introduced by the reversing unit, a small correction to the Avo-meter readings was necessary because there was a short period when the meter was not connected to the cell.

The film was held horizontally over a small Petri dish and removed in one piece by running a glass rod round the inside of the glass ring on which the film was supported. A known volume of doubly distilled water was added and when the potassium chloride was dissolved 1cc. samples were removed and transferred to the cell with a pipette. The resistance was then measured. It was found that a range of concentrations existed which gave maximum accuracy of measurement. Because an approximate value for the film mass was generally known before the measurement was made, it was often possible to achieve

this concentration by chosing the amount of water used in making up the solution.

The cell was calibrated using solutions of known concentration. Over the range of concentrations used, a linear relationship was found between concentration and cell conductance.

Because of the sensitivity of the technique to impurities, it was necessary to be scrupulously clean; all parts of the apparatus were frequently washed in distilled water. The absence of a zero error arising from soluble deposits on the film present before the evaporation of the potassium chloride, was confirmed by carrying out an analysis on a film which had been aluminised but not coated with potassium chloride. No detectable error was found.

One film was weighed on a semi-micro balance before being analysed. Direct weighing of the film gave a mass 25% greater than that obtained by conductrimetric analysis. This difference exceeded the estimated error of measurement, but as semi-micro weighing techniques are subject to errors caused by the absorbtion of water vapour, the discrepancy was not surprising in deposits of such high surface area.

From measurements of weight and thickness, it was concluded that freshly evaporated films had average

densities of 3.2% ± 0.5% bulk density. Deposits which had been exposed to damp air showed considerably higher densities, up to 10% of the bulk value.

2.8 Correlation of Mass Deposited and Optical Transmission

As a result of the measurements described above, it was found that, although the optical transmission gave some guide to the thickness of the films, it was not sufficiently consistent to predict properties of dynodes intended for use in image intensifiers. The reason for this was not understood, but was probably due to poor control of the large number of factors influencing the evaporation.

In later work four dynodes were prepared simultaneously; no difference in excess of 10% of the masses of simultaneously evaporated deposits of potassium chloride was ever found.

CHAPTER 3

The Testing of Dynodes in the Demountable Tube

3.1 The Demountable Tube

A demountable tube was used for the initial testing of the dynodes. Silver chloride seals, made by allowing molten silver chloride to solidify between the two glass surfaces to be joined, were used as it appeared that they would allow repeated sealing, and would withstand a temperature of up to 350°C.

The source of primary electrons was an electron gun removed from an oscilloscope cathode ray tube (V.C.R. 97). This gun was a tetrode having a cathode, modulator, anode and focussing electrode. Deflection was achieved by potentials on two pairs of plates at the end of the gun. A gun having electrostatic focussing and deflection was used because the position and focus of the spot would, within very wide limits, be independent of the potential between the cathode and the dynode when all the electrodes were fed from a common resistance chain.

The original oxide coated cathode was replaced by a directly heated filament which consisted of a short length of 4 thou. diameter tungsten wire bent into a hairpin shape.

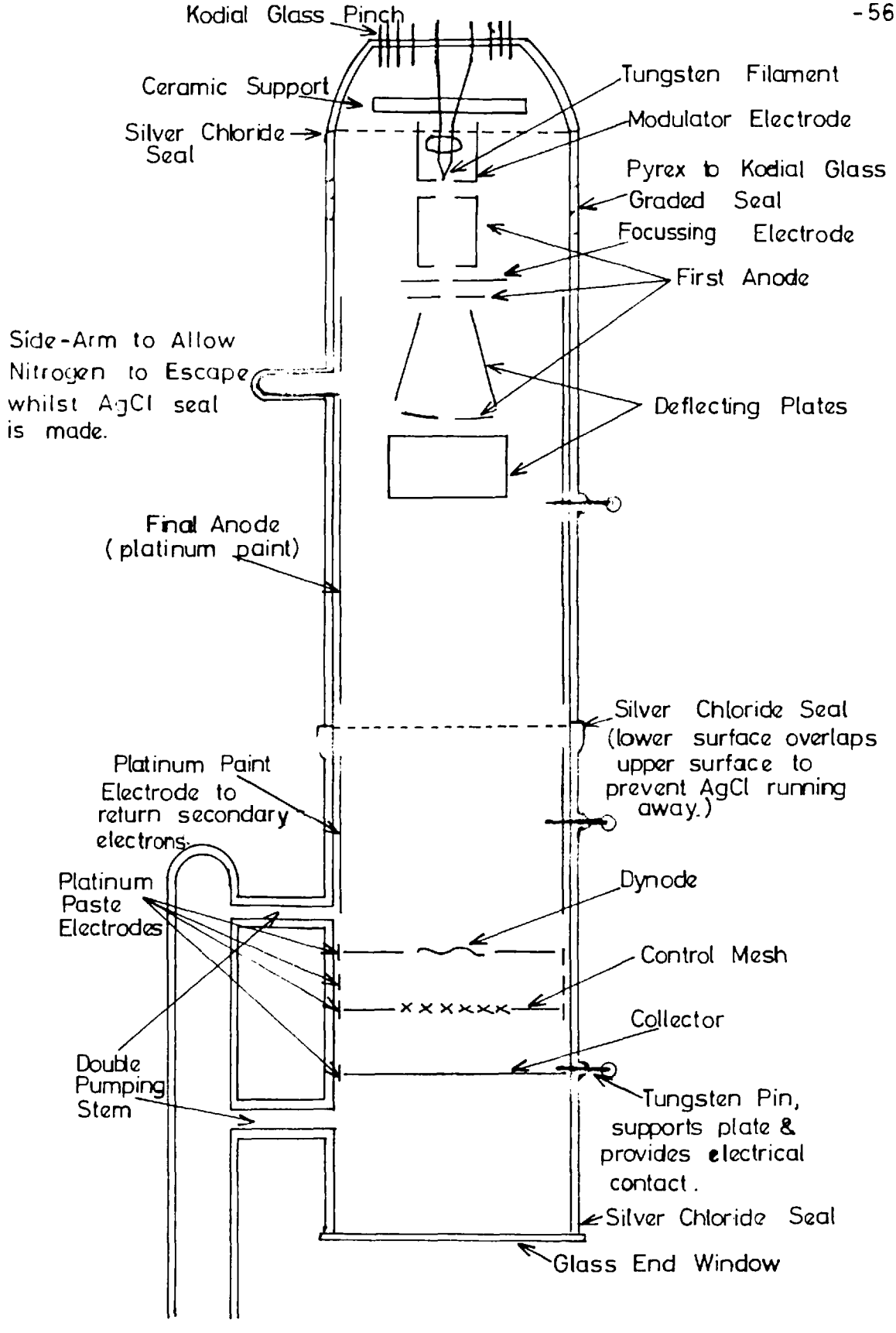

Fig. 3.1. Demountable Tube for Measurements on Dynodes.

The gun was removed from its original lead glass base and remounted by stout nickel wires on a glass pinch. This pinch was of Kodial glass and was joined to the rest of the tube which was of Pyrex glass, through a graded seal. In order to gain access to the gun a silver chloride seal was inserted close to the pinch. This seal was made and remade infrequently.

The bottom half of the tube, to which the pumping stems were sealed, contained the dynode and the associated electrodes. These were; - the dynode support, the control mesh and the collector. A guard ring was painted onto the tube wall between the mesh and the dynode support, to divert leakage currents. The dynode plate was coated with phosphor so that the gun could be focussed when the beam was deflected off the dynode.

The circuit used to control the electron gun is shown in figure 3.2. The beam current was controlled by both the filament current and the modulator potential. The current to the filament, which was at the full H.T. voltage negative of earth, was supplied by accumulators and controlled by a series transistor. The potentials for the gun electrodes were derived from a resistor chain, using both plug boards and potentiometers to give sufficiently

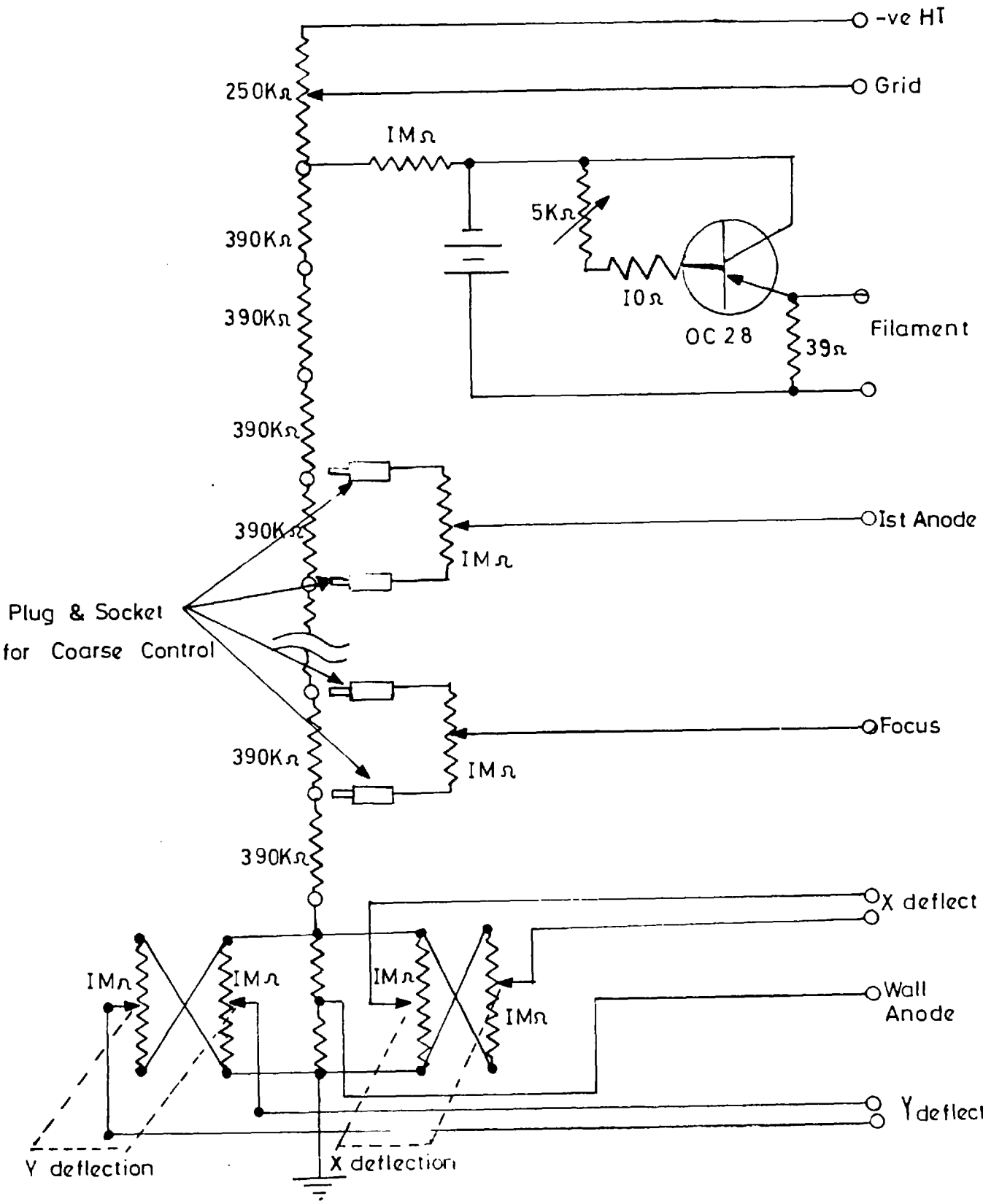

Fig.3.2.Control Circuit for Electron Gun

wide and accurate control.

In order to spread the beam over a large but well defined area, the focussed spot was made to scan a rastor by impressing sawtooth voltages on opposing pairs of beam deflecting plates.

Each sawtooth voltage was generated by a relaxation oscillator, figure 3.3, using positive feedback between the grids of a pentode. It was amplified by a double triode which generated two signals of equal amplitude, but opposing phase, which were fed to opposing deflector plates. The circuit was duplicated for the other set of deflecting plates.

3.2 The Measurement of the Electron Gain of the Dynodes

The arrangement used to measure the gain of the dynodes is shown in figure 3.4. Moving coil galvanometers were used to measure the secondary and primary currents. The beam current, i.e. the primary current, was measured directly as the total current to earth from all the electrodes, whilst the secondary current was measured as the total current to the control mesh and collector.

Errors in the measurement, caused by secondary electron emission from the support membrane, were avoided by the use of a painted wall electrode held at about 100 V negative

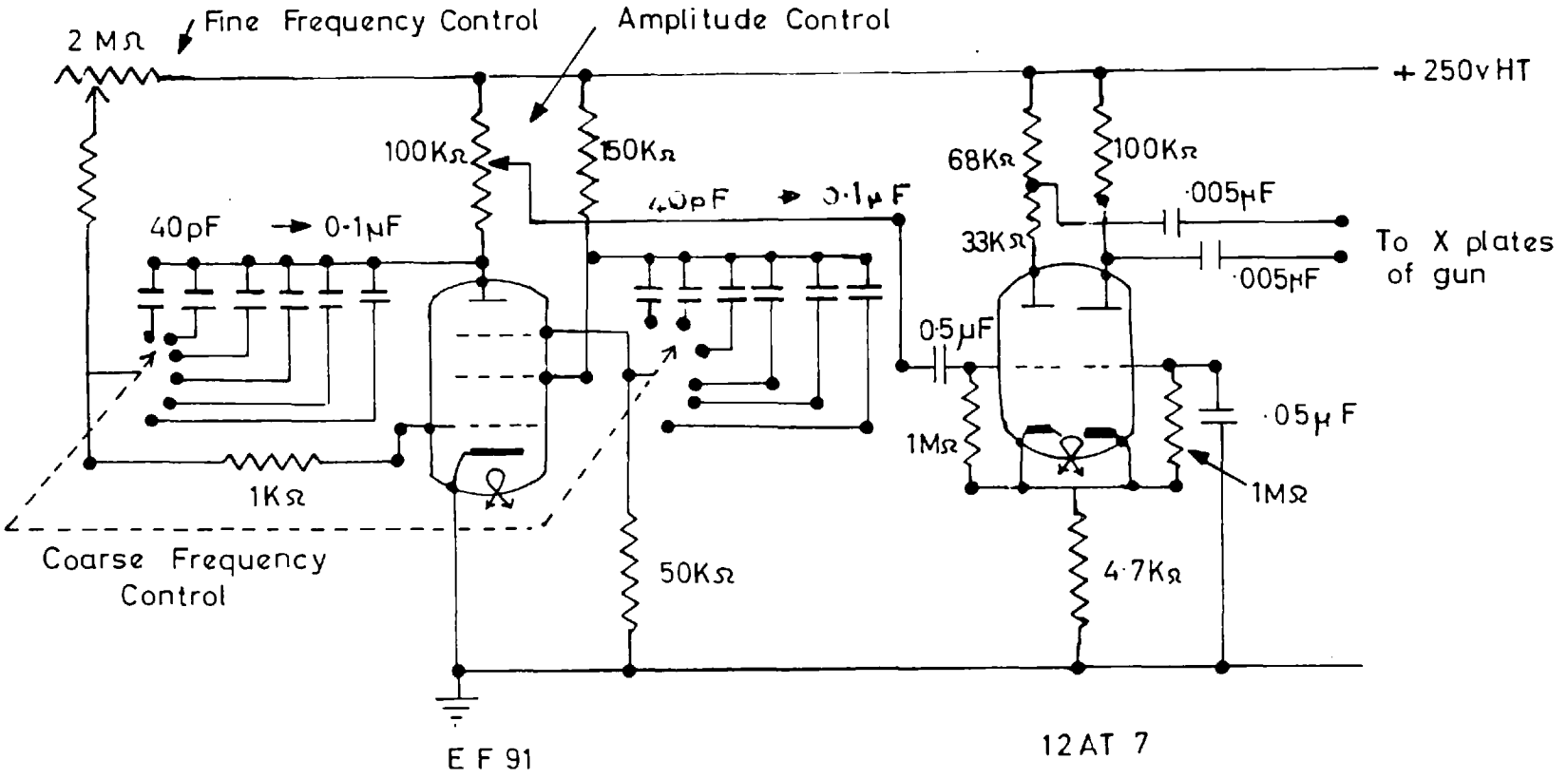

Fig. 3.3. Generator of Sawtooth Voltage for Scanning Electron Beam in Demountable Tube.

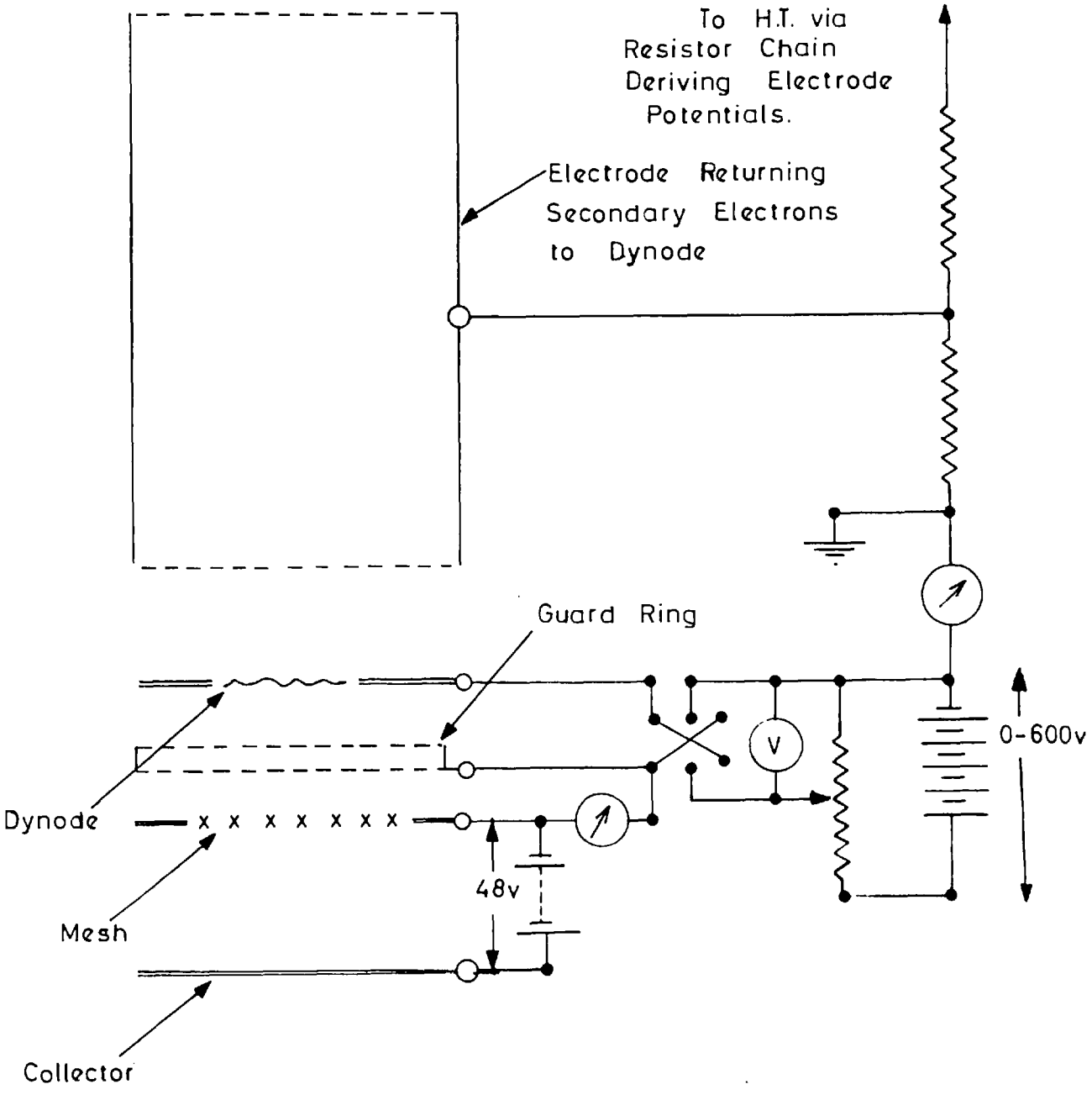

Fig. 3.4. Simplified Circuit Diagram for the Measurement of Electron Gain in the Demountable Tube.

with respect to the dynode. Without this precaution errors of up to 50% (at the lowest H.T. voltage) were introduced.

When the collector was maintained at about 50 volts or more positive with respect to the mesh, the current collected by the two electrodes was independent of the voltages between the two. Thus the two electrodes connected in this manner were equivalent to a single electrode having very low secondary emission. The effect of field penetration by the collector potential can be shown to be very small and the effective potential of this compound electrode was very nearly that of the mesh.*

3.3 Attack by Water Vapour and its Prevention

The first dynodes tested in the demountable tube were found to have gains very much lower than those reported by Goetze, although the variation of gain with primary and collector voltages was as reported. As the low density deposits of potassium chloride were known to be susceptible to attack by water vapour, and as water vapour was known to have an adverse effect on the performance of dynodes using bulk density potassium chloride for the

---

* Appendix A.3.

secondary emitter[38], it appeared likely that the low gains obtained at first might have been a result of attack by water vapour. In the next four paragraphs, possible means by which water vapour might have reached the dynodes and the steps taken to eliminate this attack are discussed.

1) The argon atmosphere in which the dynodes were prepared might have been damp. Drying towers and a cold finger were introduced into the argon admission line; these have already been described in section 2.3.

2) The dynodes might have been attacked by atmospheric water vapour between their removal from the chamber and their being placed in the dry-box in which they were inserted into tubes. When the evaporation had been completed the entire substrate assembly was placed in a dessicator containing phosphorus pentoxide. A brief exposure to the atmosphere could not be avoided but the transfer was effected as rapidly as possible, and the person making it wore arm-length rubber gloves and breathed through a mask. The dessicator was then placed unopened in the dry-box. After the dry-box was closed, the dessicator was left unopened for 15 to 20 minutes, by which time, phosphorus pentoxide showed no sign of absorbing water on being freshly exposed inside the dry-box.

3) Water vapour from the gas torch might have been

admitted on sealing a completed tube on to the pumping system. To prevent the admission of water vapour during seal-on, the tube was isolated from the section of the stem being worked by means of a valve. This consisted of a length of tube bent as in figure 3.5, with a steel ball which fitted in a ground seat. When the glass blowing was completed, the ball was lifted into a side-arm by a magnet and the tube was pumped down as quickly as possible.

4) Water vapour, and possibly some other contaminant might have been evolved from the heated surfaces as the silver chloride seal was made. During the forming of the silver chloride seal, dried nitrogen was passed through the tube in such a direction as to ensure that no gases from the seal could reach the dynode. An additional side-arm was attached to the tube to allow the nitrogen to escape. A drying tube was attached to this side-arm which was sealed off close to the tube body immediately before sealing the tube to the pump.

3.4 Results of Measurements with the Demountable Tube

The adoption of these techniques led to many dynodes showing high gains; in general, the dynodes showed maximum stable gains between 30 and 60. The variation of electron gain with primary and collector potentials of a typical

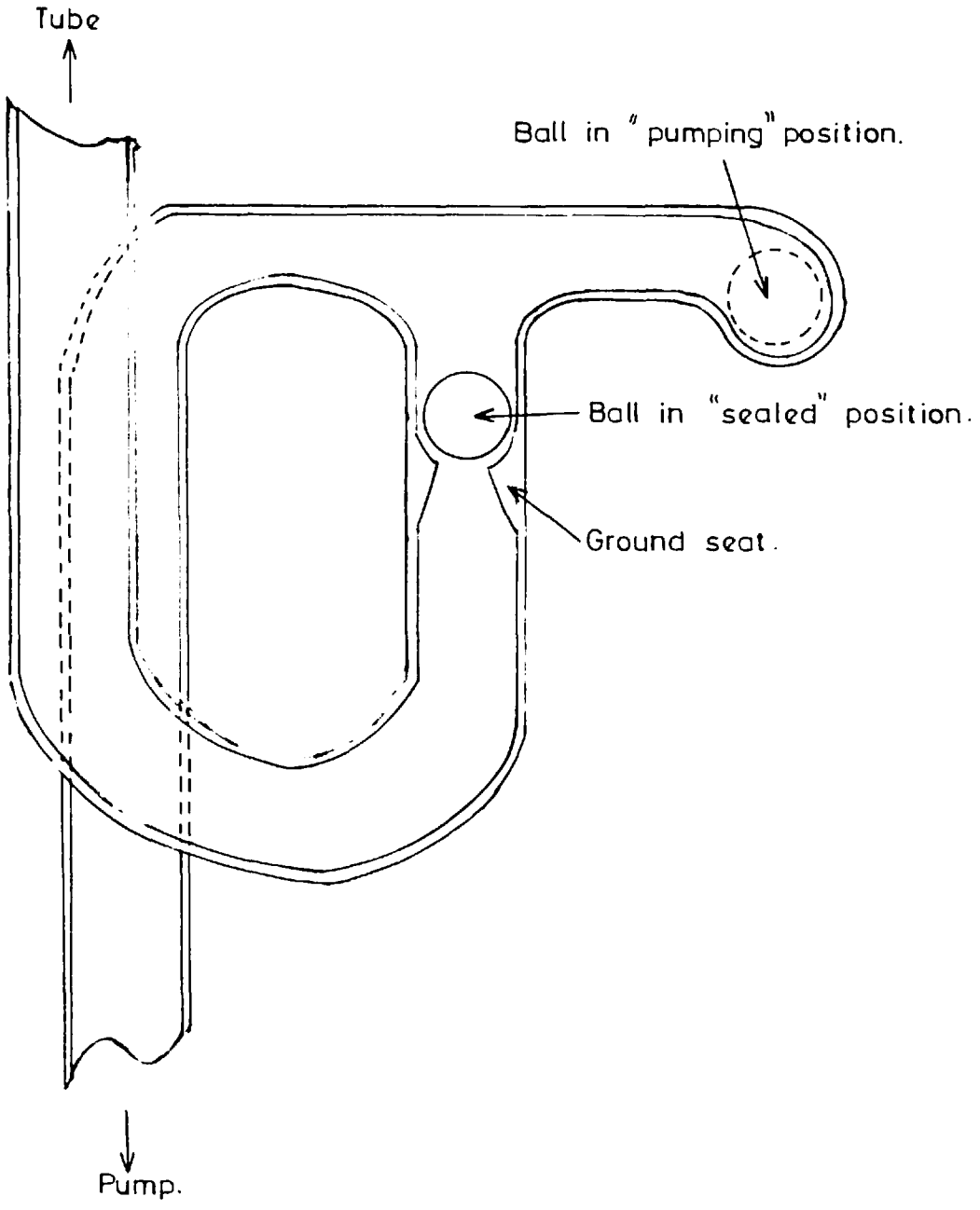

Fig. 3.5. Ball Valve

dynode is shown in figures 3.6 and 3.7. A minimum primary energy was necessary for secondary emission to be observed. At low collector potentials, the gain reached a maximum value and then fell again as the primary energy was increased. As the collector potential was increased, the maximum gain appeared at higher primary energies, and became less well defined; sometimes a maximum was no longer observed.

At low primary energies, the gain saturated as the collector potential was increased. At higher primary energies, this saturation gave way to a monotonic rise in gain with increasing collector potentials. Large collector potentials resulted in instabilities, the secondary current showing large and rapid fluctuations.

3.5 Dynode Thickness and Primary Energy

No consistent correlation was found between peak observed gains and evaporation conditions or thickness of deposit, but it was found that thicker dynodes needed higher primary voltages to achieve high gain.

This was in accordance with the theory that for enhanced emission to occur, a sufficient proportion of the incident electrons must form secondaries near the exit surface of the deposit.

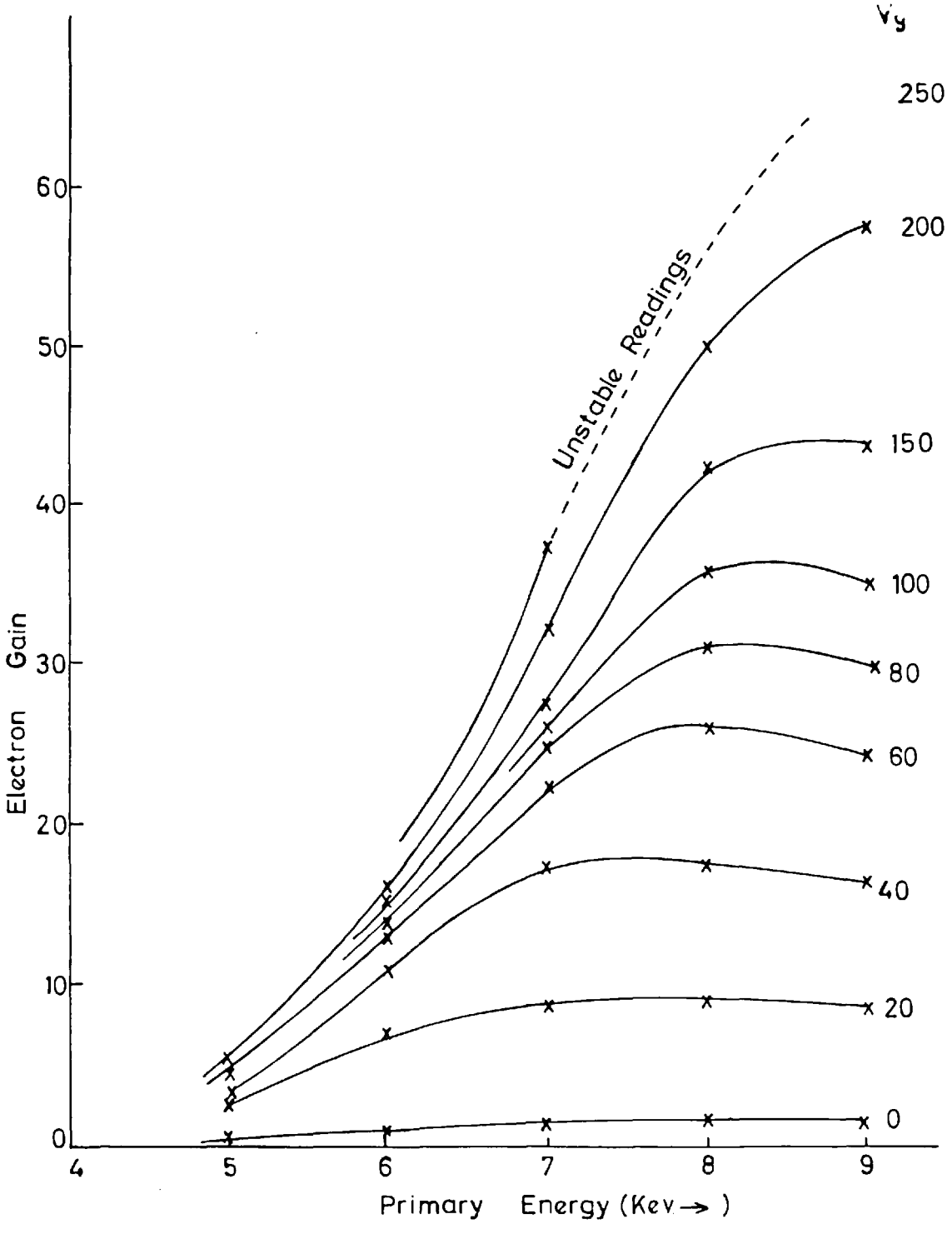

Fig. 3.6. Electron Gain of a Typical Dynode as a Function of Primary Energy for Various Constant Collector Potentials

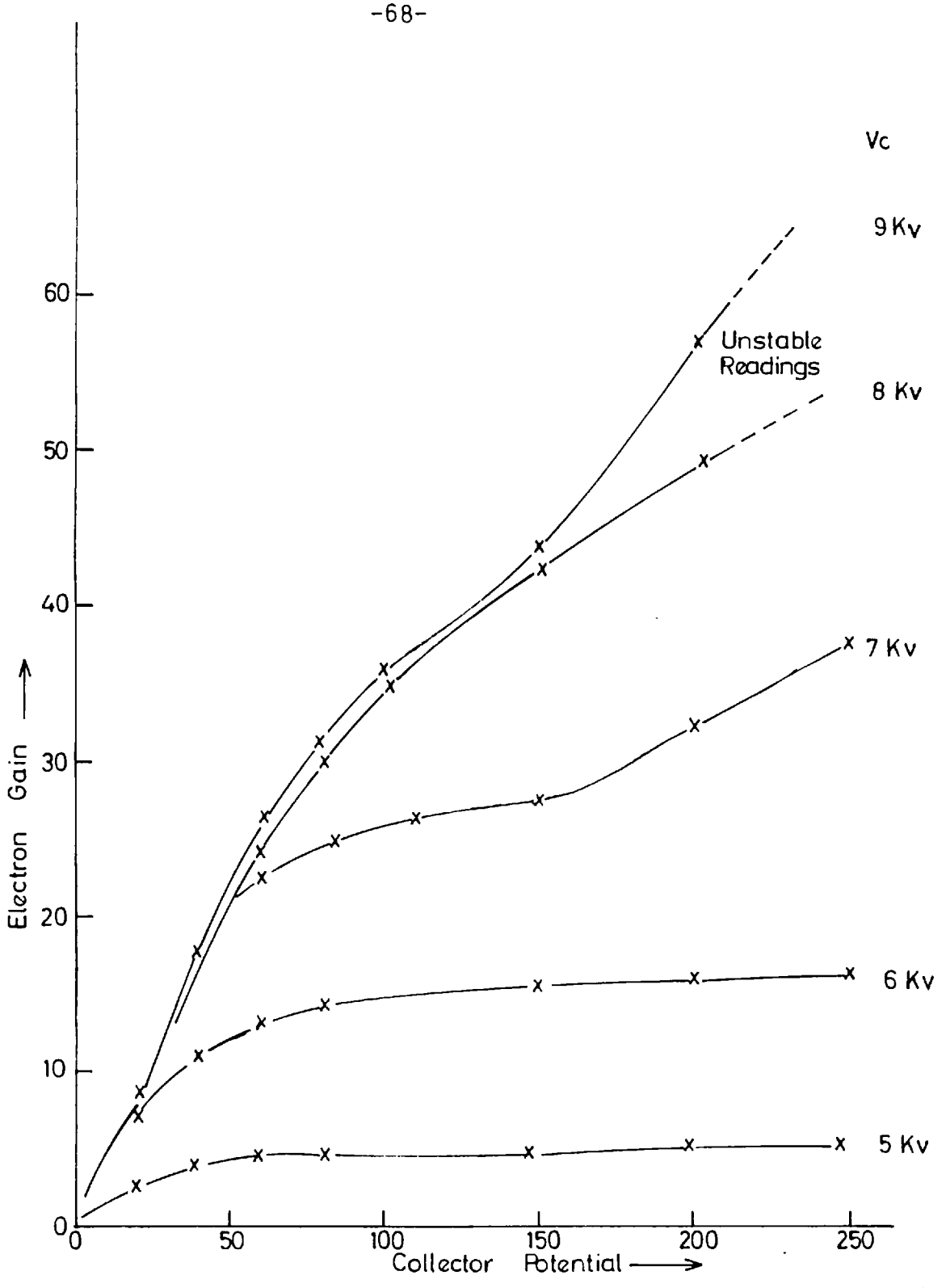

Fig. 3.7. Electron Gain of a Typical Dynode as a Function of Collector Potential for Various Constant Primary Energies

According to Feldman[62], electrons with initial energies between 1Kv and 10Kv have a range in a solid of R Angstrom units given by the general equation

$$R = bE^n \qquad (3.1)$$

where E is the initial energy in Kilovolts, and b and n are constants given by

$$n = \frac{1.2}{1 - 0.29 \log_{10} Z} ,$$

$$b = \frac{250A}{\rho Z^{n/2}} .$$

Z is the total atomic number of the compound,

A is its atomic weight,

and ρ is its density in gms./cc.

Figure 3.8 shows the electron range in 3.2% bulk density potassium chloride plotted against primary energy; the range is given in microns and was calculated from Feldman's equation.

Differentiating equation (3.1) gives

$$\Delta E = \frac{\Delta R}{nbE^{n-1}} \qquad (3.2)$$

where ΔE is the energy loss of an electron traversing a thin layer of thickness ΔR. Equation (3.2) was used to estimate the reduction in energy of the primary electrons as they passed through the aluminium support layer and the

Fig.3B.Electron Range in 3·2% Bulk Density Potassium Chloride and the Energy Losses in the Aluminium and Aluminium Oxide Layers (After Feldman)

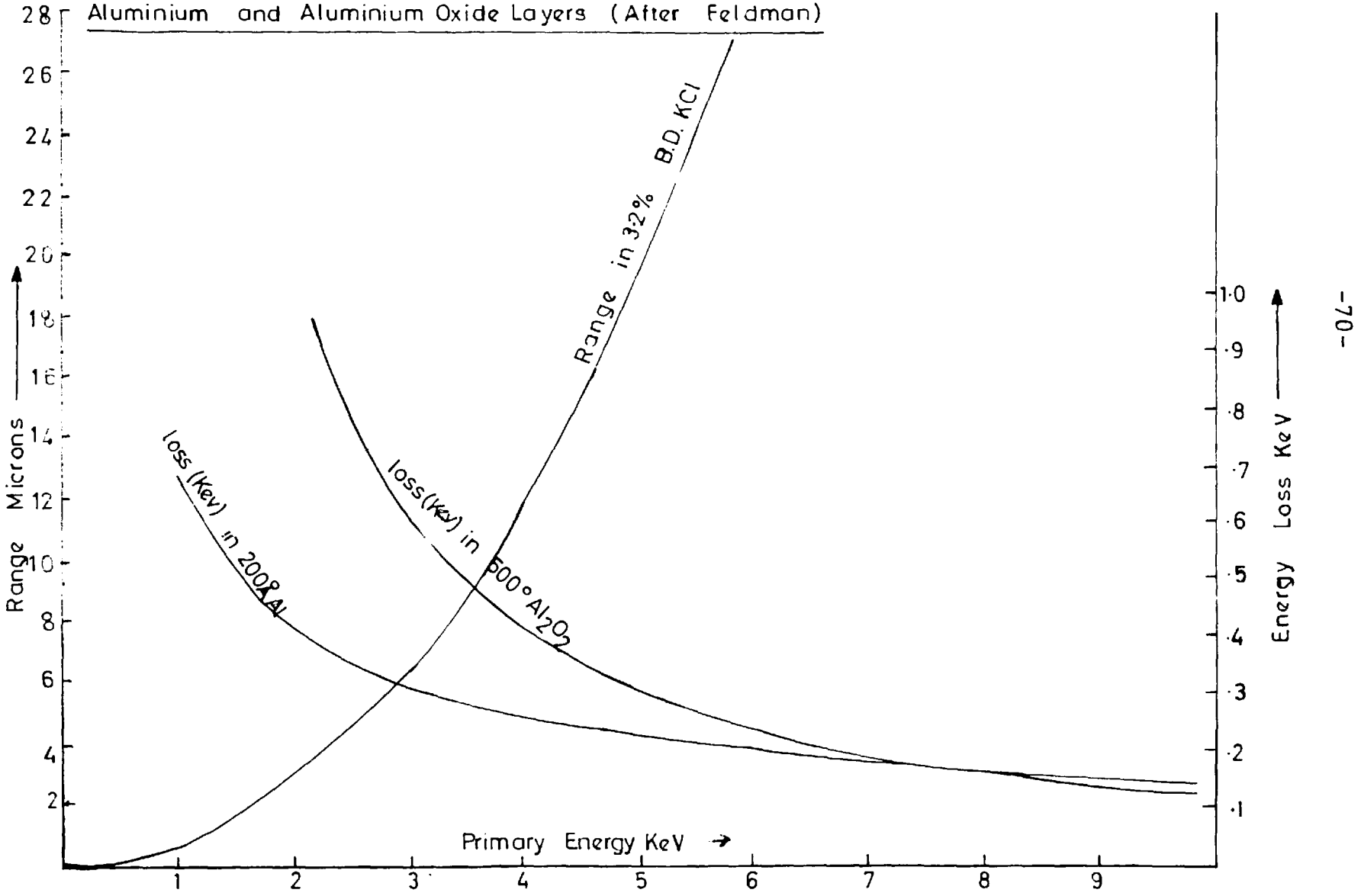

aluminium conducting layer. The reduced primary energy was substituted into equation (3.1) to calculate the theoretical curve in figure 3.9, showing the range in potassium chloride as a function of primary energy. Figure 3.9 also shows two experimentally determined energies as a function of the mass per unit area of several dynodes. These energies were related to the energy needed for an electron to penetrate the dynode; their determination is illustrated in figure 3.10. The lower energy, V_{pmin}, was the lowest primary energy which gave rise to a detectable secondary current. The higher energy, V_{pmin}, was derived from the curve of gain against primary energy; it was the intercept with the primary energy axis of the tangent to the curve at maximum $\frac{dG}{dV_p}$.

3.6 Comparison of Enhanced Secondary Emission and Electron Bombardment Induced Conductivity

The characteristic shown in figure 3.6, shows a notable similarity to some curves published by Ansbacher and Ehrenberg who measured the bombardment induced conductivity (B.I.C.) of a vacuum deposited layer of As_2S_3 bombarded with electrons in the energy range 10 to 40 Kev.[63] Two curves from their paper are reproduced in figure 3.11.

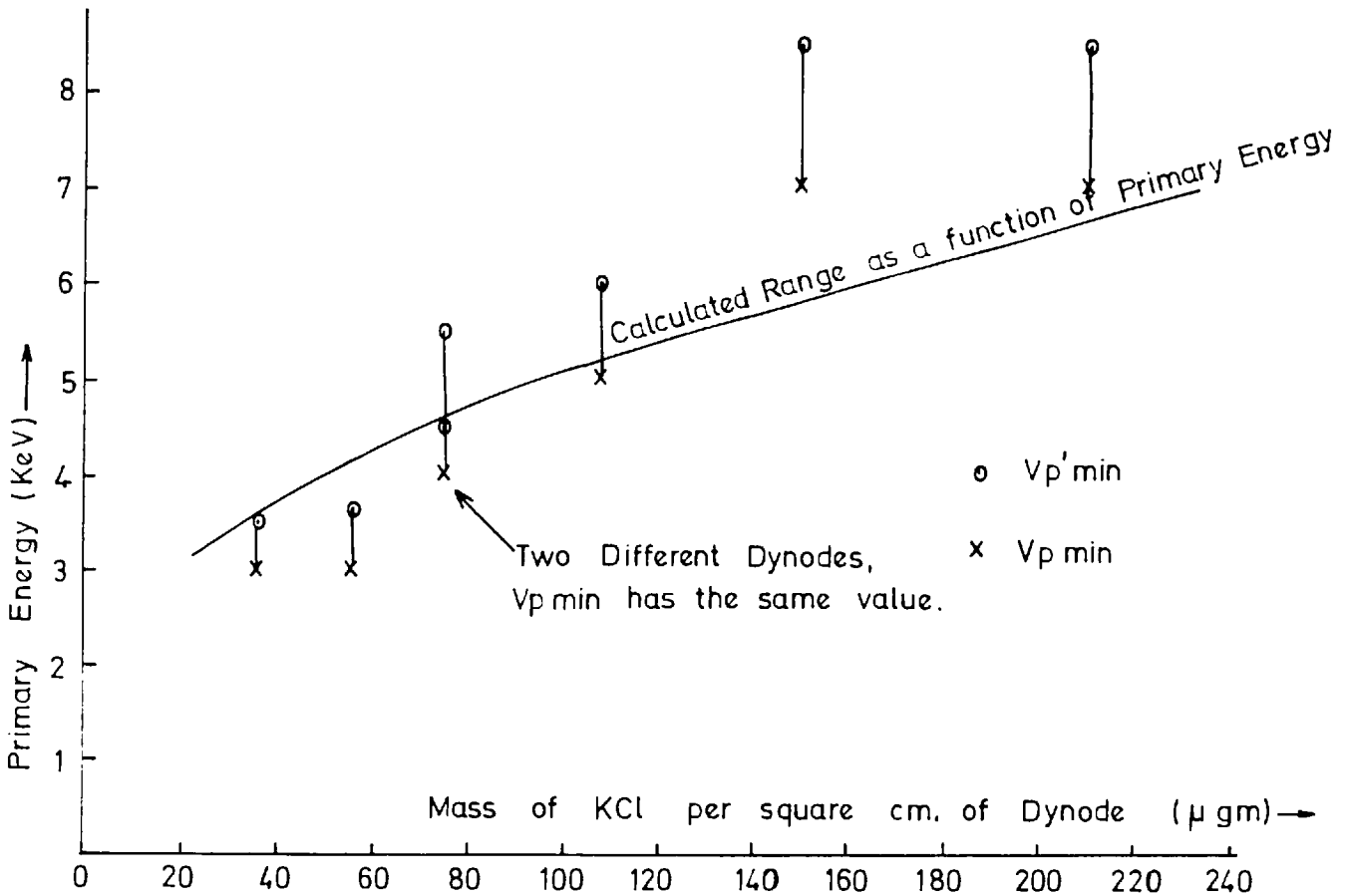

Fig.3.9.Relation between Thickness of Dynode and Primary Energy necessary to Cause Transmitted Secondary Emission.

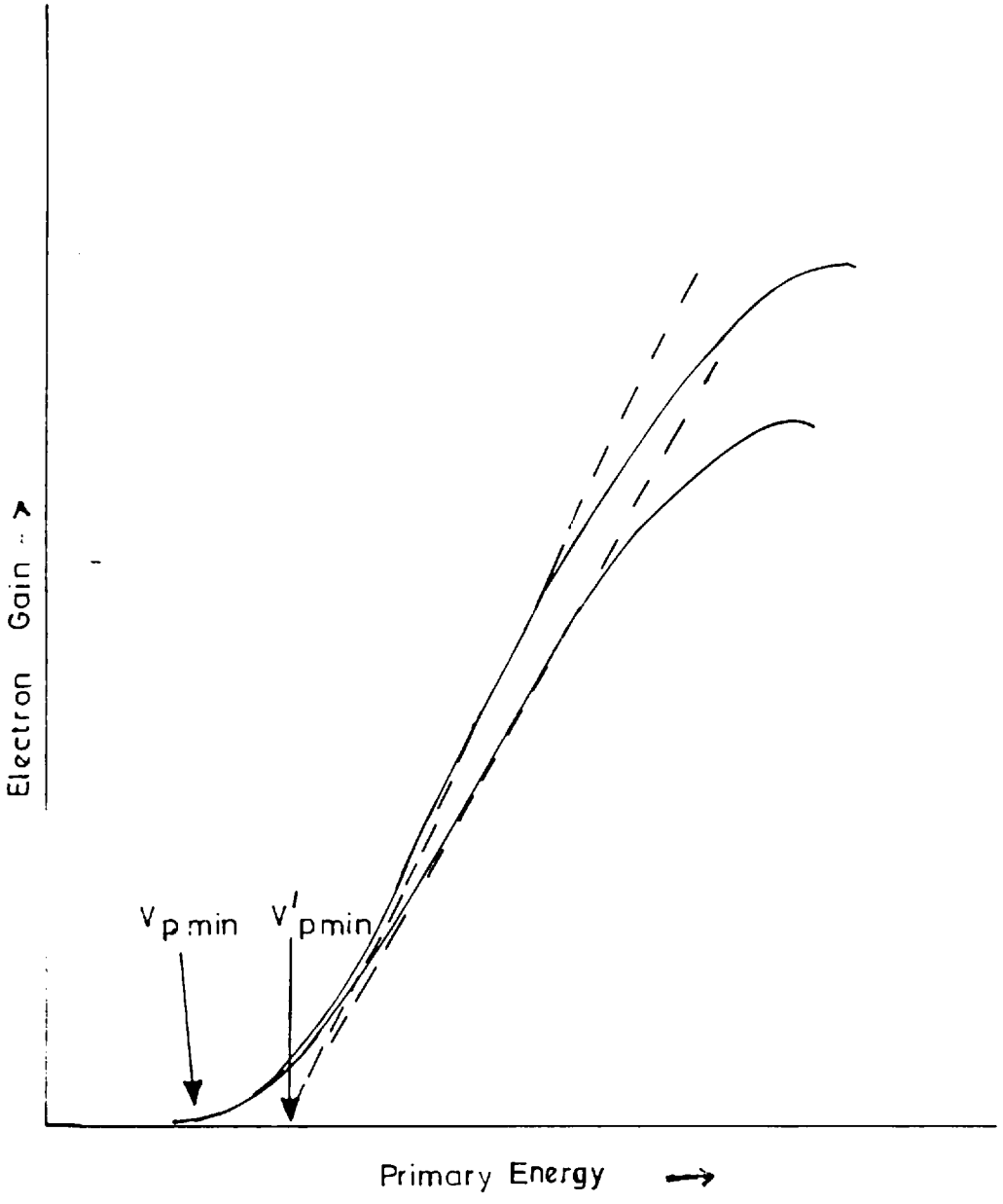

Fig.3.10. Showing the Determination of $V_{p\,min}$ and $V'_{p\,min}$

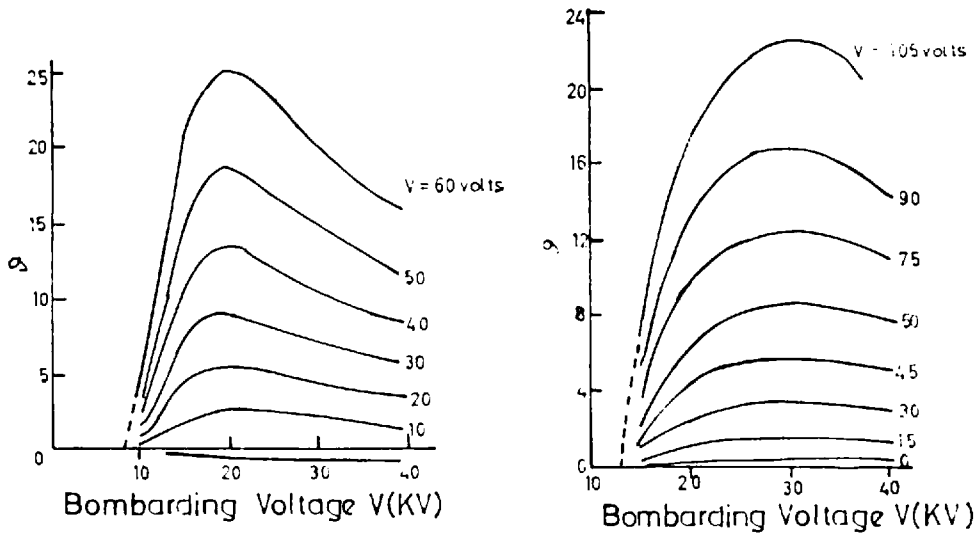

Film 1·2 μ thick
T = 26° $I_p = 27 \times 10^{-8}$ A/cm^2

Film 2·04 μ thick
T = 24°c $I_p = 27 \times 10^{-8}$ A/cm^2

Fig.3.11.Variation of B I C Gain in As_2S_3 with Primary Voltage after Ansbacher and Ehrenberg

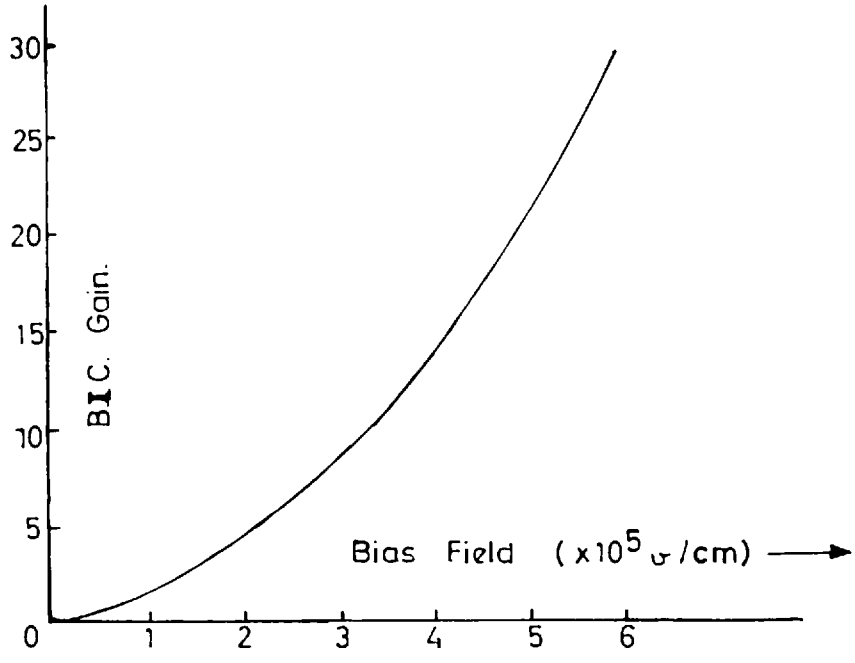

Fig.3.12.B.I.C. Gain of As_2S_3 as a function of Bias Field after Ansbacher and Ehrenberg.

These show the ratio of electron bombardment induced current to primary current (B.I.C. gain) as a function of the bombarding energy at various potentials across the As_2S_3 layer. The similarity in the form of these curves and the curve in figure 3.6, is felt to be a consequence of similarities in the processes of electron bombardment induced conductivity and enhanced transmission secondary electron emission. In both processes charge carriers are released by the primary electrons throughout the thickness of the material and accelerated by an electric field across the layer. In the case of B.I.C. the charge carriers contribute to a conduction mechanism whilst in the case of enhanced T.S.E.M. a number of the charge carriers are extracted from the deposit and appear as secondary electrons. The ways in which both processes depend on the primary electron energies are likely to have much in common.

In figure 3.12, which was derived from figures published by Ansbacher and Ehrenberg, the B.I.C. gain is seen to vary exponentially with the field across the layer. The electron gain of the dynode rose much less rapidly with the collector voltage. It was later shown* that the

---

* section 5.3

surface potential of the dynode was considerably less than the potential of the collector; when the gain of the dynode was plotted against the surface potential, a more nearly exponential relationship was observed.

No explanation has been found for the fact that a peak in the B.I.C. gain was seen at a primary energy which was independent of the potential across the film, whilst the peak in the electron gain of the dynode was seen to occur at a primary energy which increased with the collector potential.

3.7 Luminescence of Films

It was noticed that the potassium chloride deposit gave a blue glow on being bombarded. This was assumed to be connected with the excitation of electrons and their subsequent fall to lower energy states. Its efficiency as a light conversion process was not measured but comparison with the output from the phosphor around the dynode showed it to be very low.

It was also noticed, that heavy bombardment caused a permanent brown coloration of the potassium chloride. This was believed to be associated with the formation of colour centres[64].

3.8 Production of Dynodes for Image Intensifiers

For the following reasons, when dynodes were prepared for incorporation in image intensifiers, four were prepared simultaneously. The four dynodes were always found to have the same weight of KCl deposited on them, and it was assumed that by testing one in the demountable tube it would be possible to predict the properties of the remaining three. The presence of the aluminium layer enabled mechanical faults in the dynode to be spotted easily and the best dynode to be used in the intensifier. The use of four dynodes provided an insurance against breakage during assembly.

Many conditions were believed to affect the detailed structure of the low density deposit. Goetze had published the evaporation distance and gas pressure as 2 inches and 2 torr. respectively[42]. The effect of the speed of rotation and the rate of evaporation of the dynodes were not understood; it was found that with the substrate holder rotating once per second and a total evaporation time of five minutes, dynodes giving high gain could be prepared. The rate of evaporation was estimated by the rate of decrease of the optical transmission of the monitor plate around which the dynodes rotated; it was controlled

by the current through the boat. The evaporation was terminated when the transmission of the monitor plate fell to 70%. The monitor plate received a thicker deposit of potassium chloride than the dynodes. Because of the poor correlation of the mass deposited and the optical transmission, it was necessary to test one of the dynodes in the demountable tube. The boat was offset from the axis of the substrate assembly to allow the passage of the monitoring beam and consequently the distance of the dynodes from the boat varied as the substrate holder rotated.

3.9 The Baking of Dynodes

It was observed that baking the dynodes in the demountable tube caused a fall in gain. The extent of this fall depended on the temperature at which the baking was carried out, and it was found that if reasonably high gains were to be maintained, the baking temperature must not exceed 200°C.

Emberson had shown that adequate lifetime of sealed off tubes was not obtained unless a bake-out temperature of at least 300°C was used before sealing off the tubes[38]. Tubes otherwise treated showed a tendency for the photocathodes to deteriorate as gas was evolved from the tube walls.

It appeared from work by Todd[65], that although the bake-out at 300°C was necessary to drive off the gas from the walls of the tube, the walls would re-absorb gas comparatively slowly if the inside of the tube was subsequently exposed to dry air for a short time. Furthermore, it appeared that, especially if water vapour was excluded, the newly absorbed layer of gas could be driven off by baking at a lower temperature than was necessary to degas previously unbaked glass.

The following procedure was tried and found to be successful. The tube was baked in vacuo to 350°C, and sealed off containing the metal parts which had been vacuum stoved before assembly. A gas admission valve (figure 3.13) was sealed to the side-arm which later served to pass out nitrogen during the silver chloride sealing. This valve consisted of a thin glass tube which could be broken by a steel ball, thereby connecting the tube body to a source of very dry nitrogen. Once the tube was at atmospheric pressure, the silver chloride seal was broken and the tube placed in the dry box where the dynode was inserted. Dried nitrogen was passed through the tube as the silver chloride seal was remade after assembly. The tube was sealed onto the pump and baked at the reduced temperature of 200°C.

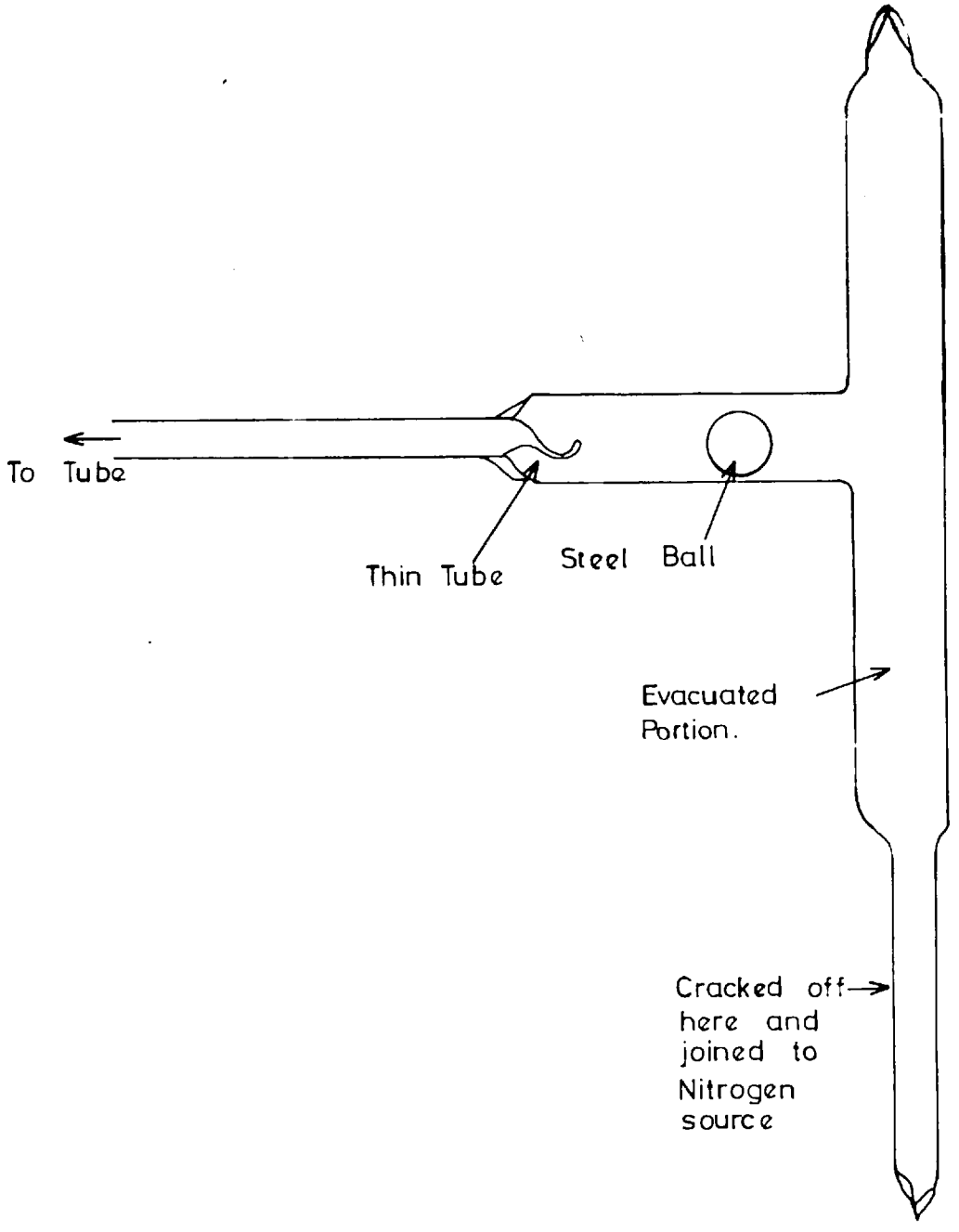

Fig. 3.13. Nitrogen Admittance Valve.

After the completion of these experiments the demountable tube was used in connection with work on bulk density KCl dynodes, and these also showed a loss of gain on baking. This lead to the conclusion that the gun was poisoning the dynodes on baking. When the gain was measured in a much simpler gun tube before and after baking it was found that the dynodes did not show a loss in gain during baking provided that the pressure was not allowed to rise whilst the dynodes were hot. On one occasion, when a small leak developed in the tube while it was at a high temperature, a drop in gain did occur. As a result of this work, it was shown that earlier conclusions on the baking of dynodes were invalid.

It was noted that dynodes using vacuum deposited KCl as the secondary emitter, frequently became transparent on being baked, and it appeared that the aluminium layer must have undergone some change. Dynodes using low density KCl, on the other hand, were never observed to become transparent. The reasons for this difference in behaviour were not established, but could have been the less intimate contact between the potassium chloride and the aluminium, the lower baking temperature, or the care taken to exclude water vapour, in the case of the low density dynodes.

CHAPTER 4

Image Intensifiers Using Low Density Potassium Chloride Dynodes

4.1 The Construction of the Image Intensifiers

Most of the sealed off image intensifiers using low density potassium chloride dynodes were as illustrated in figure 4.1.

The photocathode was of cesium antimonide[66]; in most tubes it was formed on a glass plate which fitted loosely to a metal shelf. The cathode was processed in a compartment at the end of the tube; it faced away from the dynode and after it had been processed and the tube had been sealed off, a simple mechanism[67] allowed it to be turned to face the dynode. A seal, consisting of a thin stainless steel skirt pressed against an accurately cylindrical section of the tube wall, was spot-welded to the shelf supporting the cathode; this seal prevented cesium released during the cathode formation from travelling from the compartment in which it was released to the rest of the tube. In some tubes the photocathode was formed on the end window of the tube, and the stainless steel skirt was welded on to the plate supporting the dynode.

The dynode and the control mesh were each mounted on

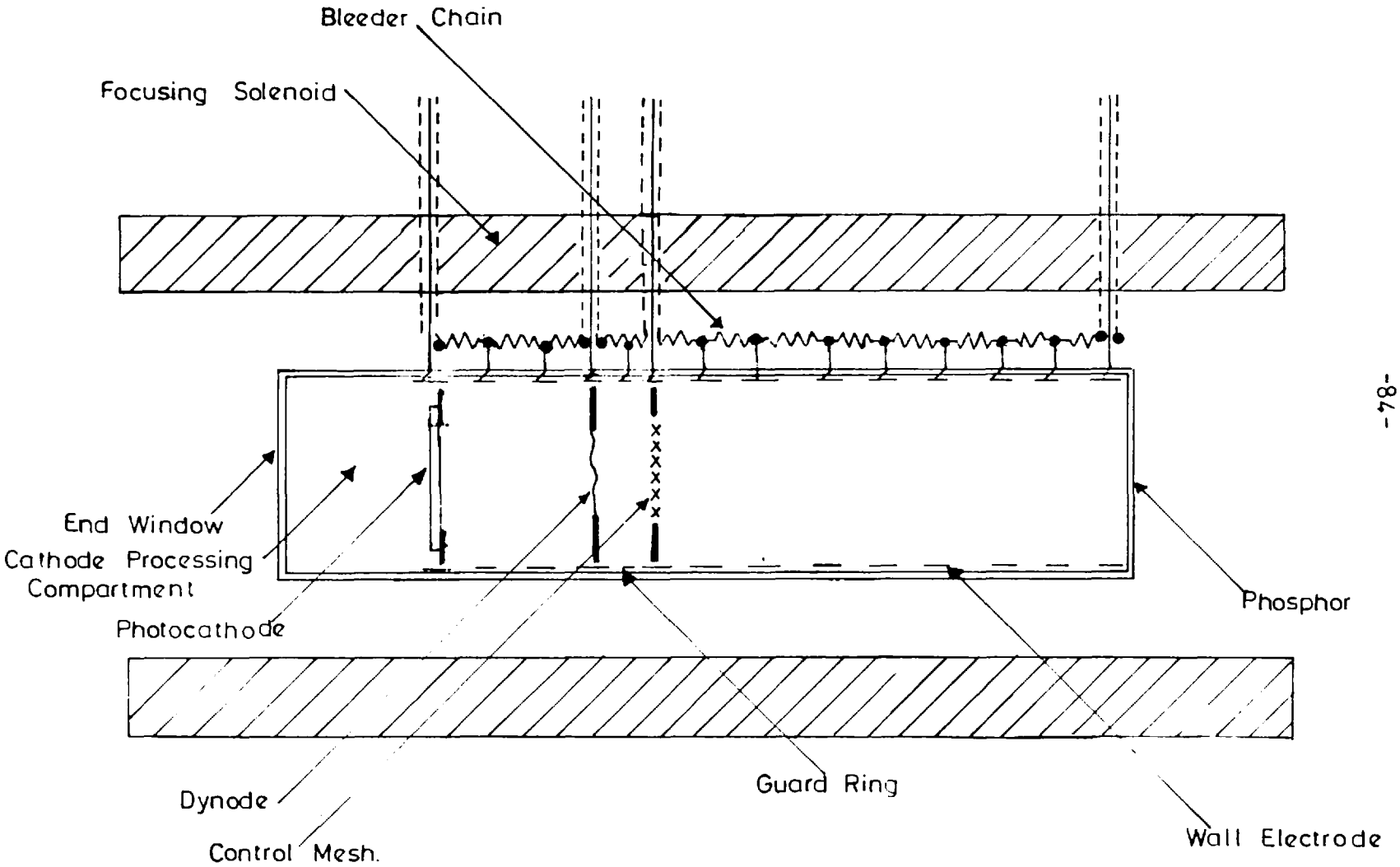

Fig. 4.1. Image Intensifier with Low Density Dynode

stainless steel plates which were supported by tungsten pins

The further end window of the tube bore a phosphor screen which was formed by allowing a suspension of silver activated zinc sulphide to settle[68]. An aluminium backing was laid behind the screen to provide electrical conduction and to increase the effective efficiency of the screen by reflecting forwards light which would have otherwise passed back into the tube; it also cut down optical feedback between the phosphor and the photocathode.

The tube was focussed by parallel electrostatic and magnetic fields*. The magnetic field was produced by a solenoid in which the completed tube was placed. The electrostatic field was produced by potentials on the metal electrodes, the cathode, the phosphor screen, and on internal circumferential wall electrodes. The latter were produced by firing bright platinum paint into the tube walls at the annealing temperature of the glass body. Contact to the internal electrodes was established by thin platinum tapes[69] sealed through the tube walls. The effects of the thermal mismatch between pyrex glass and platinum were avoided by the thinness of the metal tapes. External circumferential contacts were formed by firing silver paste into the glass walls.

---

* Appendix 1.

To gain access to the inside of the tube, the glass body was made in two halves which were joined by a silver chloride seal.

4.2 Cathode Processing

The cathode was formed after the bake-out schedule* had been completed. Antimony was first evaporated onto the cathode bearing surface to a thickness monitored by its optical transmission. Typical values used were around 83% full transmission for white light incident at an angle of 45°. The antimony was evaporated from a small movable evaporator which was slid in through a pumping stem by means of external magnets. The evaporator consisted of a shielded tungsten filament which bore a small slug of antimony and was heated by an R.F. current induced in a coil of nickel wire at its far end.

Cesium was admitted through a small side-arm, where it was prepared by a reduction process or released from a small ampoule. The cathode formation was monitored by observing the photo-current, using a wall electrode as an anode. A chopped light signal was used and the photo-current was amplified by a simple A.C. amplifier.

---

* Section 3.9.

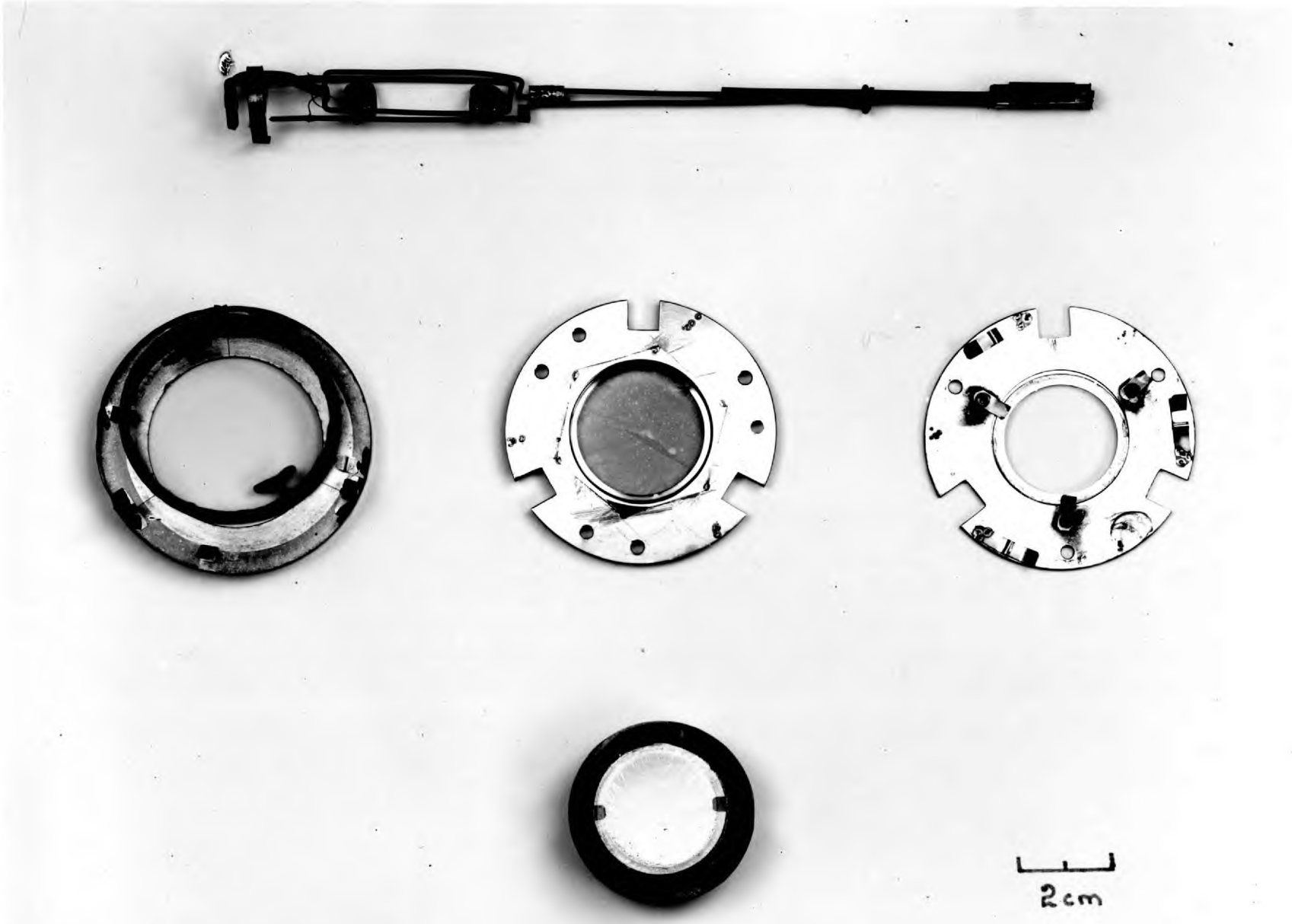

Fig. 4.2 Antimony Evaporator and Internal Parts of an Image Intensifier

The tube was heated to about 150°C, when the cesium began to combine with the antimony layer. When the sensitivity began to rise, the oven temperature was decreased and the inflow of cesium was increased by heating the side-arm with a small resistance element, until a fall in the photo-current indicated that over-cesiation had occurred. The tube was allowed to cool slowly, and the sensitivity was seen to rise as the excess cesium was driven off. More cesium was admitted until over-cesiation was again observed. This process was repeated until the tube had cooled to a temperature of about 90°C. The tube was again over-cesiated, the oven was lifted and the side-arm sealed off. The tube was then reheated until the previous highest sensitivity was again observed, after which it was cooled rapidly. When the tube was completely cool it was sealed off under vacuum.

4.3 Tube Mounting

After a tube was sealed off the pump, it was placed in a cradle for testing. In early tubes the connecting wires were soldered directly to the external silver paste electrodes, using silver loaded solder. Later tubes were mounted in the quick release cradle shown in figure 4.5; this cradle bore a series of adjustable spring contacts

which bore against the external tube contacts. The cradle also bore a resistor chain which derived the potentials applied to each electrode.

The tube and its cradle were then pushed into a 4 inch diameter polythene tube which fitted inside the focussing solenoid. The tube was cooled by water flowing through a narrow plastic tube embedded in a spiral groove around the outside of the polythene tube.

4.4 The Projectors

Two light sources and optical systems were used to project an image onto the photocathode. The optical system most useful for measuring resolutions, was that developed by W. A. Baum[70]. It was especially useful in that it included an optical arrangement which made it possible to focus the optical image onto the cathode without having to rely on the quality of the electron optical focus of the tube. This projector was generally used with the test pattern developed by W. A. Baum, which included a calibrated resolution pattern. Because of the distance between the end wall of the tube and the photocathode, it was necessary to replace the original objective lens by one of greater focal length. A correction to the calibration of the test pattern was needed because of the increased

Fig.4.5 Image Intensifier, Mounted and Ready for Testing

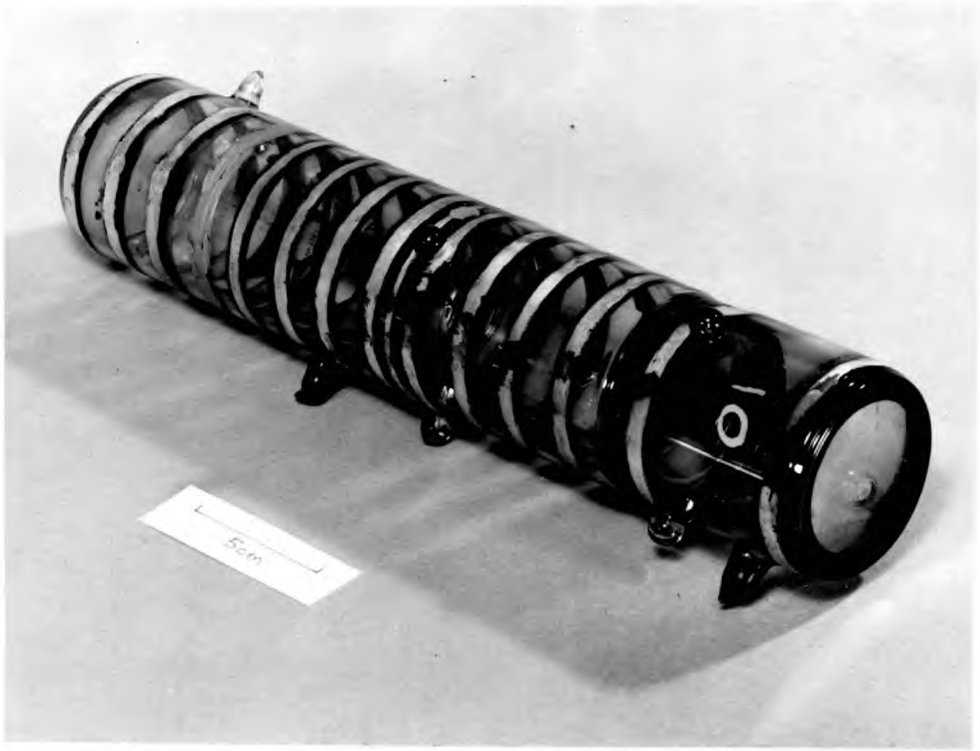

Fig.4.4 Image Intensifier with Low Density Potassium Chloride Dynode

diameter of the projected pattern.

For work involving current measurements, it was generally more convenient to use another projector and optical system. This projector consisted of a small light bulb behind a diffusing screen; the pattern to be projected was placed in front of the screen and focussed onto the photocathode by a lens whose position could be adjusted by an operator watching the phosphor of the image intensifier. To avoid the effects of mains voltage fluctuations on the intensity of the image, the lamp current was drawn from accumulators, and controlled by the transistor circuit in figure 4.6. Instabilities caused by variation of the filament temperature when the lamp was switched on and off, were avoided by running the lamp continuously, and using an electromechanical shutter to intercept the light.

4.5 Current Measurements

All the current measurements were made by measuring the voltage drop across a suitable load resistor with a vibrating reed electrometer. The load resistor was usually 10^8 or 10^{10} ohms and the currents measured were between 10^{-12} and 10^{-8} amps. When the electrometer was used to make measurements of the currents to the dynode or the mesh, it was necessary to use two H.T. power supplies, one for the photocathode supply, and one for the

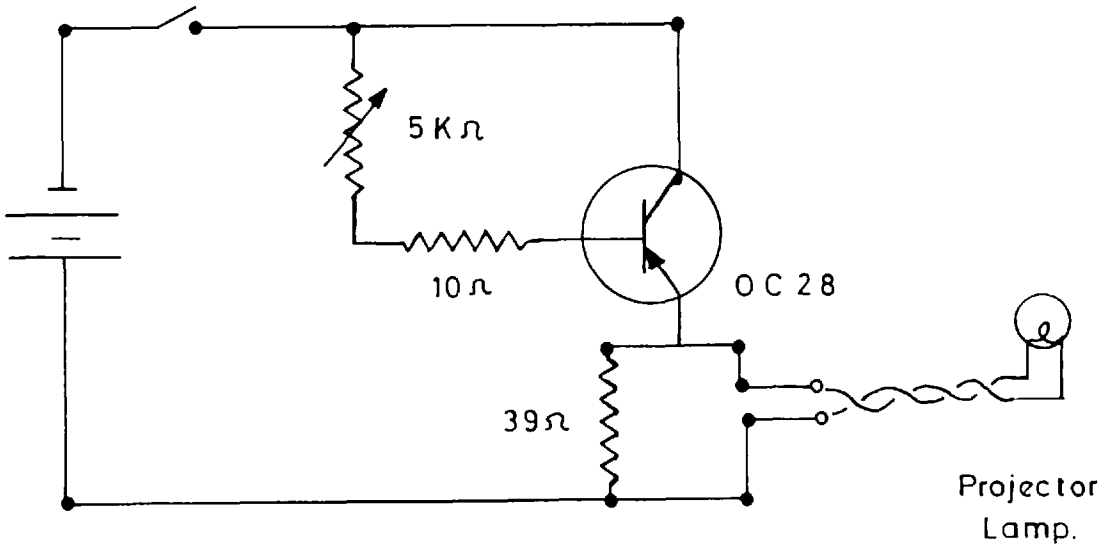

Fig. 4.6. Current Supply to Low Voltage Projector.

the phosphor supply, because the electrometer could only be used at potentials near to ground and the power supplies were earthed at one terminal. The use of two power supplies greatly simplified the focussing procedure.

4.6 Electron Gain of the Dynode

The electron gain of the dynode was usually obtained by measurements on the dynode current alone. The primary current was determined by measuring the current to the dynode as a function of primary voltage when the control mesh was at the same potential as the dynode. The curve in figure 4.7 was obtained. An initial rise in the current collected by the dynode was the result of non-saturation of the cathode current. The flat portion of the curve gave the primary current, and the fall in current to the dynode as the primary voltage was further increased, was the result of penetration of the dynode. If i_p was the primary current, and i_d was the electron current taken by the dynode, the gain G was given by

$$G = \frac{i_d + i_p}{i_p}$$

The gain showed the same variation with primary voltage and mesh voltage as was found from measurements on dynodes in the demountable tube. In general, however, high gains

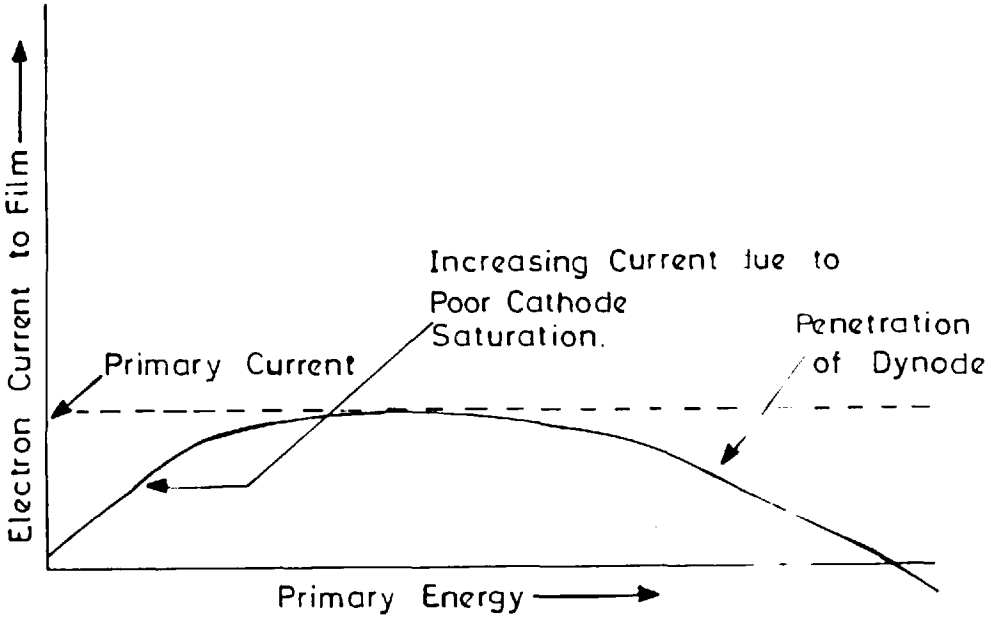

Fig. 4.7. The Measurement of Primary Current, showing External Electron Current to Dynode as a Function of Primary Energy, with Zero Control Mesh Potential.

occurred at lower values of the control mesh potential.

Considerably lower current densities (the maximum secondary current was in the order of 10^{-8} A/cm^2) were used for measurements in the sealed off tubes than had been used for measurements in the demountable tube, and the secondary current was found to depend on the time for which the primary current was incident*. In general, apart from some comparatively short lived oscillations when the primary current was changed, the secondary current increased slowly towards an equilibrium value. The time taken for readings to stabilize set a lower practical limit on the current densities used for taking readings, and few readings were taken with primary current densities below 10^{-12} A/cm^2.

4.7 The Penetrating Primary Current

The penetrating fraction^x was measured directly using a tube with two meshes*. The first mesh served as a control mesh in the normal manner whilst the second mesh was held at such a potential that only fast electrons could pass it. These electrons were collected by the phosphor

---

* Chapter 5

x Section 1.13.

which was held 2.5Kv positive with respect to the dynode. This potential effectively suppressed secondary emission from the phosphor and prevented an under-estimation of the current to the phosphor. A strong magnetic field of approximately 300 gauss, was applied to prevent electrons reaching the tube walls, and the primary current was confined to a small area in the centre of the dynode.

A graph of phosphor current against retarding potential for constant primary voltage is shown in figure 4.8. No detectable change was seen when the retarding potential was changed from 10 volts to 100 volts, and it was concluded that most of the penetrating primaries had forward velocities corresponding to energies in excess of 100 volts. The retarding potential was fixed at 100 volts for the measurements of the penetrating fraction as a function of the primary energy, shown in figure 4.9.

The dynode on which these measurements were made could yield an electron gain of fifty when the primary electrons had an energy of about 6.4Kev. It can be seen from figure 4.9 that at this primary energy about one electron in three gave rise to a fast secondary electron. Consequently, one secondary electron in 150 was 'fast' as compared with about one in ten for those emitted from a bulk density dynode. It would have been expected that

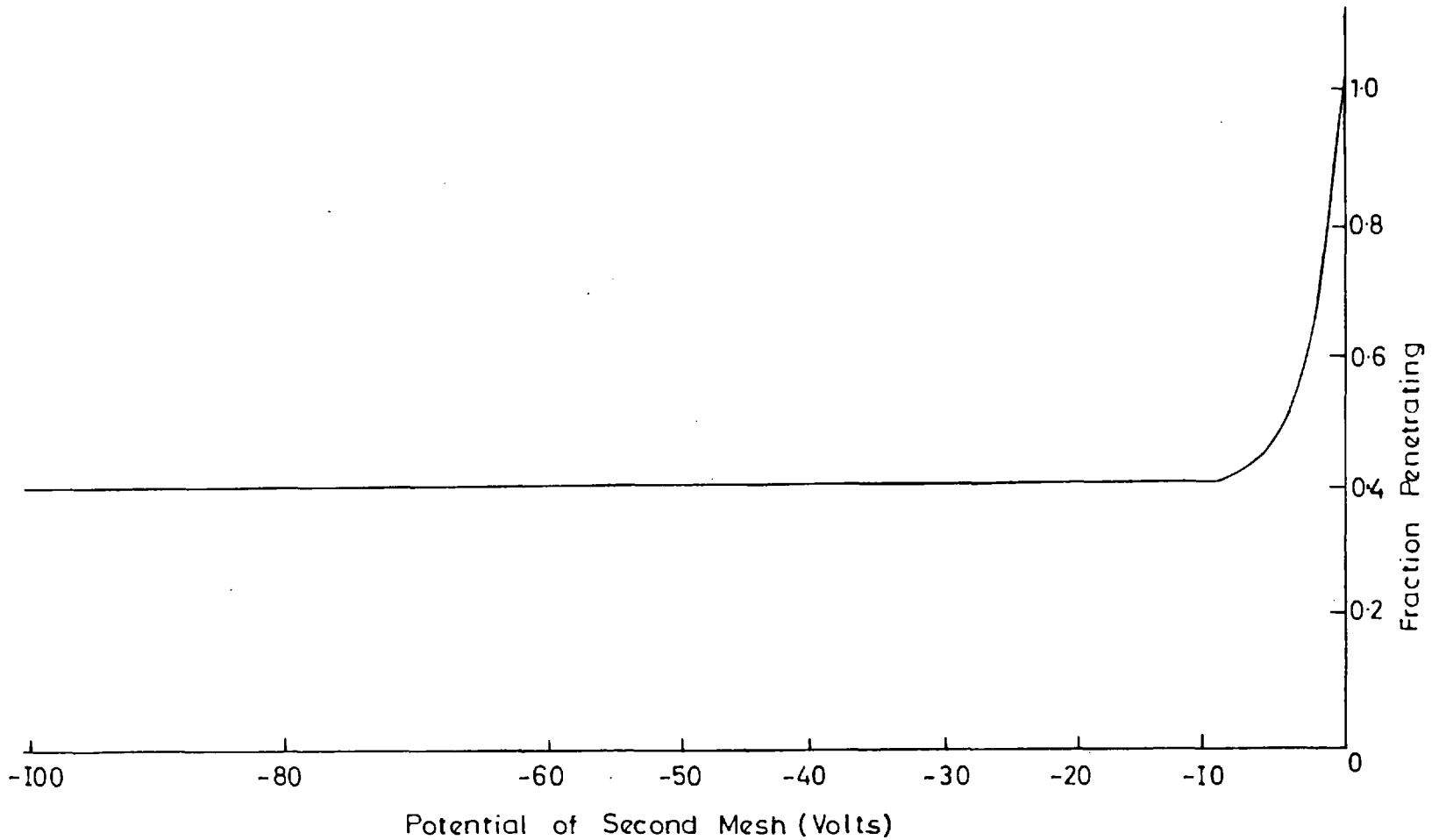

Fig.4.8 Fraction Penetrating for Various Retarding Potentials

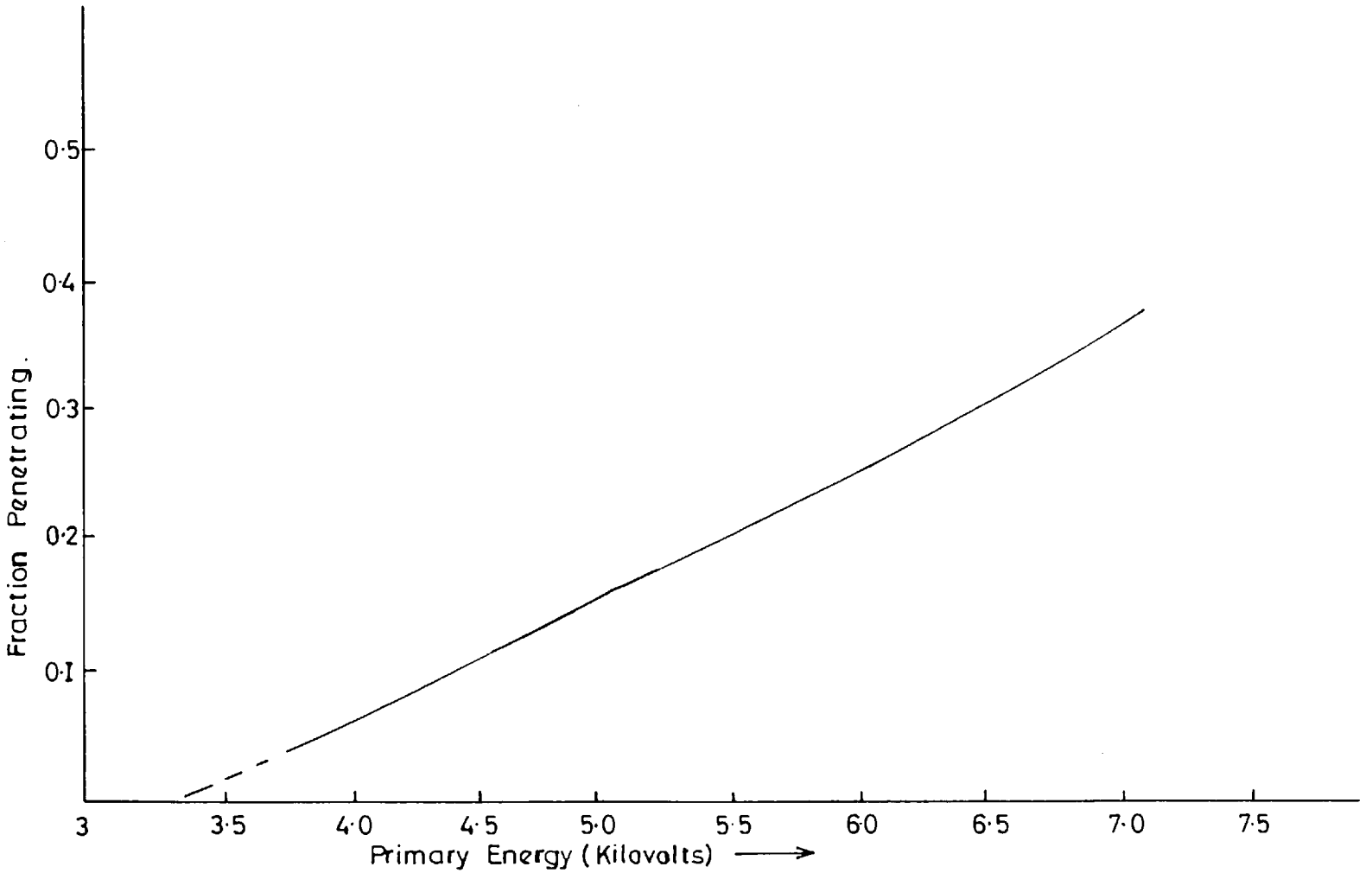

Fig.4.9.Fraction Penetrating as a Function of Primary Energy

the contrast degradation would have been correspondingly reduced; although no quantitative measurements were made, visual inspection indicated that this improvement had not been achieved.

4.8 Image Quality

Apart from the high value obtained for the electron gain, tubes using low density dynodes did not show promise. The image had a grainy appearance, and bright scintillations superposed on the image indicated local breakdown. The resolution was poor when high gains were obtained. Sustained emission was observed, and the electron gain fluctuated whenever the intensity of the incident image was changed.

4.9 Image Graininess and Localized Emission

When the control mesh and cathode voltages were low and the dynode was giving only a low electron gain, the image was free from localised emission. When both the control mesh and cathode voltages were increased to values sufficient to cause high electron gain, the image became grainy. The graininess of the image depended on the length of time for which the image had been displayed. At first, the image was relatively free from grain but it

gradually became more grainy; at the same time the secondary emission was seen to increase. The secondary emission reached a maximum value and at the same time, the graininess became very marked. The secondary emission then dropped and the graininess reduced considerably. The rate at which these changes took place depended on the current density and it was later seen that the increase in secondary emission and in graininess was associated with a maximum in the dynode surface potential.

When the mesh voltage was increased further, bright scintillations were observed to dance about the image in a random manner; their numbers increased with current density and with further increase in control mesh voltage. They were seen to persist for a time after the incident image was removed.

Different tubes varied in the extent to which scintillations occurred; there appeared to be some correlation between the occurrence of localised breakdown and dynode thickness. Tubes with thinner dynodes suffered more from localised emission. One tube, with a dynode only 3.5μ thick showed scintillations at very low mesh voltages; when the control mesh voltage exceeded 200 volts the scintillations increased with time and finally led to breakdown which could only be terminated by reducing the

control mesh voltage. On the other hand, another tube with a dynode 13μ thick could be operated with a control mesh voltage of 1,000 volts, although scintillations were observed at much lower control mesh voltages.

4.10 Sustained Emission and Image Revival

Sustained emission in the form of an 'after image' was always observed when the dynode was operated at high electron gain. This after image died slowly away and eventually disappeared. The initial intensity of the after image increased with the intensity of the incident image, it also increased with primary voltage, control mesh voltage and to a small extent with time of exposure of the image. A notable feature was that although intense images produced intense after-images, the after-images died more rapidly than those produced by weaker images. The result was that whilst the after-image initially had the same intensity distribution as the input image, the intensity distribution in the after-image changed with time. If an image had previously consisted of a very bright pattern against a faint background, the after-image may well have appeared after some time with the previously bright area dark against the after-glow from the background.

If the cathode was flooded with light after an image

had previously been projected, the image which was no longer being projected again became visible. Frequently the 'revived' image appeared bright against the flooding illumination, indicating that the gain of the dynode had been locally raised as a result of the secondary emission process when the initial image was projected. If the incident image had been very intense and sustained, however, the 'revived' image appeared darker than the flooding illumination.

It was found that an image could be 'revived' by flooding the cathode with primary electrons a considerable time after the original primary current had been interupted. On one occasion, an image was revived nine days after the tube had last been used. This particular observation led to the investigation of these dynodes as targets in charge storage television camera tubes.

An explanation of the dependence of the sustained emission and the revived image on the current density and the time of exposure, is given in section 8.6.

4.11 Resolution

In general the resolution of tubes with low density dynodes was poor. The best resolution obtainable from a tube depended largely on the dynode thickness; higher

resolutions were observed in tubes with thinner dynodes. For two tubes with dynodes about 13μ thick, the best resolution never exceeded 6-8 lp/mm. On the other hand, resolutions above 20 lp/mm. were observed in tubes with thinner dynodes. In the tube with a dynode, only 3.5μ thick, a resolution of 12 lp/mm. was observed when the control mesh voltage was only 20 volts; at this control mesh voltage most tubes gave only a diffuse glow in which few image features could be recognised. The tube used in the retarding potential measurements had a dynode 6μ thick and gave the resolutions illustrated in figure 4.10. The resolutions obtained depended on the primary voltage as well as on the focussing conditions between the dynode and the phosphor. The highest resolutions were obtained when the primary voltage was too low to give useful electron gain. Increasing the control mesh voltage was seen to increase the resolution; unfortunately, the effects of localised emission became increasingly apparent as the control mesh voltage was increased.

Two explanations can be advanced for the fact that the resolution deteriorated as the primary electron energy was increased. The first is that the dynode surface potential rose with the increasing primary voltage, and decreased the field between the dynode and the control mesh;

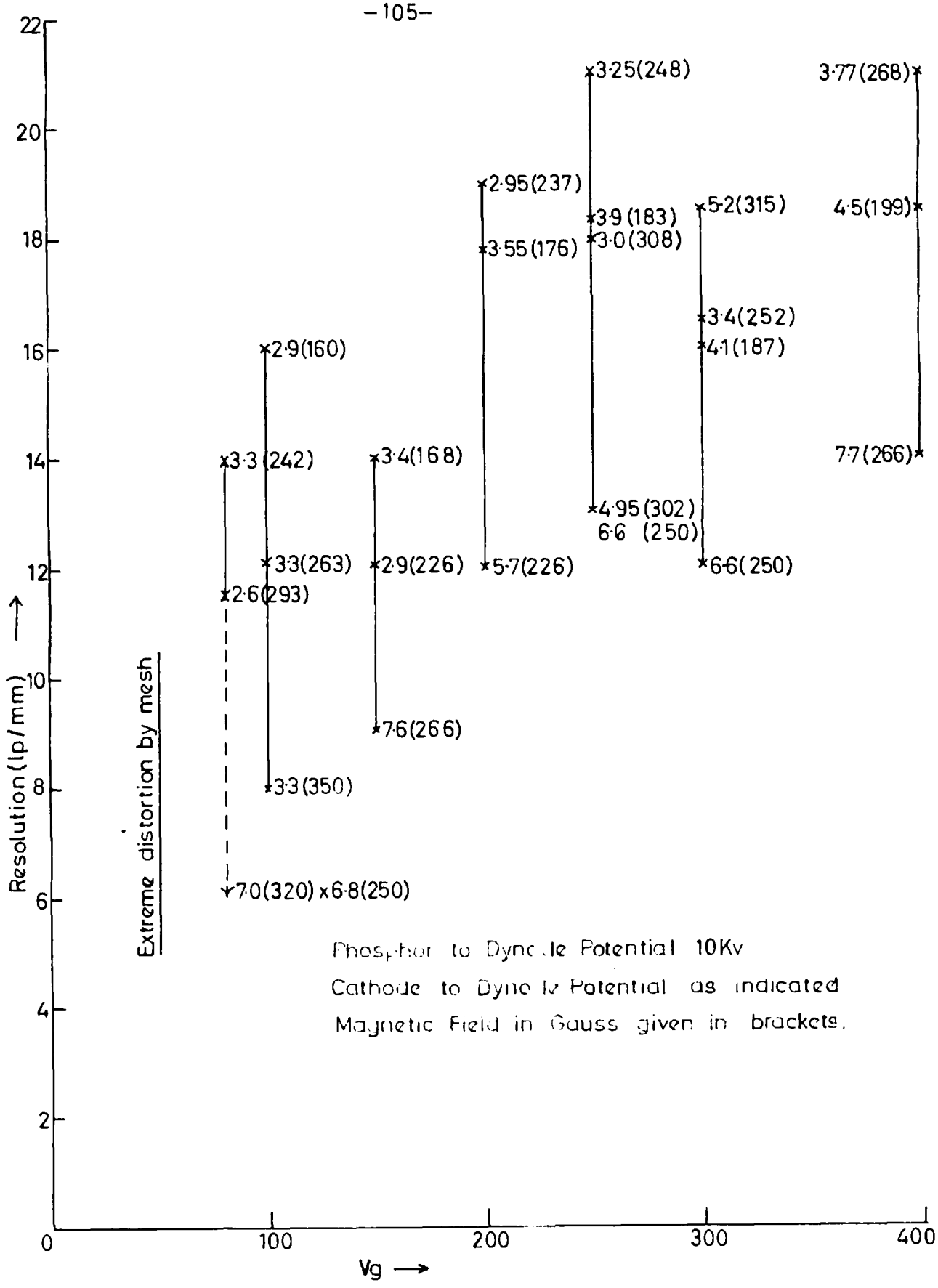

Fig4.10 Resolution as a function of Control Mesh Potential

it has been shown by measurements using retarding potentials,* that the dynode surface potential did rise slightly with increasing primary voltage. However, the cathode potential had a considerable effect on the resolution even when the control mesh potential was 400 volts; the surface potential of the dynode was known not to approach this value, and it was evident that the reduction of the field between the dynode surface and the control mesh was not a complete explanation of the loss in resolution. A second and more plausible explanation is that the energy distribution of the secondaries covered a wider spectrum as the primary voltage was increased or that the surface potential of the dynode became very uneven.

4.12 The Effect of the Control Mesh

For reasons of economy, the majority of the tubes employed a coarse woven tungsten mesh, having a spacing of two meshes to the millimetre.

The distortion in figures 4.11a and 4.11f resulted from the different electrostatic fields on either side of the mesh. Each opening acted as an aperture lens and, under some conditions, could cause independent rotation of that part of the image passing through the opening.

---

* Section 5.3

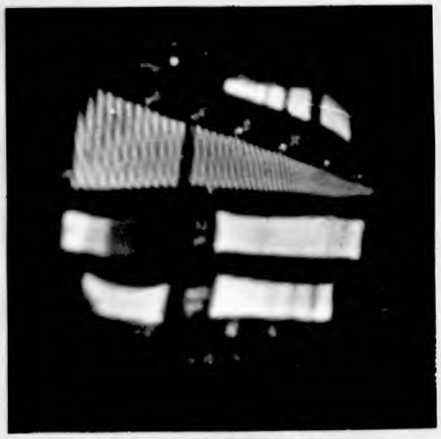

a) V_g = 150v. V_c = 4.3 Kv.
V_{ph} = 11 Kv. B = 214 Gauss

b) V_g = 100v. V_c = 4.7 Kv.
V_{ph} = 14 Kv. B = 294 Gauss

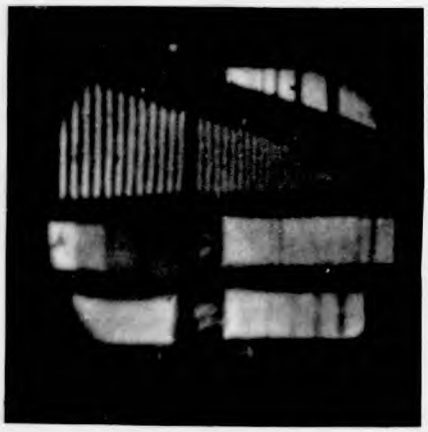

c) V_g = 150v. V_c = 4.3 Kv.
V_{ph} = 11 Kv. B = 286 Gauss

d) V_g = 200v. V_c = 4.6 Kv.
V_{ph} = 11 Kv. B = 302 Gauss

e) V_g = 100v. V_c = 39 Kv.
V_{ph} = 11 Kv. B 275 Gauss

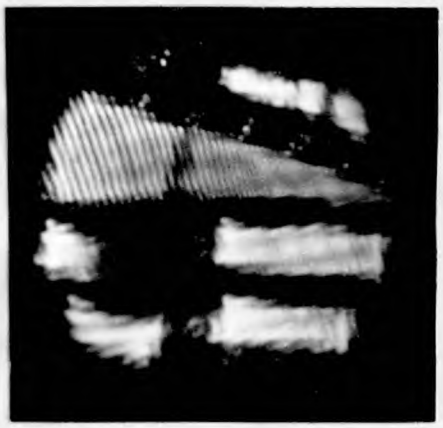

f) V_g = 100v. V_c = 5.35 Kv.
V_{ph} = 14 Kv. B = 217 Gauss

Fig4.11 Images Produced by Intensifier under Different Conditions

Besides introducing distortions in the image, the mesh itself frequently appeared in the image produced by the tube. Its appearance and state of focus could vary considerably according to the potentials between the dynode, mesh and phosphor, and the magnetic field. In the following paragraph the appearance of the mesh is described as the magnetic field was increased and the various potentials were held constant.

An unfocussed illumination of the tube photocathode produced a uniform glow on the phosphor against which the mesh appeared. At first the mesh appeared as a diffuse shadow which could be brought to a focus as the magnetic field was increased. Increasing the magnetic field further caused the mesh to disappear against the background and then to reappear, still well focussed, but brighter than the background. The bright image of the mesh then defocussed and disappeared as the magnetic field was increased still more. This train of events could be repeated at integral multiples of the magnetic field strength.

Several photographs of the phosphor of one intensifier are shown in fig. 4.11 , which illustrate different appearances of the image; in each photograph combinations of electrostatic and magnetic fields were chosen which gave an optimum focus. Some of the photographs show that some

spurious emission was occurring; the fact that the photograph with the highest resolution is also that with most spurious emission is a consequence of the increase of both resolution and breakdown with control mesh potential. The dynode in this particular tube was not a good one, in that a small area was at a substantially different surface potential to the rest of the dynode. This fault resulted in the localised distortion between the centre and the bottom of the Baum pattern. Much of the spurious emission appeared to originate in this area.

The presence of the mesh in the tube would not necessarily have been a serious disadvantage as focussing conditions could usually be found where its effect was not important. Had the low density dynodes proved more promising, the cost of finer meshes might have been justified. With the coarse meshes used, resolutions of over 20 lp/mm. were observed when the properties of the dynode were not limiting the resolution.

CHAPTER 5

The Surface Potential and Secondary Electron Energy Spectrum

5.1 Two Mesh Tube

It is easy to show that, in a single stage tube focussed by parallel electrostatic and magnetic fields, the obtainable resolution is inversely proportional to the mean energy with which the electrons are emitted[38, 71]. The spread in forward velocity of secondary electrons emitted from a bulk potassium chloride density dynode has been measured by Todkill who used a single dynode image intensifier with two meshes between the dynode and the phosphor screen[72]. The first mesh was held positive with respect to the dynode from which it ensured full emission. The second mesh acted as a potential barrier for the secondary electrons. The variation of the phosphor current with the retarding potential on the second mesh gave the forward velocity of the secondary electrons. Successful measurements, using the phosphor as both the retarding electrode and the collector could not be made because of secondary emission from the phosphor.

In order to measure the surface potential of the low density dynodes and the energy of emission of the secondary

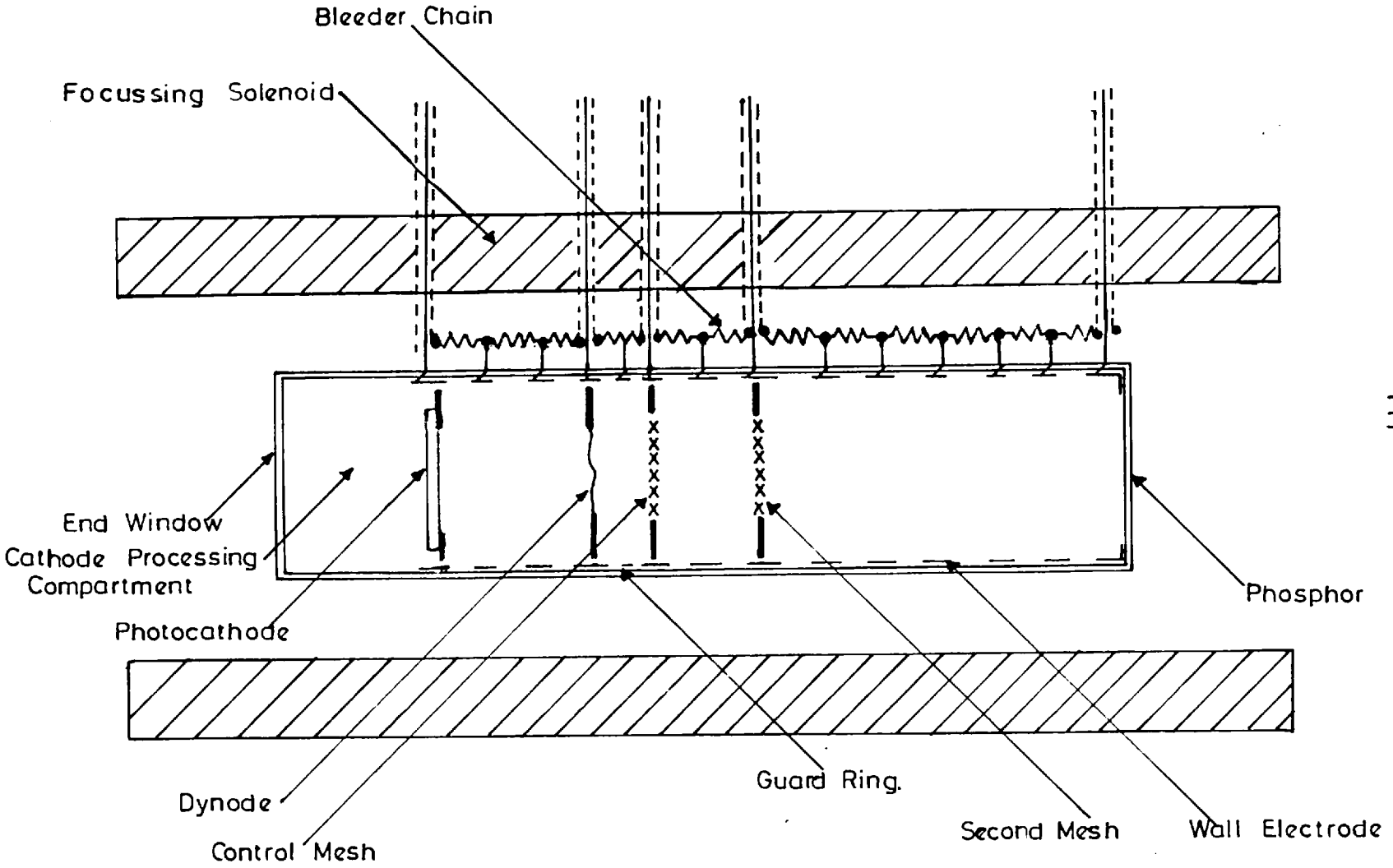

Fig. 5.1 Image Intensifier with Low Density Dynode and Two Meshes

electrons, a tube with two meshes was built. Apart from the additional mesh which was placed between the phosphor and the control mesh, the tube was identical to the established design, having a control mesh one centimetre from the dynode.

5.2 Static Current Measurements in the Two Mesh Tube

In the following chapter, let

V_g be the control mesh potential,

V_{g2} be the second mesh potential,

V_c be the cathode potential,

V_{ph} be the phosphor screen potential,

and V_s be the surface potential of the dynode,

all the potentials being measured with respect to the conducting backing of the dynode.

Figure 5.2 shows the variation of phosphor current with phosphor screen potential when V_g and V_{g2} were held constant and at such potentials to maintain enhanced secondary emission from the dynode. It is evident from figure 5.2 that secondary emission from the phosphor screen was taking place, and it was thus confirmed that a successful measurement of surface potential and electron energy could be made only if the phosphor screen was unable to emit secondary electrons.

Fig.5.2 The Current to the Phosphor as a function of the Phosphor Potential for Constant Mesh and Cathode Potentials

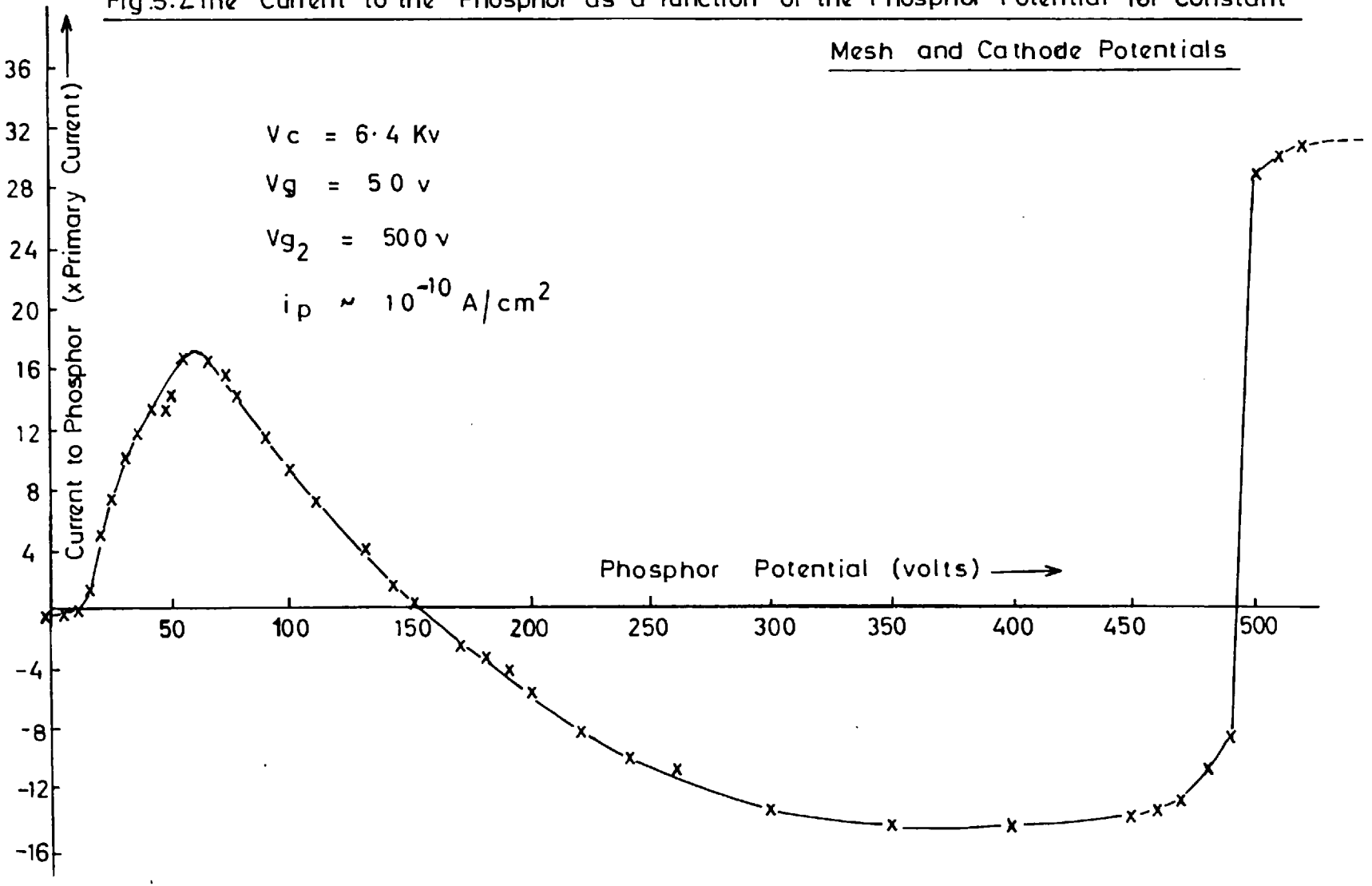

The following method of measurement was adopted. The first mesh was held at the potentials necessary to obtain high gains from the dynode and the second mesh potential was varied. The second mesh acted as a potential barrier and allowed only electrons with sufficient energy to pass onto the phosphor where they were collected. The high positive potential* at which the phosphor was held relative to the dynode, prevented errors arising from secondary emission from the phosphor.

The variation of phosphor current with second mesh potential is shown in figure 5.3 for different control mesh potentials and a constant primary energy. The curves show an initial rise in phosphor current, followed by a region where the current is almost independent of the second mesh potential.

A rise in phosphor current was seen when V_g and V_{g2} were approximately equal. Measurement of the current to the control mesh as a function of second mesh potential showed that this was caused by a reduction in the electron current to the mesh. An initial drop in the current to the control mesh as V_{g2} rose was accounted for by a larger fraction of the secondary current passing through the control mesh. As V_{g2} was further increased, the rapid rise in secondary current was sufficient to cause a net

* 1.8 Kv

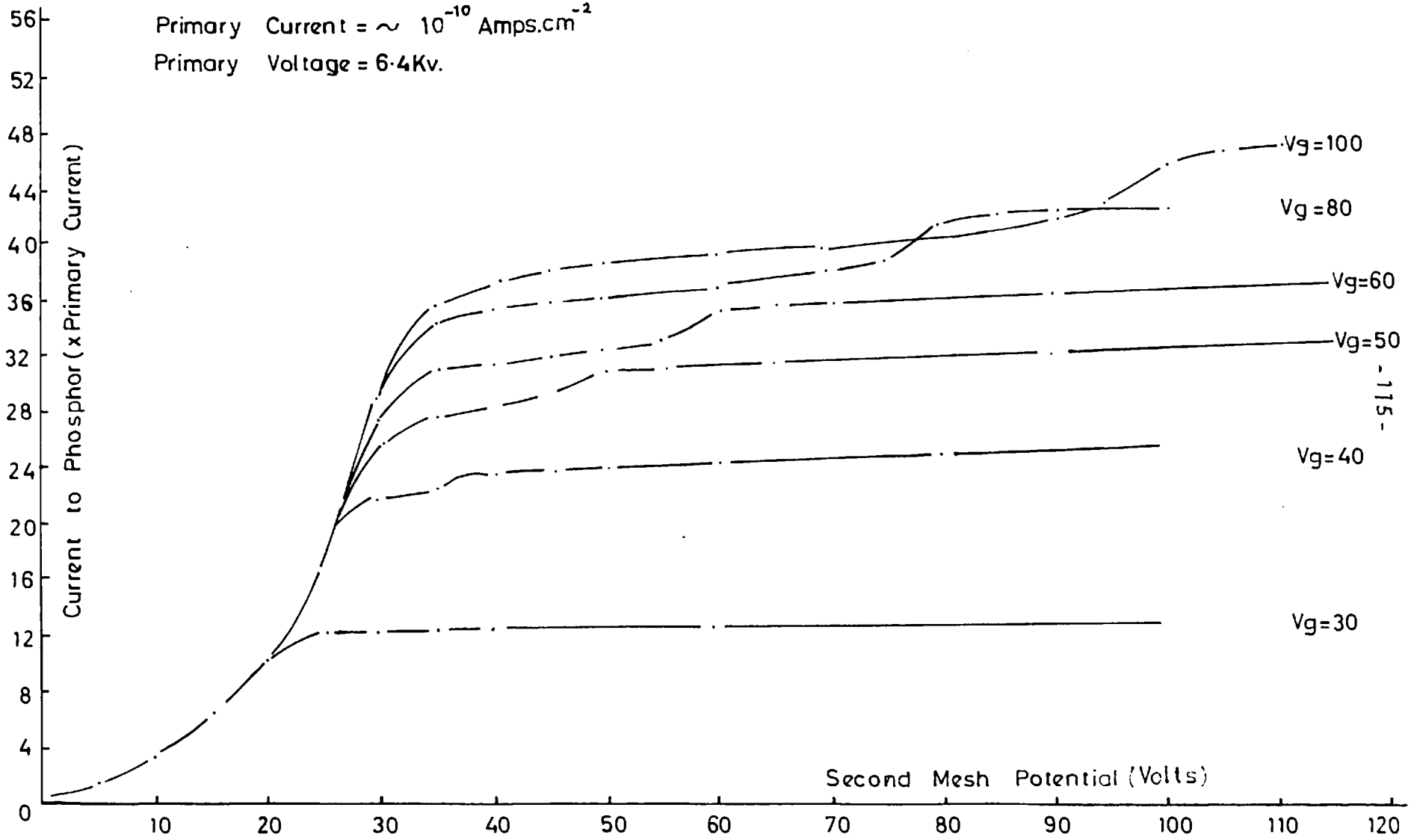

Fig.5.3 Current to Phosphor as a function of Second Mesh Potential for Various Constant Control Mesh Potentials.

rise in the current to the control mesh despite the falling fraction which it collected. When the second mesh was made positive with respect to the control mesh, most of the secondary current was drawn through the control mesh. The fraction of secondary current passing through the control mesh is shown as a function of V_{g2} in figure 5.5.

As the secondary current from the dynode was equal to the sum of the currents to the phosphor and to the control mesh, and as it was found simpler to measure the dynode current as a function of the second mesh potential, many of the experiments were performed in this way. In figure 5.6, the secondary current is shown as a function of the second mesh potential for various control mesh potentials. The curves for different V_g and V_c were all similar in form and showed a distinct knee. Below this knee the current was independent of V_g; above this knee the current depended on V_g, and only to a small extent on V_{g2}. The curved portion at the knee depended on both voltages. The following explanation was proposed:-

The knee of the curve occurred when V_{g2} was approximately equal to V_s, the surface potential of the dynode. When V_{g2} was greater than V_s, a small but steady rise in

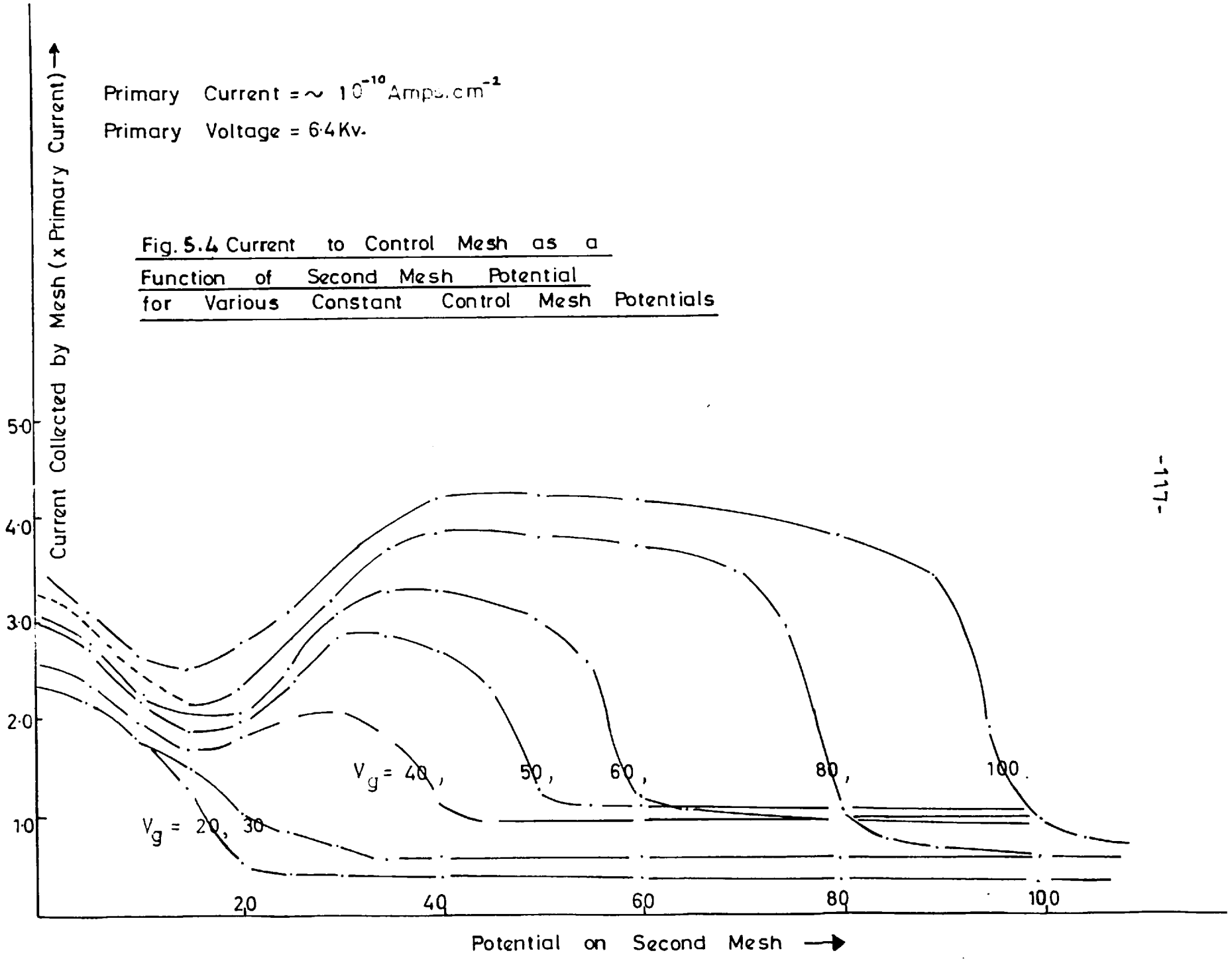

Fig. 5.4 Current to Control Mesh as a Function of Second Mesh Potential for Various Constant Control Mesh Potentials

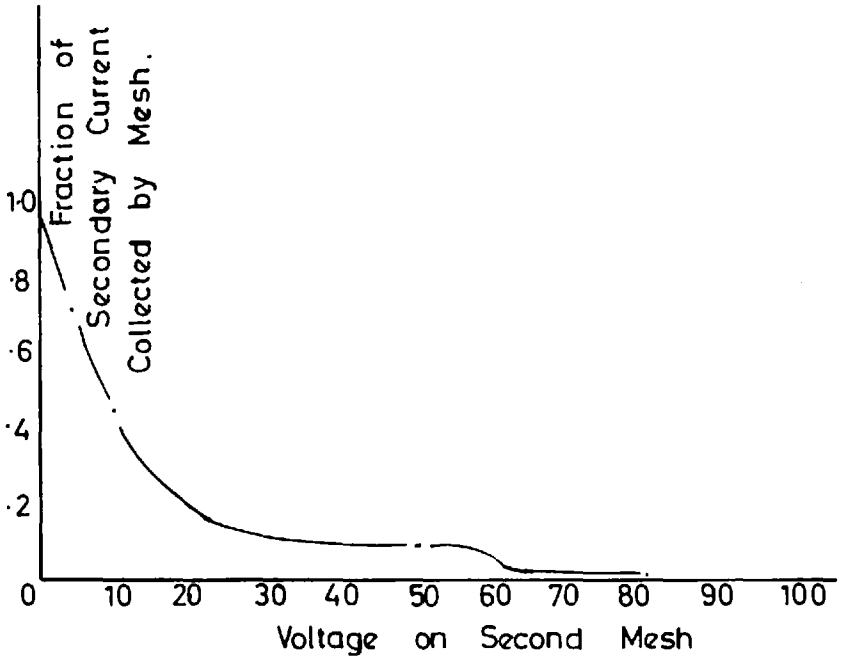

Fig.5.5 Fraction of Secondary Current Collected by Control Mesh for a Control Mesh Potential of 60 v.

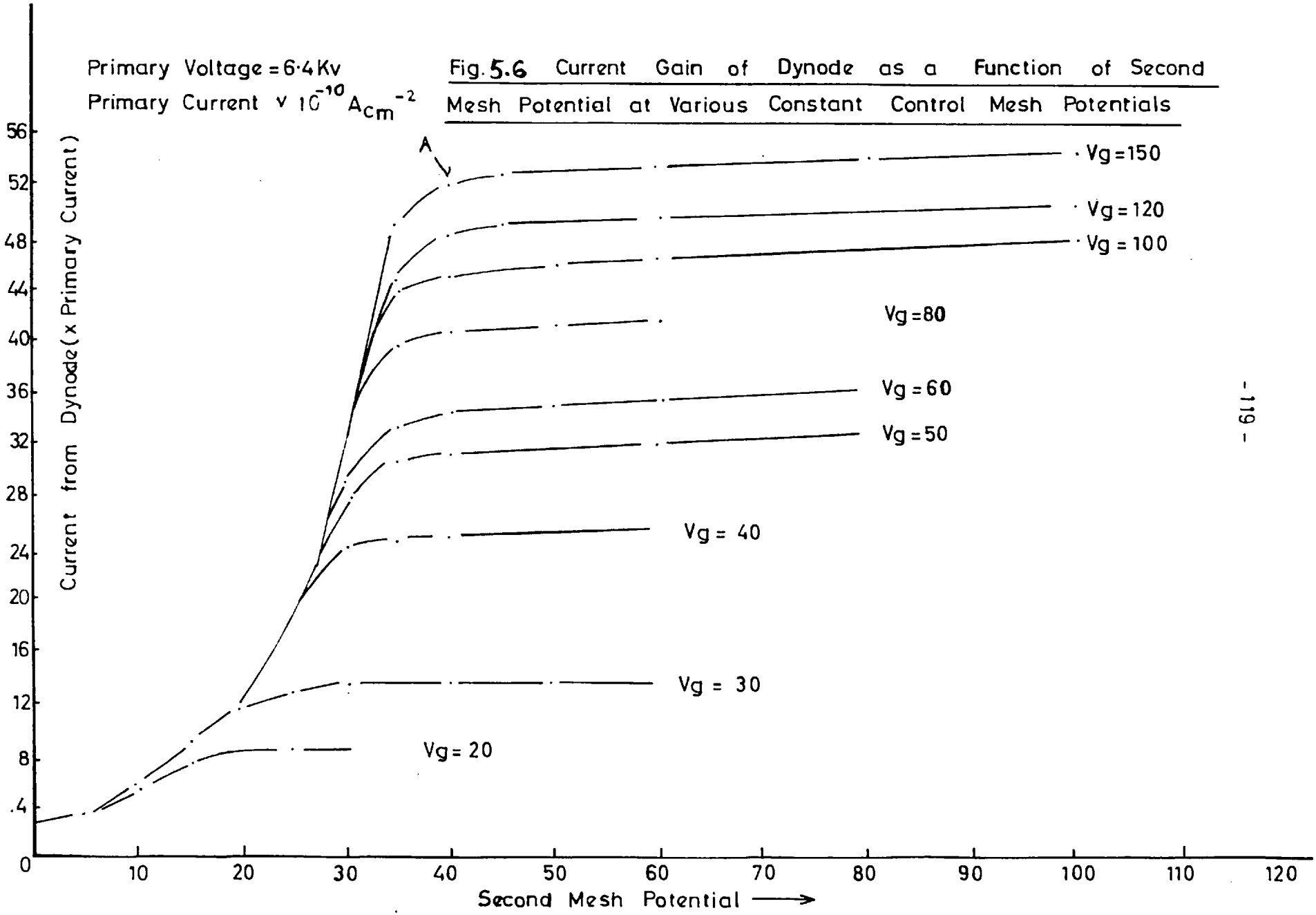

Fig. 5.6 Current Gain of Dynode as a Function of Second Mesh Potential at Various Constant Control Mesh Potentials

secondary current was observed as V_{g2} was increased which was too great, however, to be explained as a field penetration effect*. The shape of the knee was expected to depend to some extent on the energy distribution of the secondary electrons.

When V_{g2} was less than V_s, some electrons were unable to leave the dynode or else were returned. As a result, the value of V_s was reduced until a new equilibrium was reached. In this way, the dynode surface potential was controlled for low V_{g2}, by V_{g2} and not by V_g. It followed that over a limited range, the electron gain of the dynode was controlled by V_{g2}.

Because the retarding potential was able to affect the surface potential of the dynode, a static retarding potential experiment could not be expected to yield the electron energies in a simple manner. The surface potential could, however be estimated as follows. The point A in figure 5.6 indicates the point where the electron gain began to decrease rapidly as V_{g2} was reduced. The more rapid dependence of the electron gain on V_{g2} beginning at this point was a consequence of the lowest energy electrons being repelled by the second mesh, and thus

---

* See Appendix A.3.

the value of V_{g2} at A is related simply to the surface potential.*

5.3 The Variation of the Dynode Surface Potential with Control Mesh and Cathode Potentials

Within the limits of experimental error, the equilibrium surface potential was observed to depend only on the control mesh potential, and on the primary energy. The surface potential has been plotted as a function of the control mesh potential for various primary voltages in figures 5.7 and 5.8. In figure 5.9, where the four curves are shown plotted together for the sake of comparison, it can be seen that the surface potential decreased as the primary energy fell. Except at low control mesh voltages, the surface potential depended to only a small extent on V_g. This fact was explained by the surface potential being determined, not only by the control mesh potential, but by an equilibrium between the emission of secondary electrons from the outer layers of the dynode and an opposing internal current to the surface which developed as the potential across the dynode

---

* The surface potential of the dynode will be equal to V_{G2}, the effective potential of the second mesh, c.f. section 5.5.

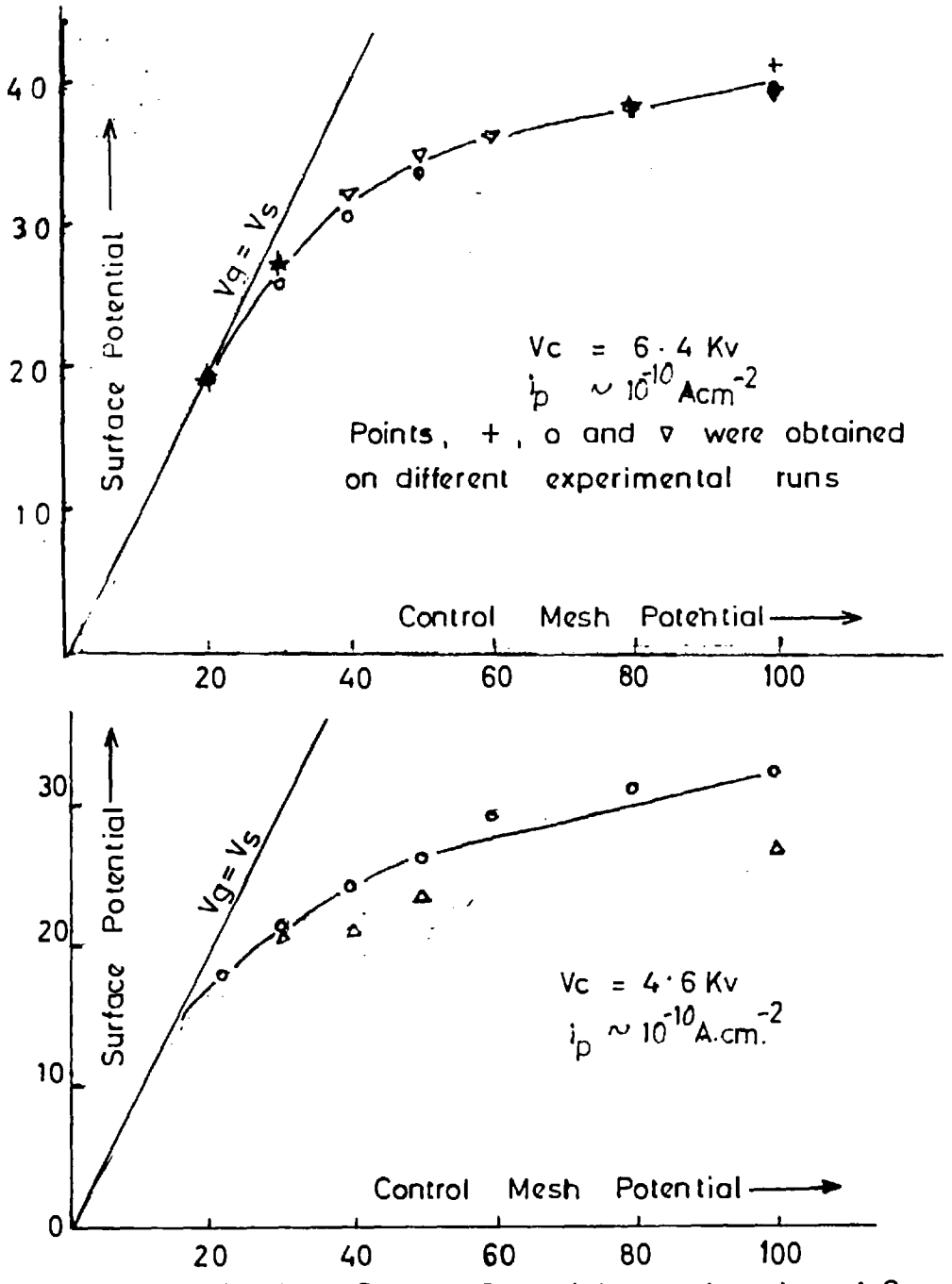

Fig 5.7 Equilibrium Surface Potential as a function of Control Mesh Potential at Various Primary Energies.

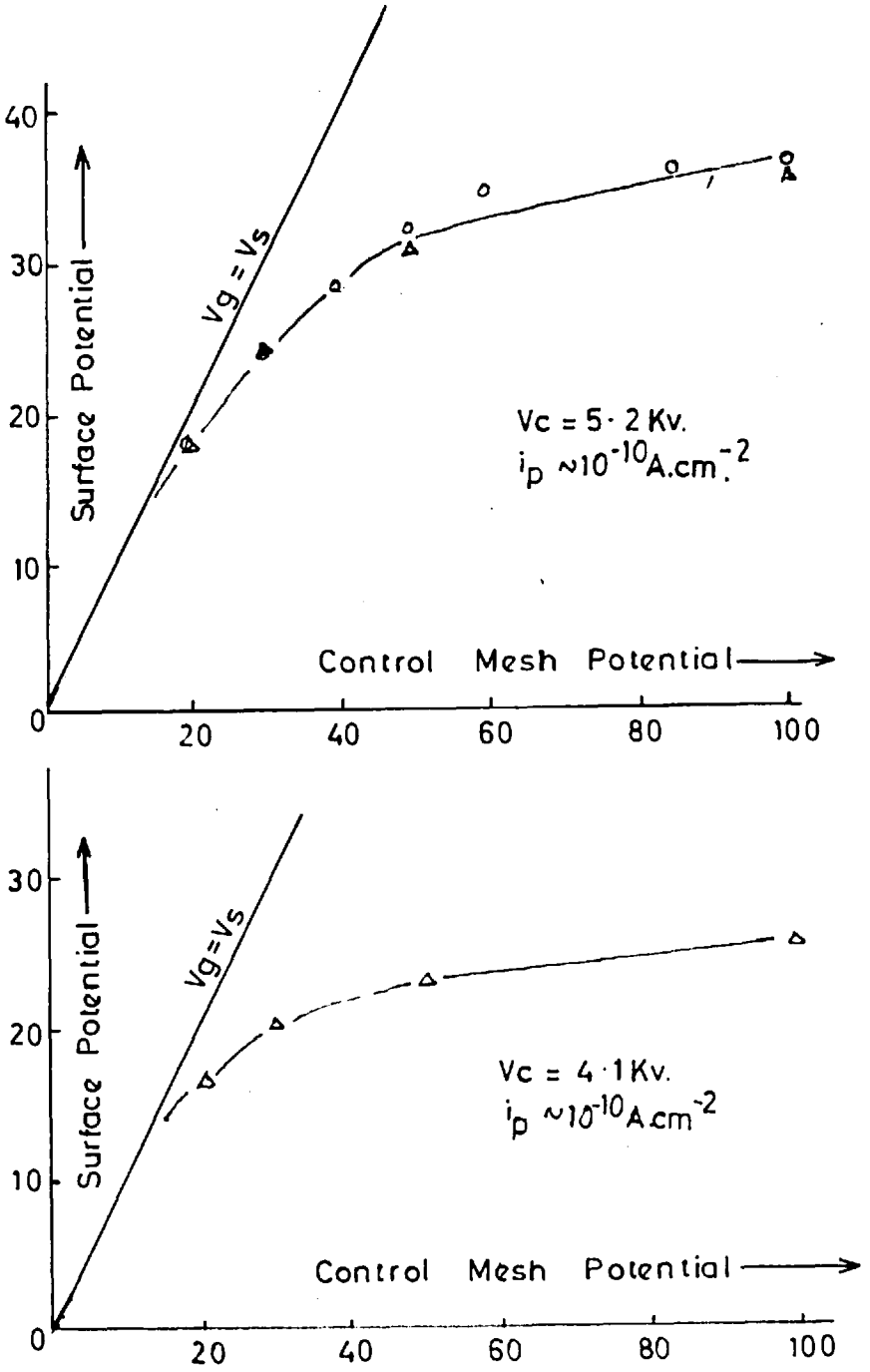

Fig5.4. Equilibrium Surface Potential as a function of Control Mesh Potential at Various Primary Energies.

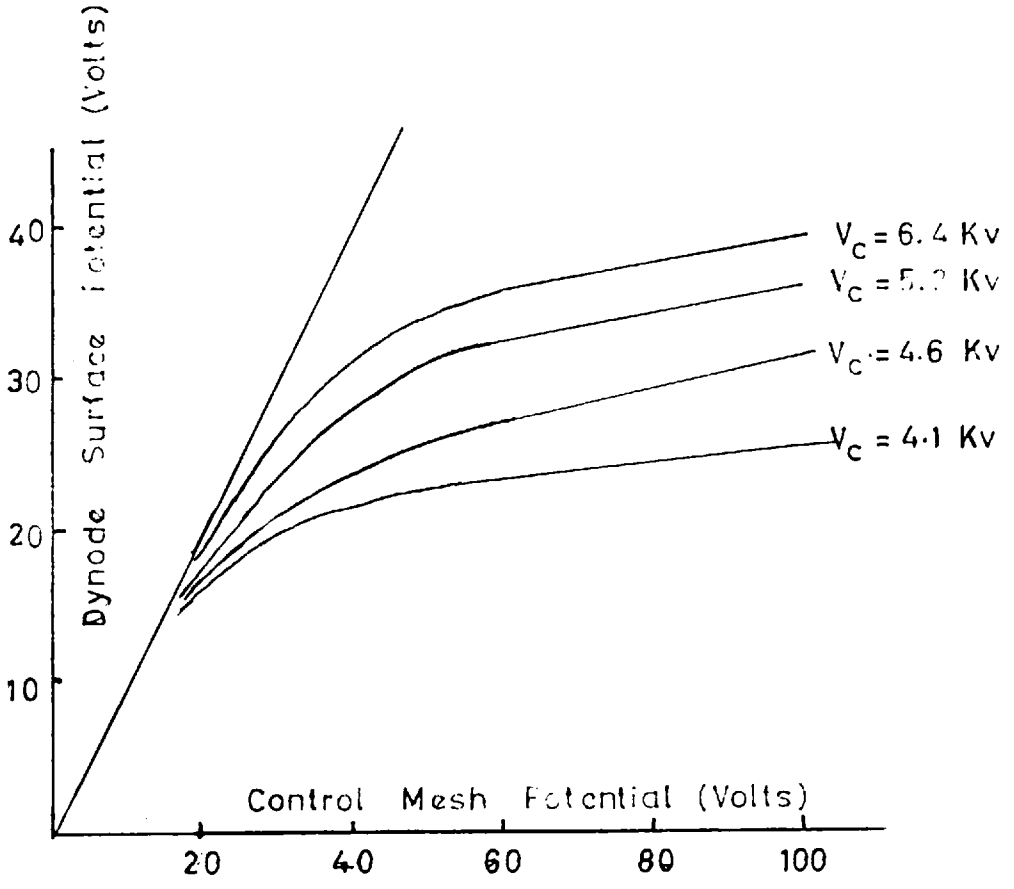

Fig. 5.9 The Curves of Figs 5.7 and 5.8 Superimposed

increased.

It had always been postulated that the surface potential of the dynode differed from that of the control mesh. Had only a small potential existed between the surface of the dynode and the control mesh, little or no focussing of the tube would have been possible. The focus improved with increasing control mesh potential; this improvement suggested an increasing potential difference between the dynode surface and the control mesh.

It was often found possible to focus the cathode stage with two or more different cathode to dynode voltages at a given magnetic field. To maintain the focus between the dynode and the phosphor, it was usually necessary to make a small correction to the potential of either the control mesh or the phosphor screen. For example, it was necessary to increase the mesh potential by 30 volts when the cathode voltage was changed from 3.0 to 6.8 Kv. This example indicated a change in dynode surface potential of 30 volts and provided confirmation for the results just described.

5.4 The Variation of Gain with Surface Potential

Figure 5.10 shows the electron gain as a function of the surface potential at various primary energies. An

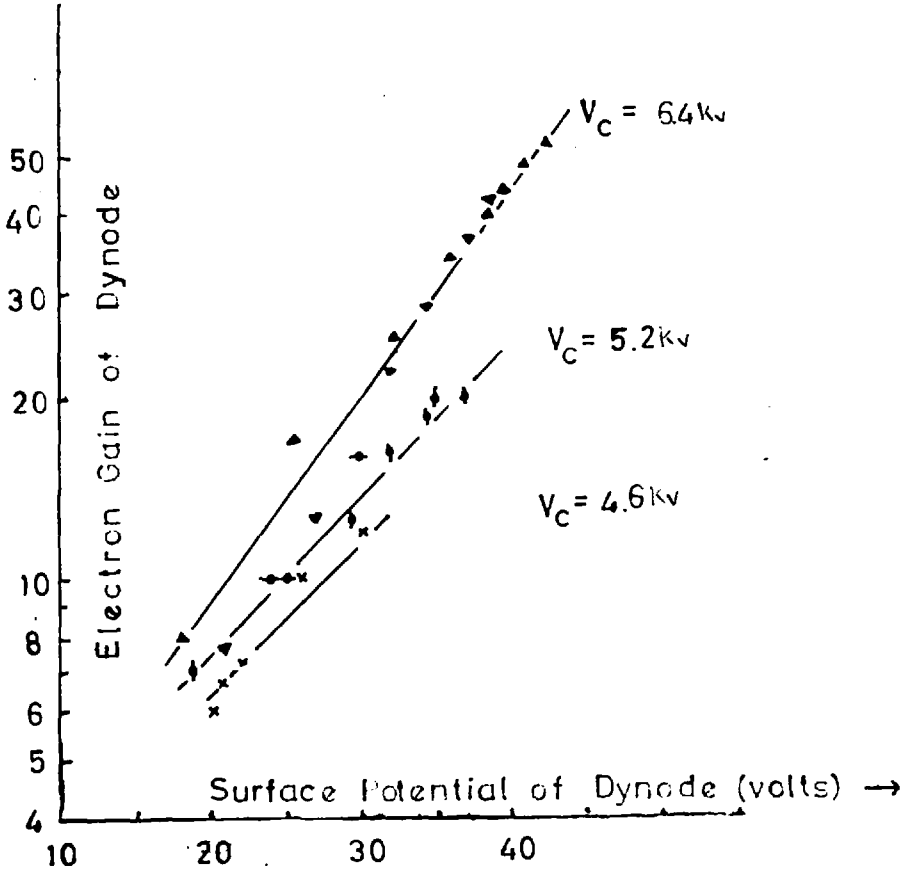

Fig. 5.10 Electron Gain as a Function of Surface Potential at Various Primary Energies

approximately exponential variation of gain with surface potential was observed. As well as the rapid dependence of gain on surface potential, the gain at a given surface potential increased with primary energy.

5.5 The Effect of Phosphor Field Penetration

Calculation* shows that the effect of the penetration of the mesh to phosphor field was small and equivalent to an increase in the effective potential of the second mesh by an amount proportional to the phosphor voltage, i.e.

$$V_{G2} = V_{g2} + 5 \times 10^{-4} V_{ph}$$

where V_{G2} was the effective potential of the second mesh.

This expression has been approximately confirmed by varying V_{ph} and V_{g2} in such a manner as to keep the secondary emission from the dynode constant+. The results of this

---

* See Appendix A.3

+ The values of V_{g}, V_{c} and i_{p} were held constant and V_{g2} was chosen so that the secondary current was a rapidly changing function of V_{g2}. The secondary current did not change when V_{g2} and V_{ph} were varied as in figure 5.11, because V_{G2} the effective value of the second mesh potential, remained constant.

experiment are shown in figure 5.11, whence the emperical relationship

$$V_{G2} = V_{g2} + 10 \times 10^{-4} V_{ph}$$

was obtained. This equation was used to correct the dynode surface potential in figures 5.7 to 5.10. In graphs where the second mesh potential occurs as a co-ordinate, the uncorrected value has been used.

5.6 The Forward Velocity Distribution

It was not possible to measure the velocity spectrum of the secondary electrons, by applying steady retarding potentials, because the electrons which were returned to the dynode reduced its surface potential with respect to the retarding electrode. This problem is common in work on electron emission from insulators and has previously been attacked by the use of pulse techniques similar to that about to be described.[44, 73]

The retarding electrode was held at a D.C. level which allowed all the electrons to pass; a negative going square pulse was applied to the electrode, and when it was of sufficient amplitude, some of the electrons were unable to pass and were returned to the dynode. By making the duration of the pulse short, the charge returned to the dynode surface was unable to lower its potential significantly

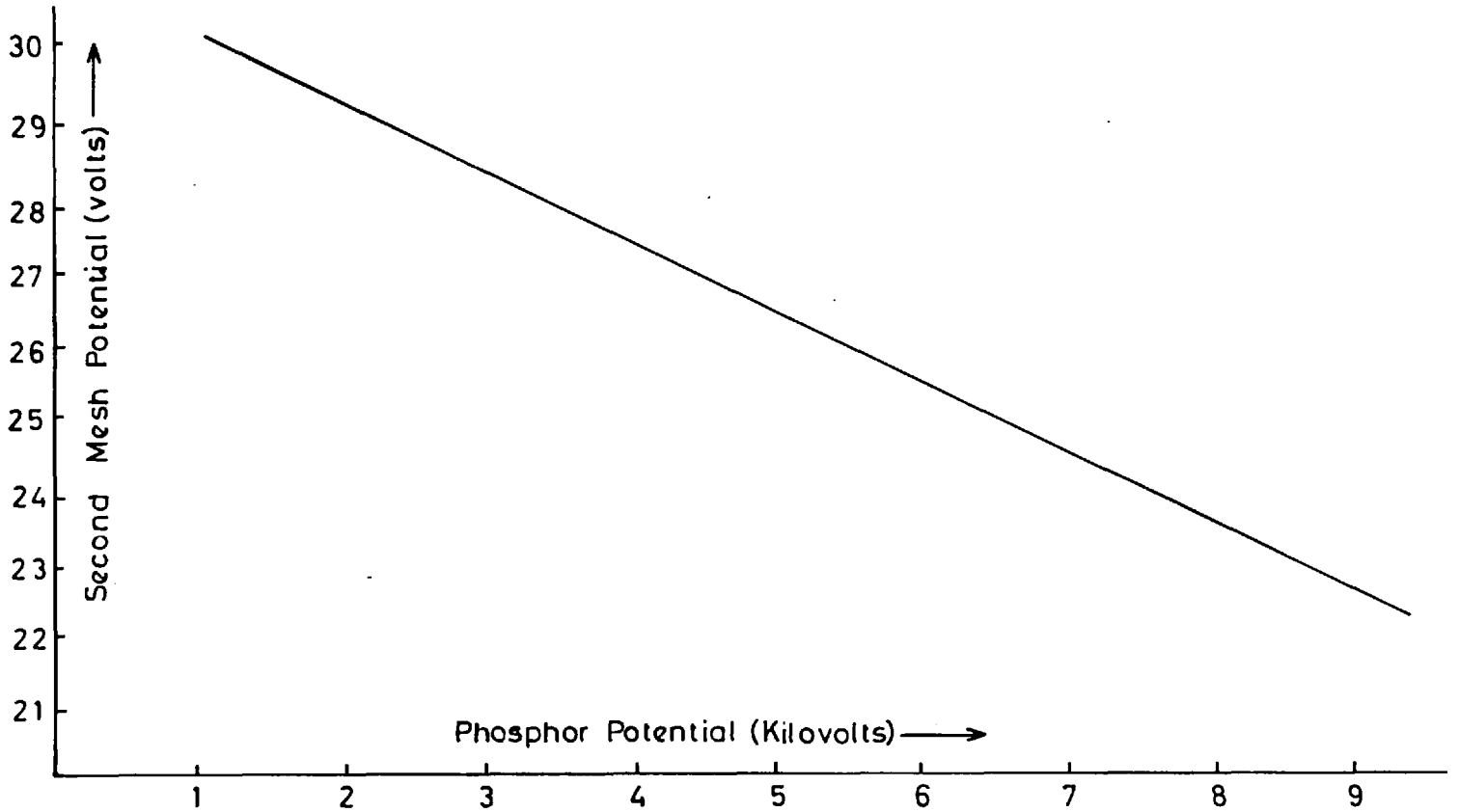

Fig 5.1 Field Penetration Experiment, the Variation of Second Mesh Potential and Phosphor Potential for Constant Secondary Emission From The Dynode

and the current flowing through the mesh remained constant for the duration of the pulse*. The secondary current passing the mesh was collected by the phosphor which was connected to ground by a resistor. The change in secondary current was displayed on an oscilloscope connected across the resistor. Because the current during the negative pulse remained effectively constant, a square waveform was displayed whose amplitude was proportional to the change in the secondary current passing the retarding electrode. The spread in the forward velocities of the secondary electrons could then be deduced by measuring the change in the secondary current as a function of the amplitude of the negative pulse applied to the retarding electrode.

The experimental arrangement used is shown in figure 5.12. The negative going square pulses were produced by a Naggard pulse generator, attenuated by means of a potentiometer, and then measured on an oscilloscope. The attenuated pulses were fed onto the second mesh of the two mesh image tube. The phosphor current was passed

---

* 200μ second pulses were used, and a secondary current of the order of 10^{-8} amps. was collected. The capacity of the spot bombarded was estimated from the dynode thickness as 100pf, and the change in surface potential could not have exceeded one fiftieth of a volt.

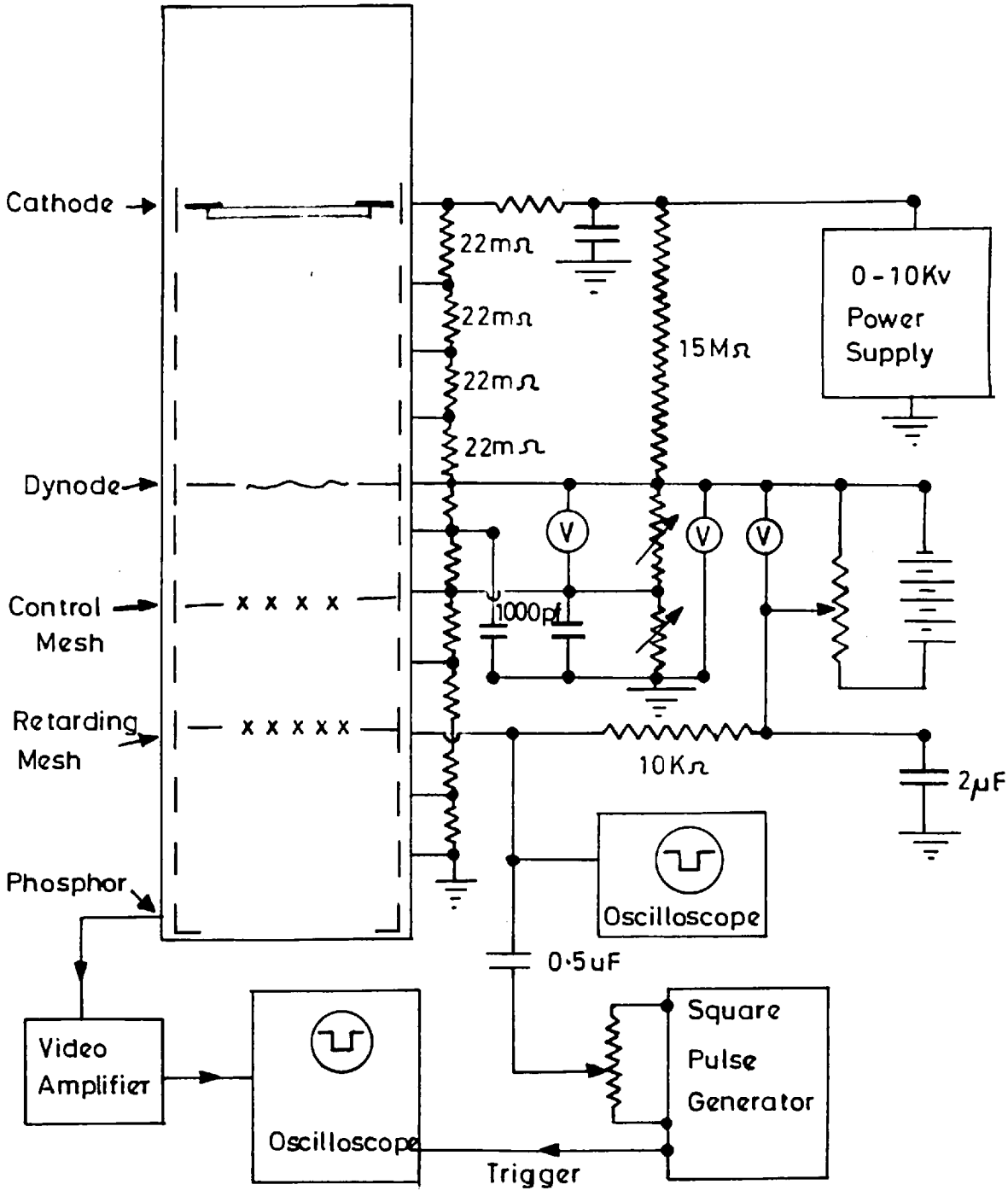

Fig.5.12 Diagram Showing Measurement of Forward Velocity Distribution

through the input impedance of a television head amplifier whose output was displayed on a second oscilloscope. The television head amplifier was necessary to avoid high frequency attenuation of the output pulse by stray capacities. It was designed so that the stray capacities became part of the feedback network in the first amplifying stage, thereby reducing the negative feedback and increasing the gain at high frequencies.

Figure 5.13 shows the amplitude of the output pulse as a function of the amplitude of the pulse fed onto the second mesh. The experiment was repeated for different D.C. potentials on the mesh and larger pulse amplitudes were needed as the D.C. potential was made more positive. Except for a very small increase in the secondary current as the D.C. potential was increased, the curves obtained for higher values of V_{g2} were very similar in form. The fact that the shift in these curves was almost equal to the difference in D.C. levels on the mesh indicated that the surface potential of the dynode was not significantly affected by the D.C. potential of the second mesh.

The output pulse amplitudes in figure 5.13 have been normalised by dividing by the change in phosphor current produced by very large negative retarding pulses. Consequently figure 5.13 shows the fraction f of the

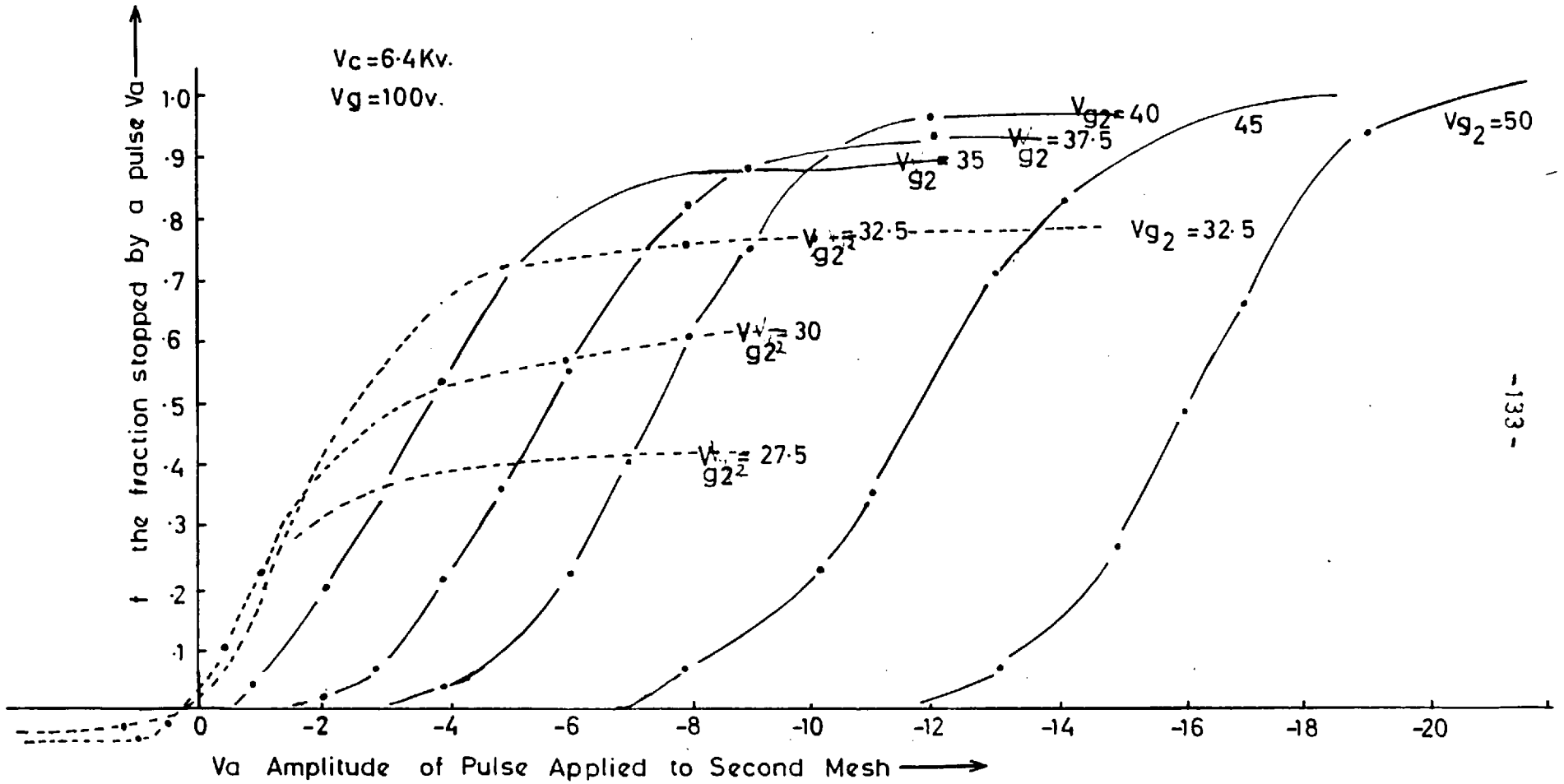

Fig 5.13 Change in Secondary Current as a function of the Retarding Pulse Amplitude, for Various D.C. Potentials on the Second Mesh.

secondary current which was stopped by a pulse of amplitude V_a. It can be seen that $\frac{df}{dV_a} \delta V_a$ is the fraction of the electrons stopped by pulses in an amplitude range δV_a about V_a.

Figure 5.14 shows the results of a numerical differentiation. The curves obtained for $V_{g2} = 40$, $V_{g2} = 45$, $V_{g2} = 50$, were very similar and are replotted in figure 5.15 as a function of a new variable, v, where,

$$v = V_S - V_{G2} + V_a.$$

V_a is the amplitude of the negative pulse applied to the retarding electrode.

Because of the planar geometry used in the retarding experiment, v is the potential difference through which an electron would have had to have been accelerated to acquire a forward component of velocity of emission u_f where,

$$\tfrac{1}{2} m u_f^2 = ev,$$

and v is not the total energy in electron volts with which the electrons were emitted. The mean value of v was 4.5 volts with a standard deviation of 2 volts. It can be seen that the electrons emitted from the low density dynodes had a large variation of forward velocities (and therefore emission energies) compared with those emitted from vacuum deposited dynodes where the average emission energy was about 2 ev.

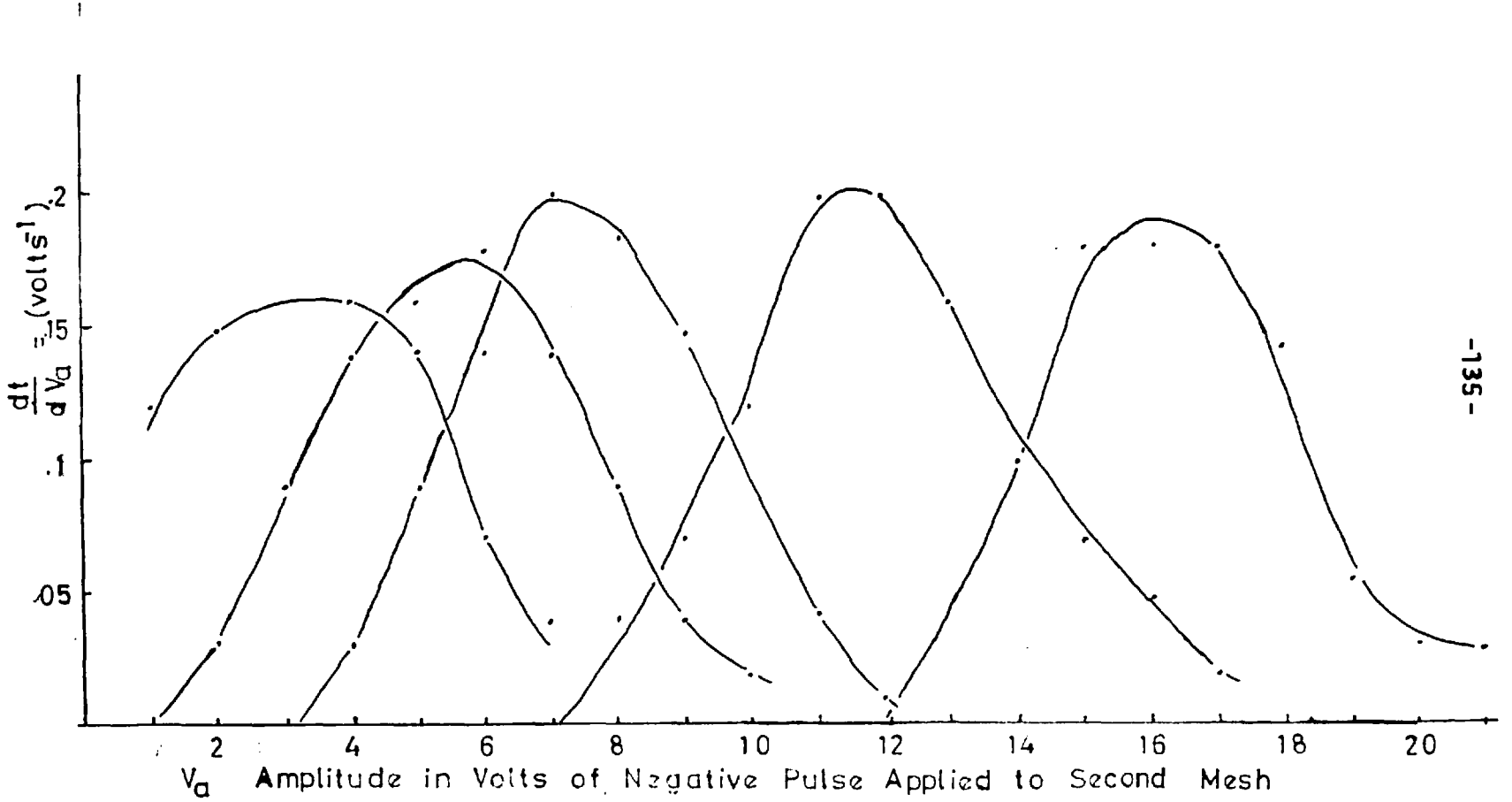

Fig. 5.14 The Curves of fig. 5.13 Differentiated

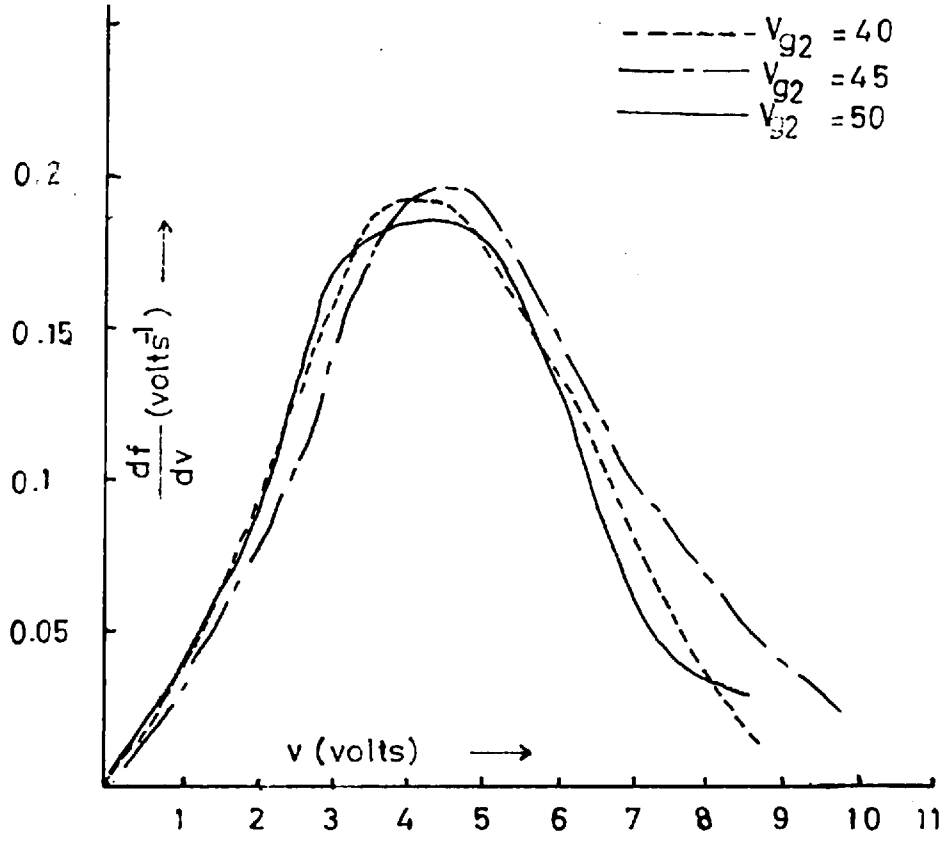

Fig. 5.15 Velocity of Distribution of Secondary Electrons

The experiment just described provided no means of establishing whether the spread of forward velocities was a consequence of enhanced secondary emission, or merely reflected non-uniformity of the surface potential. An experiment (section 8.9) in the camera tube suggested that the range of surface potential between different parts of the dynode was only of the order of two volts provided the areas were not immediately adjacent to the edge of the KCl deposit. Although the spot used in the measurement of the velocity spectrum was not small (about 8 mm. in diameter), it was well removed from the edge of the deposit.

It would not be surprising if the emergent electrons had a large variation in energy; electrons released within the deposit would be able to acquire energies from the field across the deposit which increased as the distance they travelled before escaping. Scattering would reduce these energies, but the presence of an accelerating field across the deposit provided a mechanism which would not occur in dynodes with bulk density KCl, whereby the secondary electrons could acquire a large variation in energy.

CHAPTER 6

The Response of Dynodes to Changing Primary Currents

6.1 Introduction

On projecting an image on to a tube, the intensified image takes a finite time, determined by the properties of the phosphor and of the dynode, to build up. The response times of the dynodes can be considered in two very distinct cases. In the first case, the dynode is not at its final working condition when the tube is exposed to light. The particular case when the dynode starts with no potential gradient across it is discussed in chapter 8. The second case occurs when the dynode has been previously brought to its working condition, the surface potential and the electron gain having reached their final values. According to Goetze[42], the working condition of the tube could be attained by flooding the cathode with diffuse light when the unfocussed primary electrons caused the gain of the dynode to rise towards an equilibrium value. The flooding light was interrupted once the surface potential and the gain of the dynode had reached their final value.

6.2 Experimental Observations

Observations at primary current densities of the order. ..

of 10^{-10} amps/cm^2 showed that it was possible to follow the variations in gain by means of a pen-recorder. The pen-recorder monitored the current flowing through the display meter of the electrometer which was measuring the secondary current drawn from the dynode. Identical scale readings could be obtained on both the electrometer and the pen recorder by adjustment of the potentiometer shown in figure 6.1.

A large uniform spot of light, typically 1 cm. in diameter, was projected on the cathode. When the gain had reached an equilibrium value the primary current was interrupted by means of the electro-mechanical shutter attached to the projector.* After a timed period, the same spot of light was again allowed to fall on the photo-cathode. It was felt that this procedure would simulate working conditions where a short time with no primary current incident on the dynode, would elapse between bringing the dynode to its working condition and projecting an image on to the tube.

The behaviour of the dynode following this procedure was complicated; it was however, reproducible provided that an equilibrium was reached before the primary current was interrupted. The variation of gain on re-applying the image was found to be affected by the primary current

* Section 4.4.

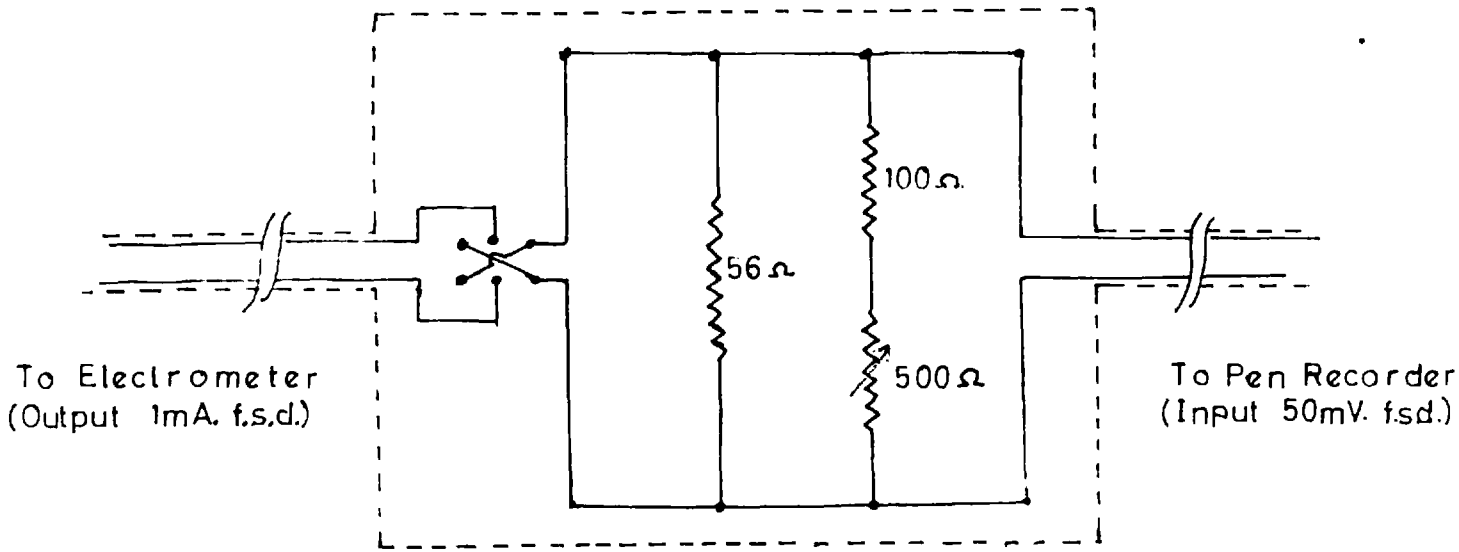

Fig 6.1 Matching Circuit for Electrometer and Pen Recorder

density and the time for which the primary current was interrupted. The latter period will be referred to as the 'off period'.

The effect of a range of 'off' periods varying from one second to two hours when the primary current density was 2×10^{-11} amps/cm^2, was investigated; the results are shown in figures 6.2a to 6.2c. In general the response was a series of heavily damped oscillations superimposed on a slow recovery of the gain towards its equilibrium value.

The first peak was always found to coincide with a marked increase in graininess in the image, and it appeared that its cause might be a rise and fall in surface potential and that further fluctuations in surface potential caused the subsequent variations in gain. The experiments described in this chapter were performed using the two mesh tube described in the last chapter, and it was a simple matter to demonstrate the origin of the first peak by repeating the experiment for a constant 'off' period and decreasing retarding mesh potentials.

Figure 6.3 shows the variation with V_{g2} of the amplitudes of the first two peaks, the first two minima, and the equilibrium value of the gain when the 'off' period was held constant at 10 seconds. The displacement of the

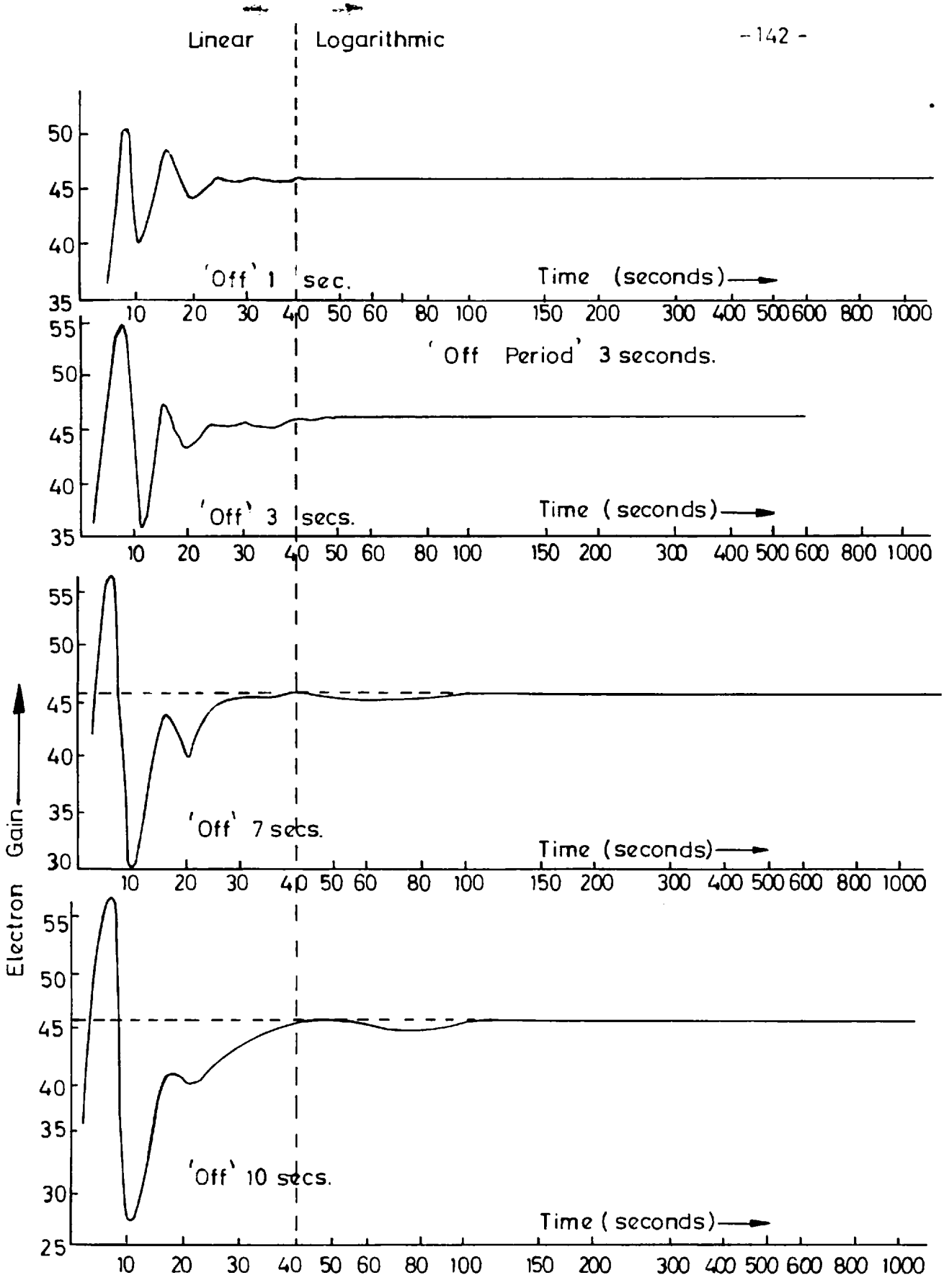

Fig.6.2 a. Dynode Time Response.

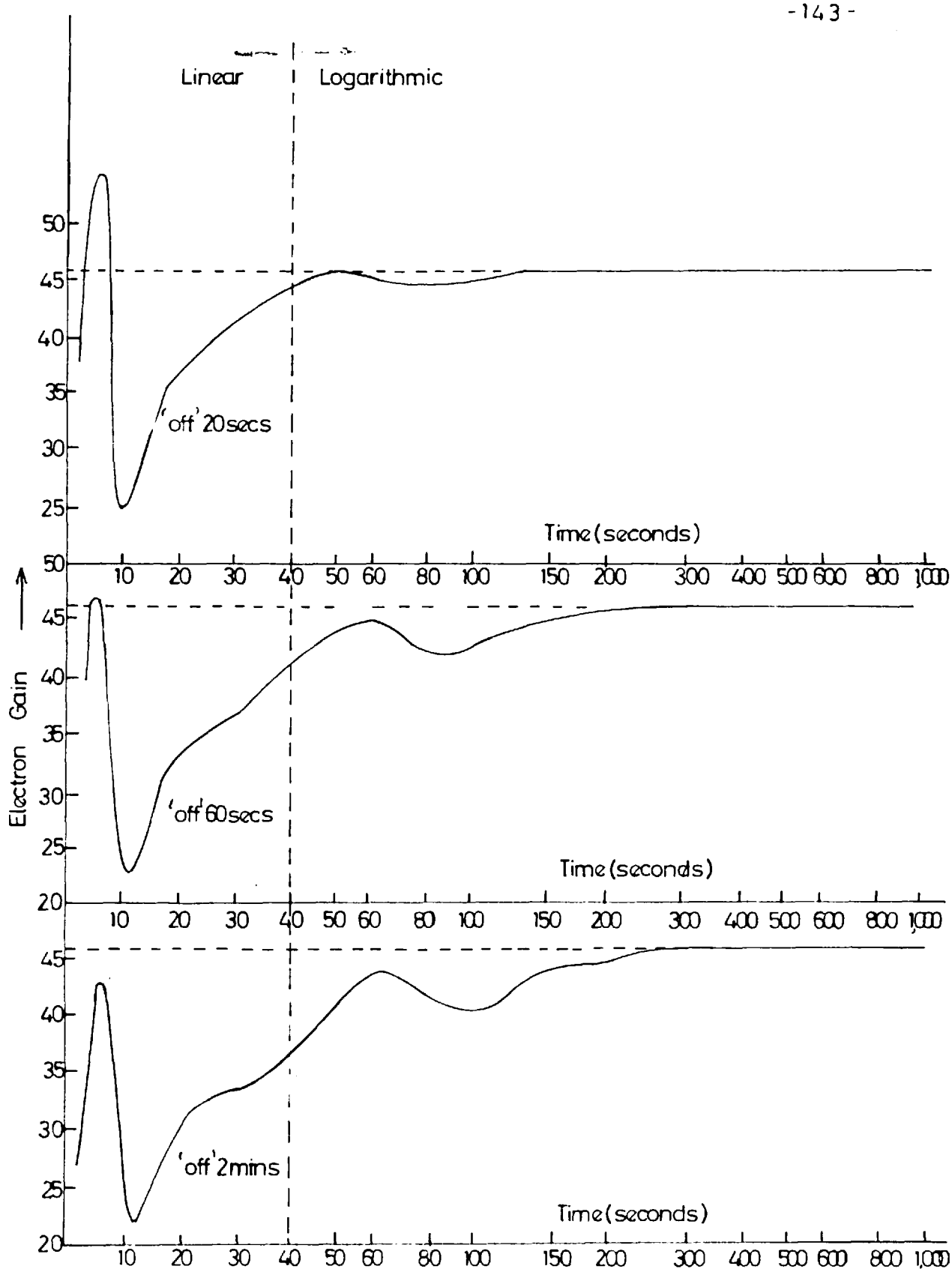

Fig. 6.2 b. Dynode Time Response

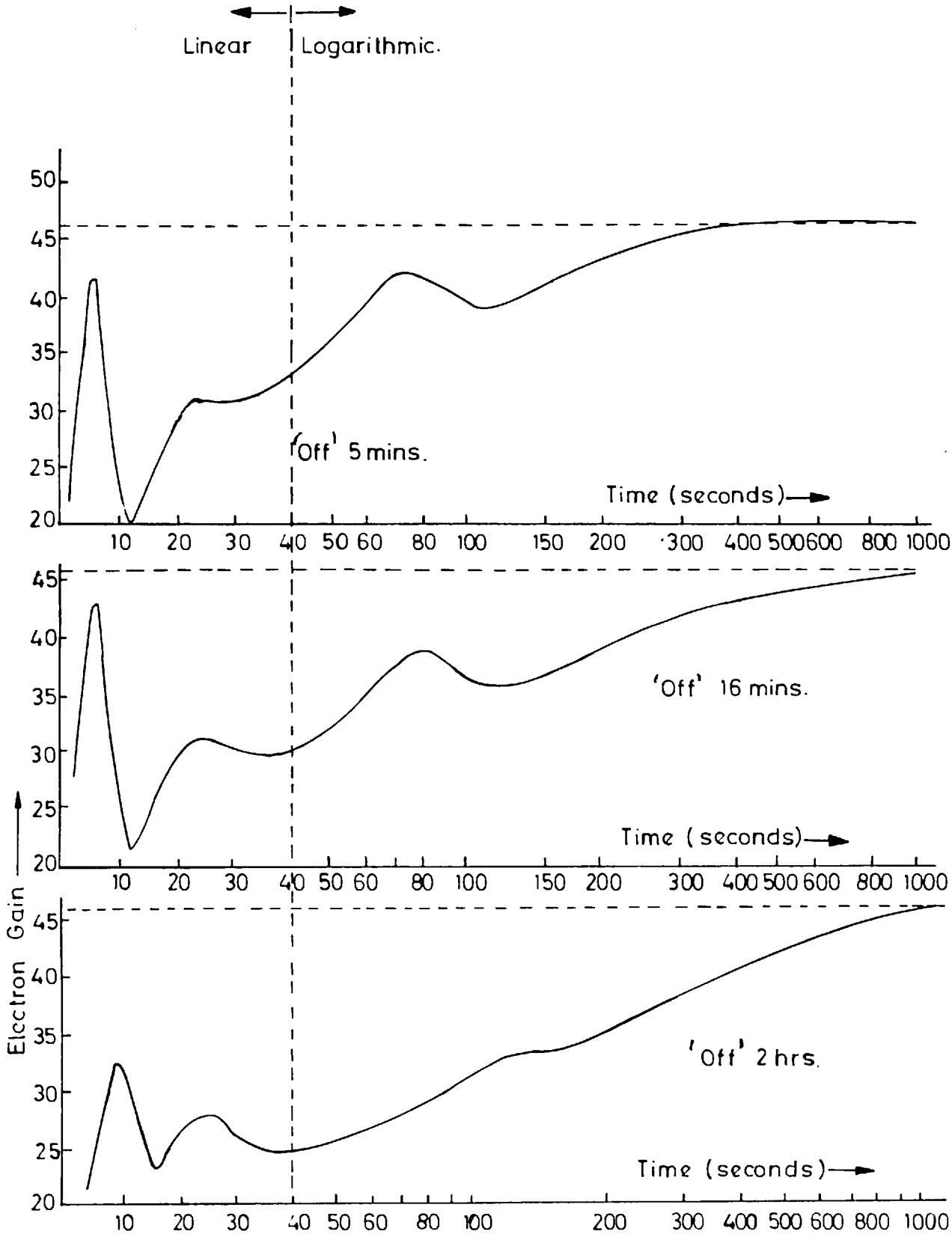

Fig.6.2 c. Dynamic Time Response

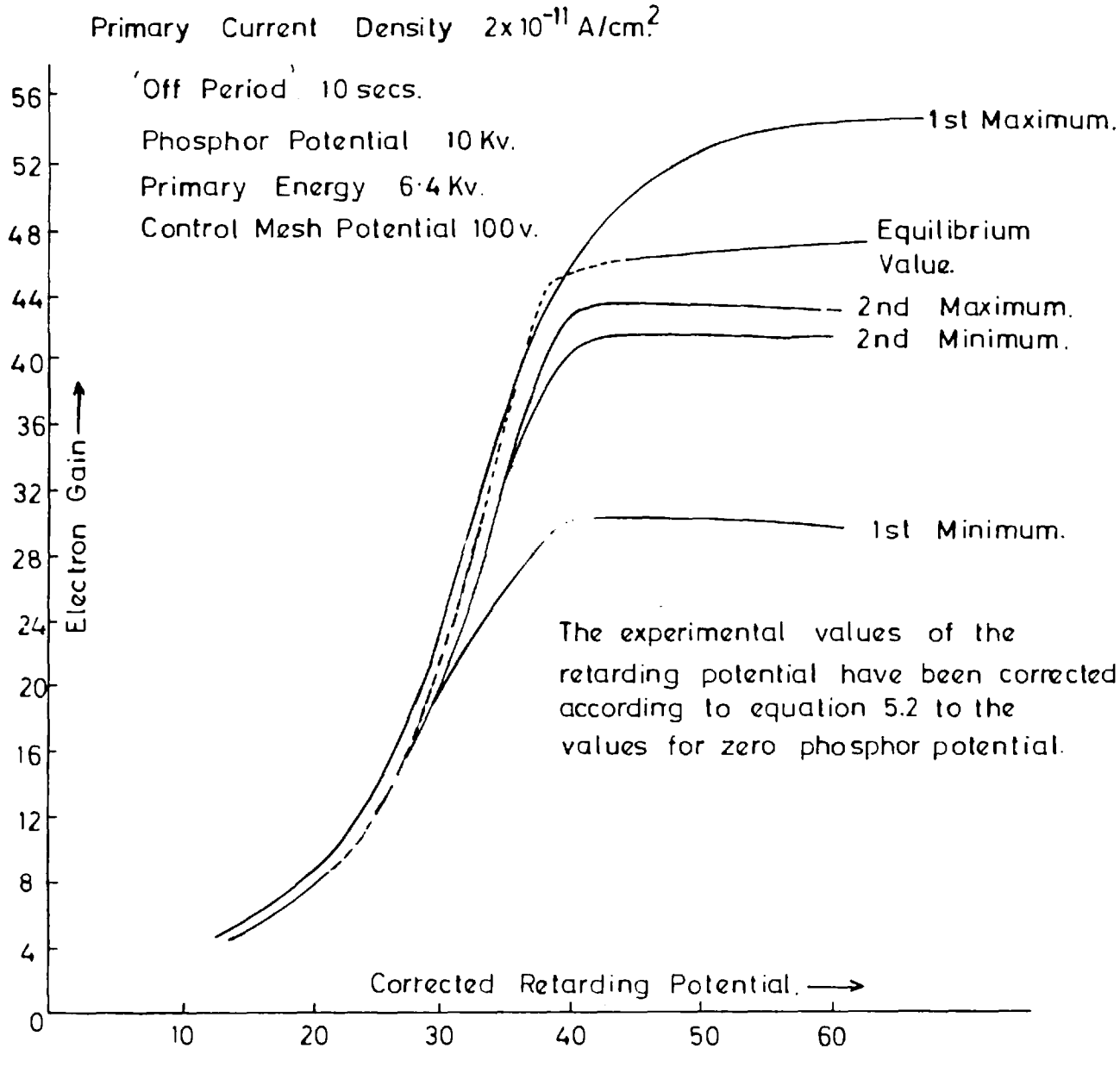

Fig 6.3 Fluctuations of Electron Gain as a function of Retarding Potential.

knee in the plot of the amplitude of the first peak against retarding potential towards a higher potential confirmed that the surface potential of the dynode did exceed its equilibrium value. Measurement of the rise in surface potential was rendered difficult by the broadness in the knee of the curve of P_1 against V_{g2}. The broadness of the knee could have been a result of an increase in the variation of emission energies of the secondary electrons during this period of high surface potential; however, in view of the very wide range of energies which would be required to account for the broadness of the knee, a more plausible explanation was that the surface potential during this initial rise was very non-uniform.

As well as the comparatively rapid fluctuations in gain which occurred when the primary current was interrupted, a slow build up of gain towards an equilibrium value was also observed. It can be seen from figures 6.2a to 6.2c that this slow build up of gain became increasingly apparent as the time for which the primary current was interrupted increased. If the primary current was again interrupted for a short time after the initial fluctuations had subsided but before the equilibrium value had been attained, fluctuations similar to those described in this

chapter were again observed; when they died down the gain continued to follow the same path it had before the interruption occurred. From these observations it was apparent that some factor other than the surface potential was involved in the slowly increasing value of the electron gain; indeed it has been shown in section 8.3 that the slow increase in gain towards the equilibrium value was associated with a fall in surface potential.

The failure of the secondary current to remain proportional to the primary current when the latter was changing must inevitably set a severe limitation to the use of these dynodes in practical image intensifiers.

CHAPTER 7

The Use of Low Density Potassium Chloride Deposits as a Charge Storage Medium

7.1 Introduction

It has already been reported (section 4.4) that the dynodes used in image intensifiers were capable of retaining information for periods in the order of days. It was decided to exploit this memory ability which resulted from the high resistance of the low density deposit of KCl, in a charge storage television camera tube.

The principle of operation of such a camera tube, is that a charge proportional to that released from the photocathode in the period between successive scans is stored on a high resistance target. When a picture element is scanned by an electron beam, the charge released is proportional to the number of photons incident since the last scan and thus the process of charge storage is a means of integration. Numerous attempts[71,74,75,76,77] have been made to increase the integration period of television cameras as a means of evaluating images of low contrast. Charge storage camera tubes were currently being investigated at Imperial College by R. Filby and S. Mendel under the supervision of Dr. N. D. Twiddy and the work described in

this chapter was undertaken as a joint venture by the afore-mentioned and the author.

Apart from the high resistance of the low density deposits, which would lead to long integration times, it appeared that other advantages might be gained from the use of a low density KCl dynode as a target. These were:

1) The electrostatic capacity of a target in the order of 10μ thick would be near the optimum value for many purposes. The upper limit to the signal to noise ratio at a given resolution is set by the storage capacity of the target. Because the maximum allowable voltage excursion produced by the input signal is limited in practice to about 2 - 4 volts, the storage capacity of the target is effectively determined by its electrostatic capacity. An upper limit is set to the target capacity by the discharge process. For small signal voltages the discharge efficiency falls as a result of poor beam acceptance; if the capacity of the target is large, the beam is unable to discharge the target in a single scan[78]. A generally accepted value for the optimum target capacity is in the range 500 - 1,000 pf[79].

2) Some electron multiplication could be expected from the dynode. Because this multiplication would occur before the video signal was fed to the video amplifier, an increase

in signal to noise ratio might result*.

3) A tube could be designed with the scanning gun and the photo-cathode on opposite sides of a multiplying target. This arrangement is used in the image Orthicon but the necessity for residual target conductivity leads to a loss of resolution on attempting to prolong the integration period[80].

It was hoped that a camera tube with a low density KCl dynode as a target would yield information on the operation of these dynodes in image intensifiers.

7.2 Camera Tube Design and Construction

In order to make use of existing apparatus, which included a conventional tube focussing solenoid and a complete closed circuit television channel together with miniature C.P.S. Emitron scanning coils, the tube was designed as in figures 7.1 and 7.2. The scanning section was identical in design and dimensions to the miniature C.P.S. Emitron and used the same type of electron gun[81].

The target and control mesh assembly was made and mounted as one unit. The film was mounted on a plate which was skirted to prevent cesiation of the rear end of the tube

---

* Appendix A.4.

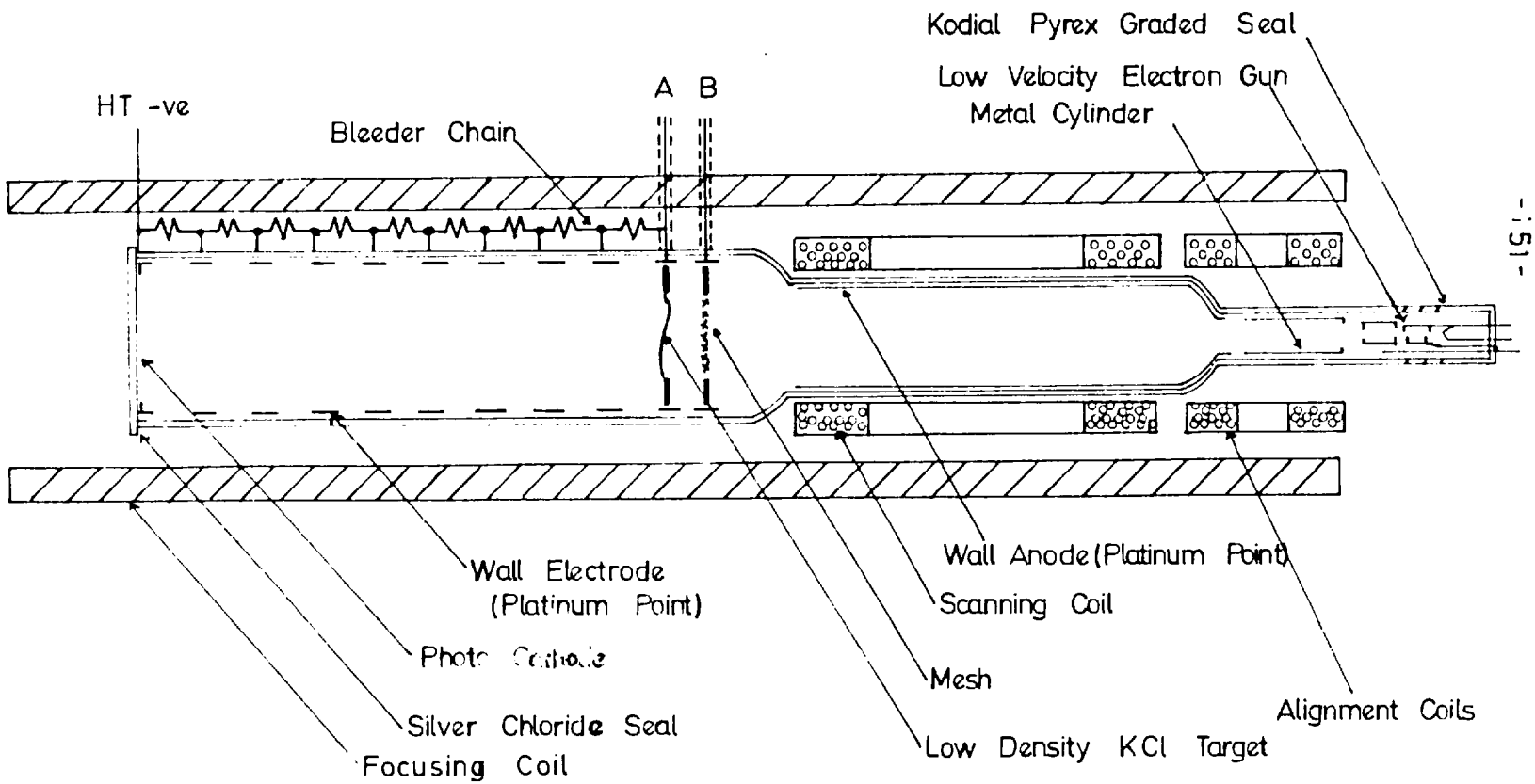

Fig. 7.1 Camera Tube.

Fig. 7.2 Camera Tube and Internal Parts

during photo-cathode processing. A mesh of electro-formed copper was mounted 1 cm behind the exit surface of the film. When the tube was used as a television camera tube, this mesh acted as an electron collector and defined the decelerating field for the scanning electron beam. In experiments on the behaviour of the dynode in image intensifiers, it also acted as a control mesh. It was supported by a plate which was attached to the outer film bearing plate by ceramic rods. A spring contact on the mesh plate bore against a platinum paste electrode on the tube wall.

The image section of the tube was similar in most constructional details to the image intensifiers. It was focussed by parallel electro-static and magnetic fields. Its unusually long length (19 cm) was a result of the low magnetic field recommended for focussing the C.P.S. Emitron electron gun. The photo-cathode was formed on an end window which was sealed to the tube with silver chloride.

7.3 Low Velocity Scanning

Low velocity scanning was used to read the charge image on the target and a short description of the mechanism of signal generation follows. The optical image was converted to a positive charge image on the surface of the target

which was scanned by a finely focussed electron beam. The target was arranged to be at a potential near that of the scanning gun cathode and as a result, the scanning electrons emitted very few secondary electrons from the target and stabilized the surface of the target at the potential of the cathode of the scanning gun. The discharge of successive picture elements induced a current to flow to the signal electrode which was capacitively coupled to the target surface. This current formed the video output of the tube.

Several physical processes can be used to convert the optical image into a positive charge image. The charge image is formed in the C.P.S. Emitron by photo-emission from an insulating photo-cathode. In the camera tube developed here, two processes, secondary electron emission and a form of bombardment induced conductivity, contributed to the formation of the charge image.

7.4 Operation of the First Camera Tube

The external circuit for the camera tube is illustrated in figure 7.3. The closed circuit T.V. channel was of conventional design and is not described. Suppression of the electron beam for charge integration experiments was achieved by connecting the modulator grid of the electron gun

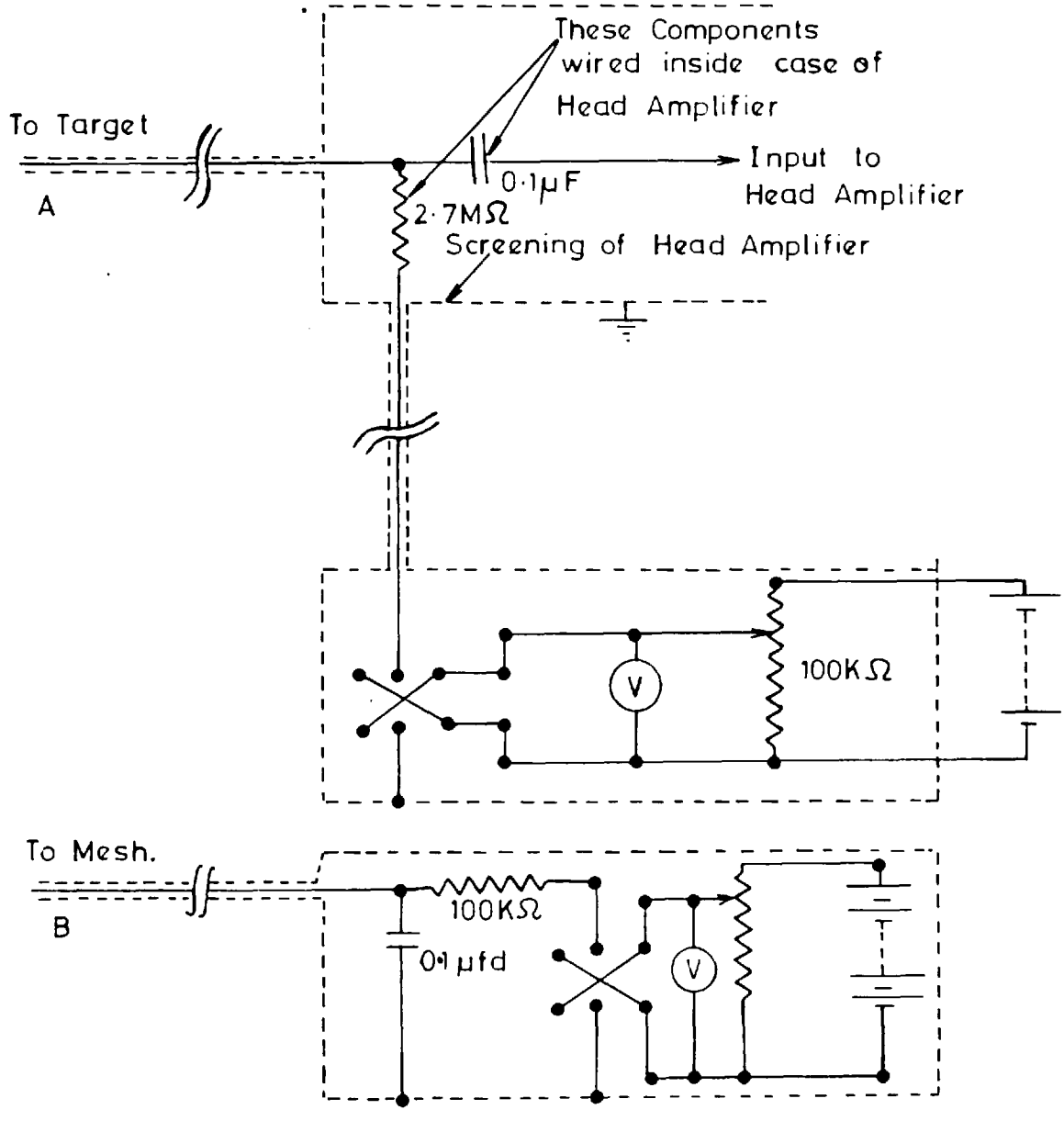

Fig. 7.3 Connections to Camera Tube

to the negative H.T. line of the head amplifier. The tube was supported at the image section end by a conventional cradle and was pushed into the scanning and alignment coils which were permanently mounted in the focussing solenoid.

The preliminary experiments were made with a tube which was later shown to have a high resistance contact between the film backing and the supporting plate. This tube functioned well as a camera tube, exhibiting resolutions in the region of 5 - 6 lp/mm, and most of the characteristics of the successful tube were discovered with this tube.

At low backing positive voltages* the tube gave good pictures without observable lag. The image produced on the monitor, became progressively weaker as the film backing was made more negative of the electron gun cathode. Increasing the positive backing voltage caused brighter images. As the backing was made more positive, localised bright spots appeared and increased in intensity and an increasing instability towards overloading was noted.

From these observations it was decided that two

---

*Throughout this and the next chapter, the term 'film backing' is to be understood to refer to the aluminium layer between the Al_2O_3 support layer and the potassium chloride deposit.

independent mechanisms were involved in picture formation.

7.5 Formation of the Charge Image by Secondary Electron Emission

Primary electrons from the photocathode were sufficiently energetic to penetrate the film and liberate secondary electrons from the potassium chloride nearest the mesh. Because of the high secondary emission ratio of potassium chloride* a net positive charge was left as a result of bombardment. The emission of these secondaries was, to a large extent, determined by the surface condition of the crystallites and the energies of the electrons striking them and independent of the potential gradients within the film.

7.6 Formation of the Charge Image by Bombardment Induced Conductivity

Many normally insulating materials become conducting when bombarded by high energy electrons[63,82,83]. Bombardment induced conductivity has already been employed in camera tubes [84,85]. In these tubes a thin layer of

---

* The secondary emission ratio of KCl has been reported by Theodorou to reach eleven[30] on reflection.

insulator or semi-conductor was deposited on a signal plate which was held positive with respect to the cathode of a low velocity electron gun. The electron beam scanned the free surface of the deposit and continued to land until the surface was cathode potential stabilized. When the insulator was bombarded with high velocity electrons, it became conducting to an extent determined by the bombarding current density. Because the side of the deposit facing the gun was at cathode potential and the signal plate was held positive, a positive charge image was transferred to the target surface.

It was believed that a similar mechanism contributed to the formation of the charge image in the camera tube described here, when the film backing was held positive with respect to the gun cathode. When the backing was held negative with respect to the gun cathode, the induced conductivity resulted in a reduction of the intensity of the positive charge image produced by secondary emission.

It is important to note a difference between the conduction mechanism operating in low density KCl deposits and true bombardment induced conductivity which arises in continuous solids. In the latter, the conductivity occurs due to a conduction mechanism within the solid. The low density KCl deposit was believed to consist of finely divided

particles between which little contact existed; the charge carriers must have been able to drift between the particles and were almost certainly secondary electrons which were emitted from the surfaces of the crystallites.

It was even more unlikely that BI.C. in the normally accepted sense was significant in view of work reported by Collins and Hirsch[86]. They showed that although it was possible for alkali halides in general, and KCl in particular, to exhibit B.I.C. and show a current gain, the effect was small. The maximum gain for KCl was about 18 and this could only be maintained for a short time unless the potential across the layer was periodically reversed. No sustained conductivity was observed.

For the sake of convenience, the term B.I.C. will be used to indicate the process just described, which has been termed S.E.C. (secondary electron conduction) by Westinghouse in reference to their S.E.C. Vidicon. This is a tube, essentially similar to that described here which was announced shortly after the construction of the last tube described in this thesis[87,88].

7.7. Electron Skipping

Certain combinations of electric and magnetic field gave rise to the considerable increases in primary current

illustrated in figure 7.4. Complete suppression of the rise in primary current could always be achieved by increasing the magnetic field to large values; no evidence of more than one peak was ever obtained at a given magnetic or electric field. The peaks in primary current were always accompanied by noise on the monitor screen. When making measurements of the primary current* it was necessary to increase the magnetic field to get a correct reading because the measurements were made at photo-cathode potentials which otherwise gave rise to an apparent increase in primary current.

Firing the getter in the tube reduced but did not eliminate these effects which persisted when the tube showed no other signs of softness. This reduction did however, indicate a connection of the effect with residual gas in the tube. A possible explanation of the gain was that ions or electrons striking the walls of the tube produced secondary electrons which were accelerated and returned to the tube walls whence they released yet more secondaries. A cascade of electrons was established along the walls of the tube.

---

* Section 4.6.

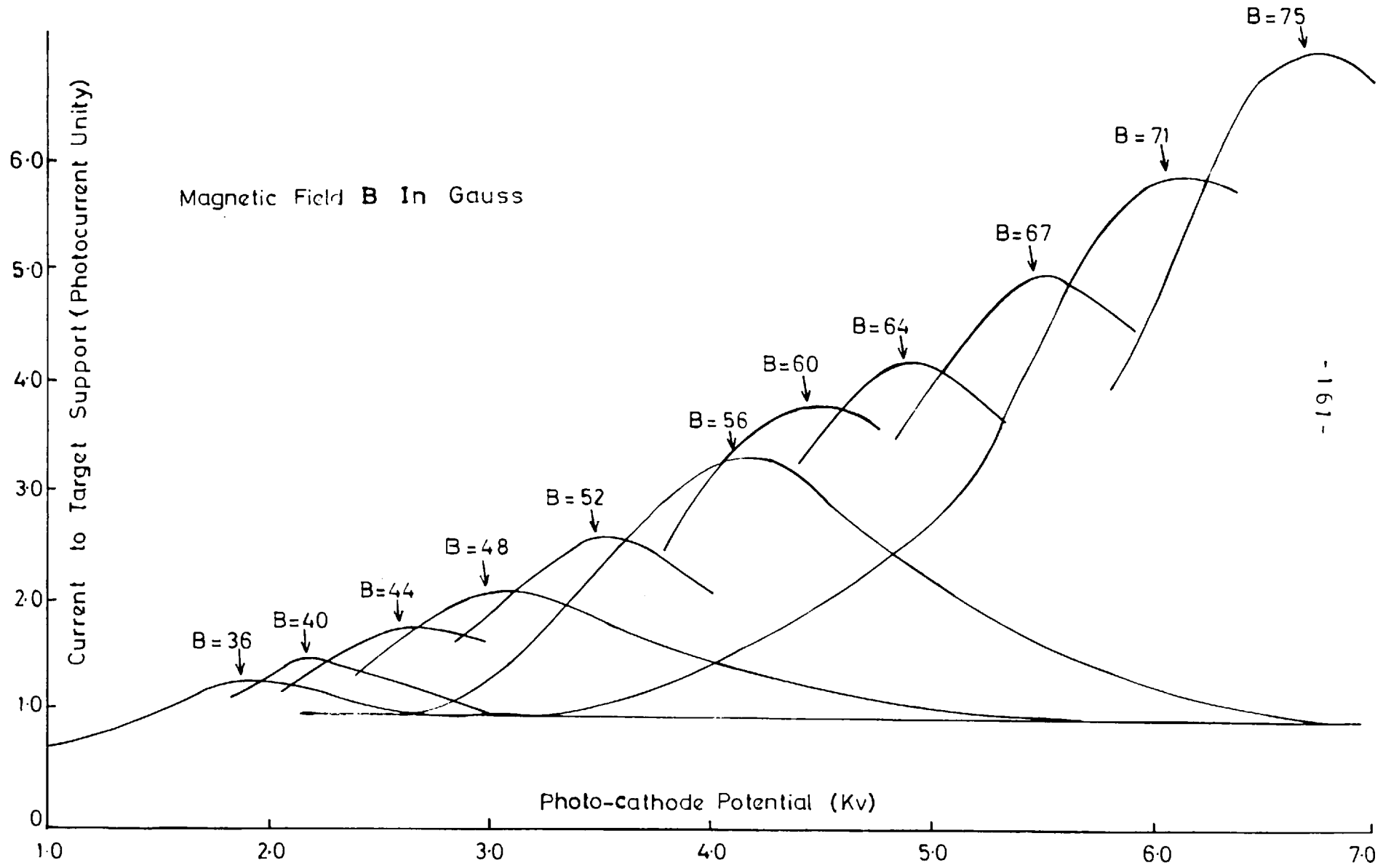

Fig 7.4 Photocurrent as a function of Photocathode Potential at Various Constant Magnetic Fields.

It was found that

$$B^2_{max} = kV_{max} + c$$

where B_{max} was the magnetic field, and V_{max} the cathode potential at which the apparent primary current had a maximum value. c was a small constant of unexplained origin and k was another constant. Evaluation of the constant k showed that this equation corresponded to electrons striking the walls of the tube after travelling an average distance of 2.2 to 2.45 cm along the tube from the point at which they were emitted*. This distance was not very different from the spacing of the platinised glass wall electrodes. Since metals invariably have secondary emission ratios below those of insulators it was postulated that the tube wall consisted of alternate bands of high and low secondary emitting surfaces. An electron cascade was only possible when electrons from one region of unpainted glass were focussed onto the next. The resonance arose because of the large number (nine) of evenly spaced electrodes. Further confirmation of this hypothesis was obtained when two electrodes near the centre of the tube were connected together. A large reduction in the primary current gain was observed to result from the defocussing and non-acceleration of one generation of electrons.

---

* Appendix. A.5.

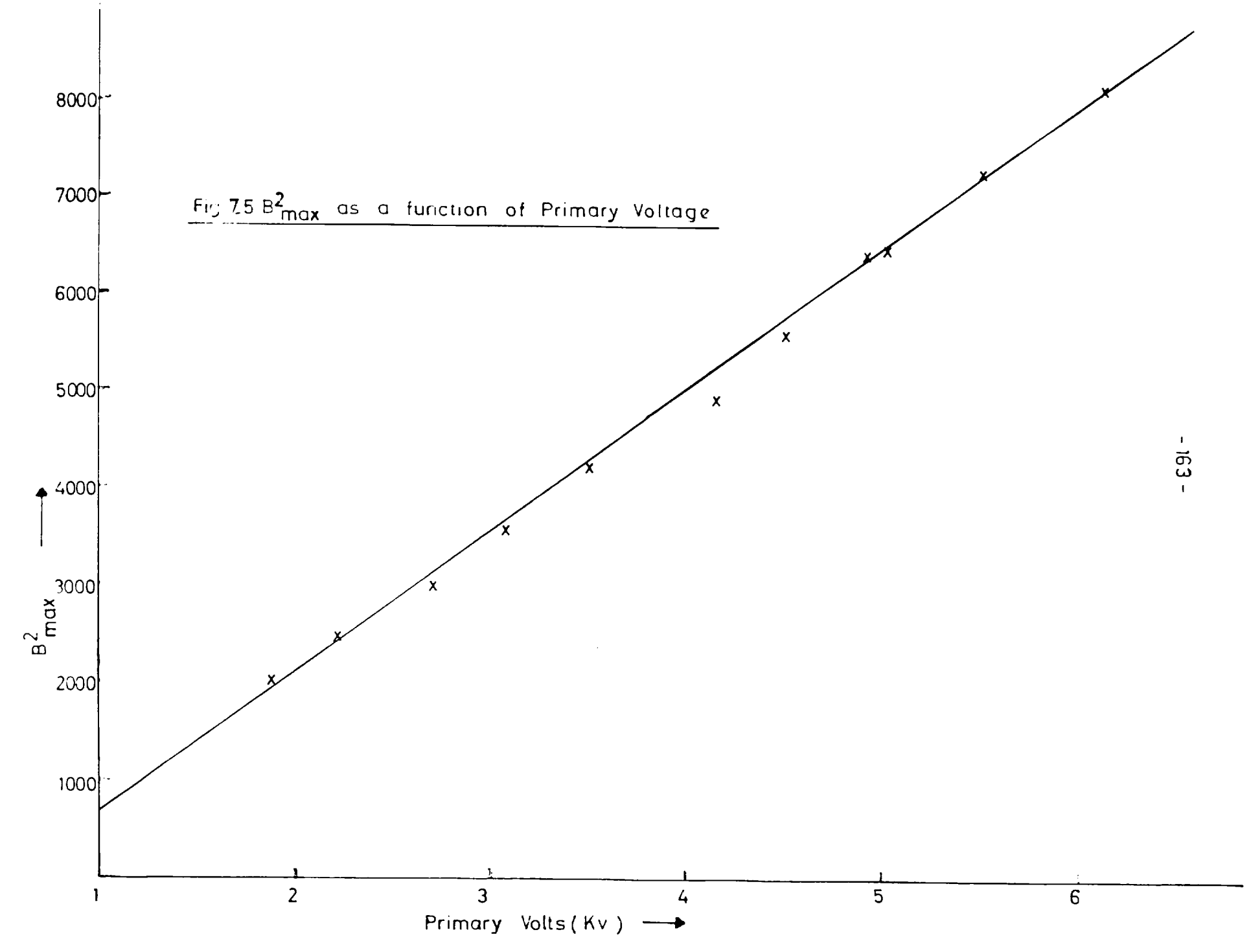

Fig 7.5 B^2_{max} as a function of Primary Voltage

The observation that the cascade was associated with noise over the entire monitor screen, and that the image within the area of the film was not affected, confirmed that the electron showers were confined to the walls of the tube; the position and length of a flash on the screen indicated the time of arrival of a shower initiated by a single electron or ion, and also its duration. The flashes were always about picture point size and hence were probably of shorter duration than the response time of the head amplifier.

It is interesting to compare this result with that of Zacharov, who found a high background in his tubes only in the presence of a magnetic field.[26] Zacharov reduced this background, which was augmented by ions from the tube walls striking the cathode, by means of anuli spaced down the walls of the tube.

The camera tube had a high background which limited the integration time to two hours. It was felt that this background was associated with electron cascading even though the normal tube operating conditions were some way off resonance. For this reason it was decided that future tubes (built after the author had left) should have shorter image sections and anuli similar to those suggested by Zacharov.

7.8 The Effect on the Film of Processing the Thermionic Cathode

Before the construction and processing of a second and a third camera tube, the demountable tube (chapter 3) was modified and used in an experiment to see if the low density KCl deposit was attacked by gases evolved during the processing of the thermionic cathode. The end plate below the electrode structure was replaced by a tube to which a side-arm containing an unprocessed Emitron gun was sealed. A low density KCl dynode was mounted in the tube and its electron gain was measured at intervals while the electron gun was processed. No fall in gain was observed. Care had been taken to ensure that the pumping stems were sufficiently constricted that the chance of contamination was not minimised by rapid removal of gas.

7.9 The Final Camera Tube

Although the first tube operated reasonably well it became evident that there was a very high resistance between the film backing and the plate supporting the target, and the tube was abandoned. A second tube was made, but had to be abandoned because of a fault in the gun section, and a third tube was successful. This tube

showed no significant deviations in behaviour from the first tube, except that there was no evidence of a poor contact to the film backing. A more searching investigation was made into the performance of this tube as a television camera, and it was found to exceed all expectations. A limiting resolution of 13 lp/mm, at the photo-cathode was observed. This resolution was obtained only when the 'zoom' control on the monitor was operated so that the scanned area of the target was reduced and the limitations imposed by the frequency response of the television channel were removed.

7.10 The Measurement of the Signal to Noise Ratio

The signal to noise ratio was measured when a potential of 6Kv was applied between the photo-cathode and the target, the film backing was 5 volts positive of earth, and the image was of the maximum intensity which did not cause overloading of the tube. The signal and the noise were measured by means of an oscilloscope, as voltages at the output of the head amplifier.

In order to avoid confusion on the oscilloscope screen, and to be able to identify deflections on the oscilloscope trace with features in the image, measurements were made on only one line. A 'line selector' caused the

oscilloscope to trigger for only one line scan per frame; the line selected was identified as a dark line on the monitor screen.

The head-amplifier, which had a gain of unity, produced an R.M.S. noise of 1mV, when the tube was not connected. The noise of the complete system was 3mV R.M.S. when the tube was connected and the cathode was at full H.T. volts. A focussed image was shone on the photo-cathode at the maximum intensity which did not show, by a loss of resolution on the monitor screen, that the tube was being overloaded.* The signal was found to be 200mV giving a signal to noise ratio of approximately 70+

---

* When areas of the target charge beyond a certain voltage, the beam is deflected towards these points away from less heavily charged neighbouring areas. The effect, which is known as 'beam pulling' is indicated by an apparent growth of the white areas and a loss of resolution.

+ Later measurements[89] by Filby and Mende, have indicated that the signal to noise ratio is higher, being between 100 and 200.

7.11 The Charge Gain of the Target

The incidence at the target of a charge Q_{in} from the photo-cathode causes the appearance of a positive charge Q_{out} on its scanned surface. The ratio $\frac{Q_{in}}{Q_{out}}$ is defined as the charge gain. If we confine our attention to the charges q_{in} and q_{out} incident on, and scanned off the target, respectively, in a single frame period and at a single picture point, then;

$$\frac{Q_{out}}{Q_{in}} = \frac{q_{out}}{q_{in}}$$

Now if N is the number of lines per frame,

T is the frame scan period,

i_p is the primary current,

f is the fraction of the scanned area occupied by the image,

and a is the aspect ratio of the picture,

then $$i_p T = afN^2 q_{in} \qquad (7.1)$$

Also, if i_v is the current generated by the discharge of a picture point

$$i_v = \frac{aN^2 q_{out}}{T} \qquad (7.2)$$

The current i_v flows across a load resistor R producing a video signal v_{out}. Re-arrangement and substitution gives

$$G = \frac{q_{out}}{q_{in}} = \frac{f v_{out}}{R i_p} \qquad (7.3)$$

v_{out} was measured directly in the manner described in the preceding section. The charge gain is shown in figure 7.6 as a function of the film backing potential at a constant primary energy of 5Kev. The charge gain was not measured at very high positive backing voltages because the camera tube was becoming increasingly unstable, and the image produced was spoilt by blemishes.

7.12 Image Blemishes

As the backing was made more positive, localised blemishes in the form of white spots became increasingly apparent. These blemishes were probably holes in the potassium chloride layer through which scanning electrons were attracted by the positive potential on the film backing. The collection of electrons when areas very near a hole were scanned, resulted in a signal corresponding to a bright spot.

7.13 Overloading of the Camera Tube

When an excessive signal was applied to the photo-cathode

Fig:7.6 Charge Gain of Camera Tube as a Function of the Film Backing Potential

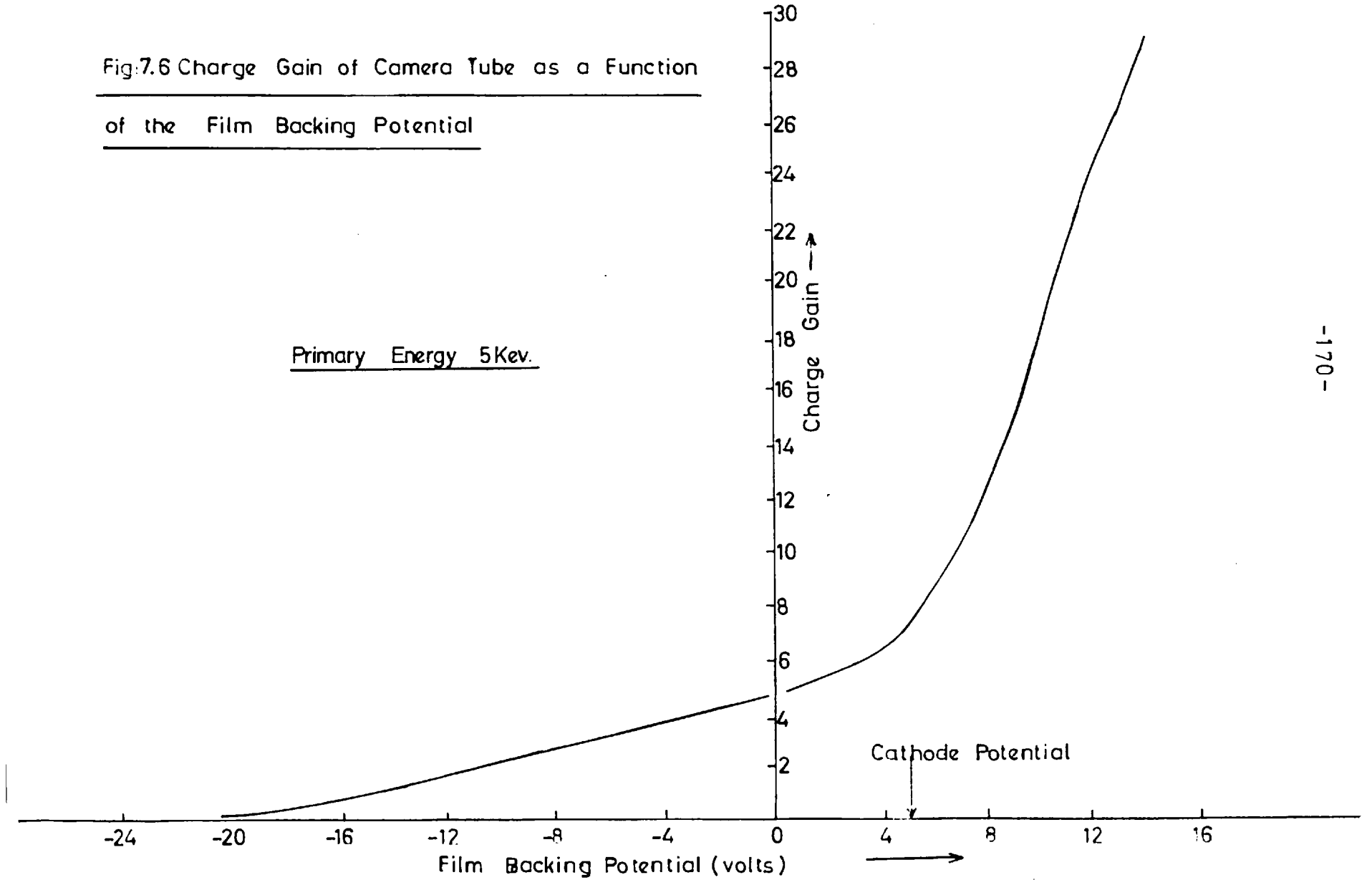

more positive charge was generated on the target surface than could be removed by the scanning beam. As a result the surface potential of the target rose and the scanning electrons were accelerated and acquired sufficient energy to liberate secondary electrons from the target. When the potential of the film surface rose to first crossover,[+] the scanning electrons, instead of neutralising the positive charge on the film surface, added to it. The potential across the film rose until the film broke down.

Overloading was observed on the monitor screen, first as beam pulling, and then as a loss in intensity in the highlights which rapidly became black and spread over the film area if the overloading was allowed to continue. The black appearance was due to a net loss of electrons as the target was scanned. The picture finally disappeared in a burst of horizontal flashes as the film broke down and the head-amplifier was overloaded. This condition was self maintaining and could only be stopped by lowering the mesh potential until secondary electrons liberated by the scanning beam were returned to the target, or by reducing

---

[+] First crossover is that potential at which the secondary emission ratio of the surface first rises to unity as the potential is increased from zero.

the film backing potential until the target surface potential was near that of the cathode of the electron gun.

7.14 Tube Linearity

Figure 7.7 shows the output of the tube (measured as the voltage output of the head amplifier) as a function of the incident current when the film backing was at the same potential as the gun cathode. Within a range which was shown by beam pulling to be in excess of the normal operating range, the tube had a linear response.

7.15 Charge Integration

The tube appeared to be able to integrate weak signals over a prolonged period with no apparent loss of resolution provided that excessive excursions of the target surface potential were not allowed to occur. The period of integration was limited by tube background to about two hours.

In section 8.4, it is shown that the target had a leakage resistance in excess of 5×10^{13} ohms; it can be expected that in the absence of a primary current, very little deterioration of a stored image would take place over a period of several hours. In sections 8.3 and 8.5 it

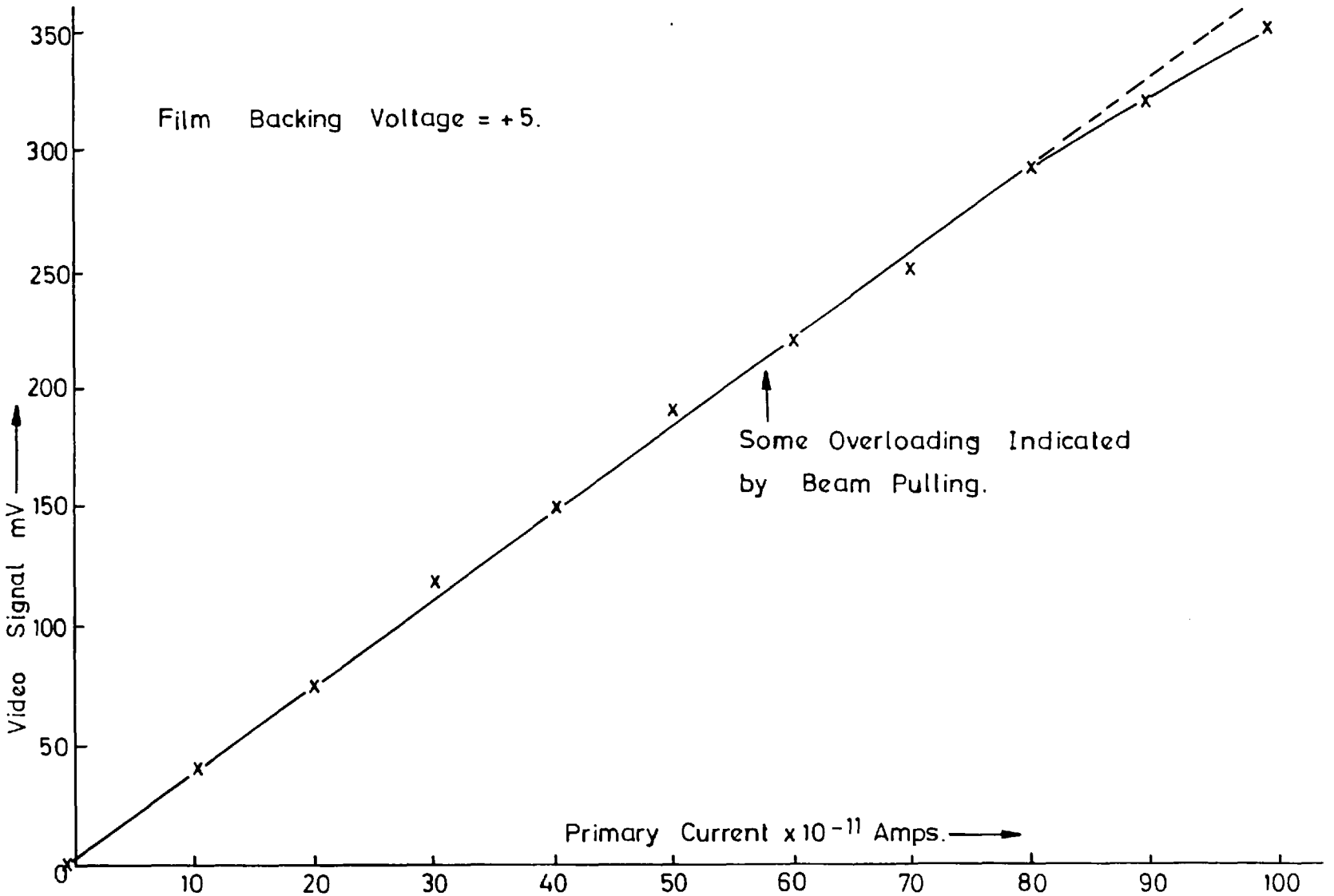

Fig.7.7 Linearity of Response of Camera Tube.

is shown that complicated effects took place when large potential gradients were allowed to develop across the KCl layer; in normal storage applications the potential gradients would be too small for these effects to occur and detract from the usefulness of the tube as a charge storage device.

CHAPTER 8

The Use of the Camera Tube to Investigate the Behaviour of the Dynodes in Image Intensifiers

8.1 Introduction

In the experiments described in this chapter, the camera tube was used to investigate the variation of surface potential of the low density KCl film under conditions very similar to those which it would have experienced as a dynode in an image intensifier. The scanning electron beam was prevented from landing on the film surface and primary electrons were allowed to land on the film; at the same time, the mesh was held at similar potentials with respect to the conducting backing as was the control mesh in an image intensifier. Under these conditions it was to be expected that the film would behave in the same manner as it would have done in an image intensifier, the surface potential being determined by the cathode and mesh voltages, the current density and time. The surface potential was then found by adjusting the film backing potential until the electrons were just able to land on the dynode surface and a picture was produced on the monitor screen. It was then known that

the surface potential was near that of the cathode of the electron gun and thence the potential across the KCl deposit could be estimated.

Two means were available for preventing the electron beam from landing. Either the scanning beam was suppressed by the application of a large negative potential to the modulator of the electron gun, or the film backing was held sufficiently negative with respect to the cathode of the electron gun that the electrons were unable to land.

Before any experiments on the variation of the surface potential were made, the secondary emission gain was measured as a function of the collector potential and the primary energy. From these measurements it was established that the film in the camera tube was representative of dynodes which had been tested in image intensifiers.

8.2 Experiments in which the Film was Continuously Scanned

Some preliminary experiments were made in which continuously displayed images were produced when the backing was negative of the gun cathode. In order to be able to distinguish the image above the noise level, it was necessary to increase the intensity of the incident

image as the backing was made more negative; at the same time the quality of the image dropped markedly. When the backing was more than about 32 volts negative of the gun cathode the appearance of the image depended strongly on the time for which primary current was incident on the target. When the backing was between 35 and 50 volts negative with respect to the gun cathode, only transient images could be obtained. When the backing was between 32 and 35 volts negative of the gun cathode images of longer duration could be obtained; these however, faded slowly and eventually disappeared. Continuous pictures could be displayed indefinitely when the backing was less than 32 volts negative of the gun cathode. Under no conditions was an image ever produced when the backing was more than 50 volts negative of the gun cathode.

Switching off the H.T. for a short time* caused the image to appear and then disappear when the H.T. was again

---

*The voltage between the photo-cathode and the film is referred to as the H.T. In experiments where the primary current to the film was interrupted, the H.T. was switched off rather than the projector to avoid any possibility of the tube background current affecting the behaviour of the film.

switched on, provided that the time lapse between successive exposures was long enough.

It appeared from these experiments that the potential across the film rose steadily at first until it reached a value of about 50 volts; it then dropped rapidly to a value in the neighbourhood of 35 volts and thereafter fell slowly to an equilibrium value of approximately 32 volts.

8.3 Experiments on the Surface Potential in which the Film was not Continuously Scanned

In two parallel sets of experiments the surface potential was investigated whilst the primary current was incident and after it had been stopped. To perform the first experiment the film backing potential was set at -50 volts, and the mesh potential at 150 volts, so that the mesh was 200 volts positive with respect to the film. With such a negative backing potential it was ensured that the scanning beam could not land. After timed intervals, the film backing potential was reduced and the negative bias on the gun modulator removed. By noting the backing potential at which a 'white up' first occurred, it was

possible to plot the surface potential as a function of time. The fact that the mesh potential relative to the film was not constant was considered unimportant for the following reasons. A comparatively high mesh potential was used so that the fractional change was small; apart from the short time for which the film surface was being explored, the film backing potential was returned to -50 volts; it had already been shown* that the control mesh potential had only a small effect on the equilibrium surface potential when it was above a certain value.

The second experiment was performed under similar conditions except that the H.T. was switched off before the film was scanned.

It was frequently observed that the initial picture on the monitor depended on the previous treatment of the film+. The film was returned to a 'normal' state before beginning a new experiment, by bombarding it with primary electrons while its surface was scanned and its backing was held at the potential of the gun cathode. The experiment was not begun until the picture on the monitor was no longer changing. In both sets of experiments, the photocathode was illuminated with a spot of light which

---

* Section 5.3.

+ Section 8.7.

coincided with the area of the film.

These experiments were repeated at several primary current densities. The results for two current densities are shown in figures 8.1 and 8.2; figure 8.1 also shows the electron gain of the dynode measured under similar conditions. It appeared that the behaviour of the surface potential whilst the primary current was incident, was determined by the total primary charge incident on the film. It was seen however , that the surface potential of the film continued to fall for a time after the primary current was interrupted. The magnitude of the fall increased with the primary current. It also increased with the time of bombardment if equilibrium had not been established before the primary current was interrupted. No fall in potential was detected if the primary current was interrupted while the surface potential was still rising.

8.4 The Resistance of the Potassium Chloride Layer

The resistivity of the KCl deposit was estimated in the following manner. After an image had been projected for a short time and the surface potential was still rising, the H.T. was switched off. It was then established by scanning the target that a potential of 41 volts had been

Fig 8.1 Electron Gain & Surface Potential as a Function of Time of Bombardment.

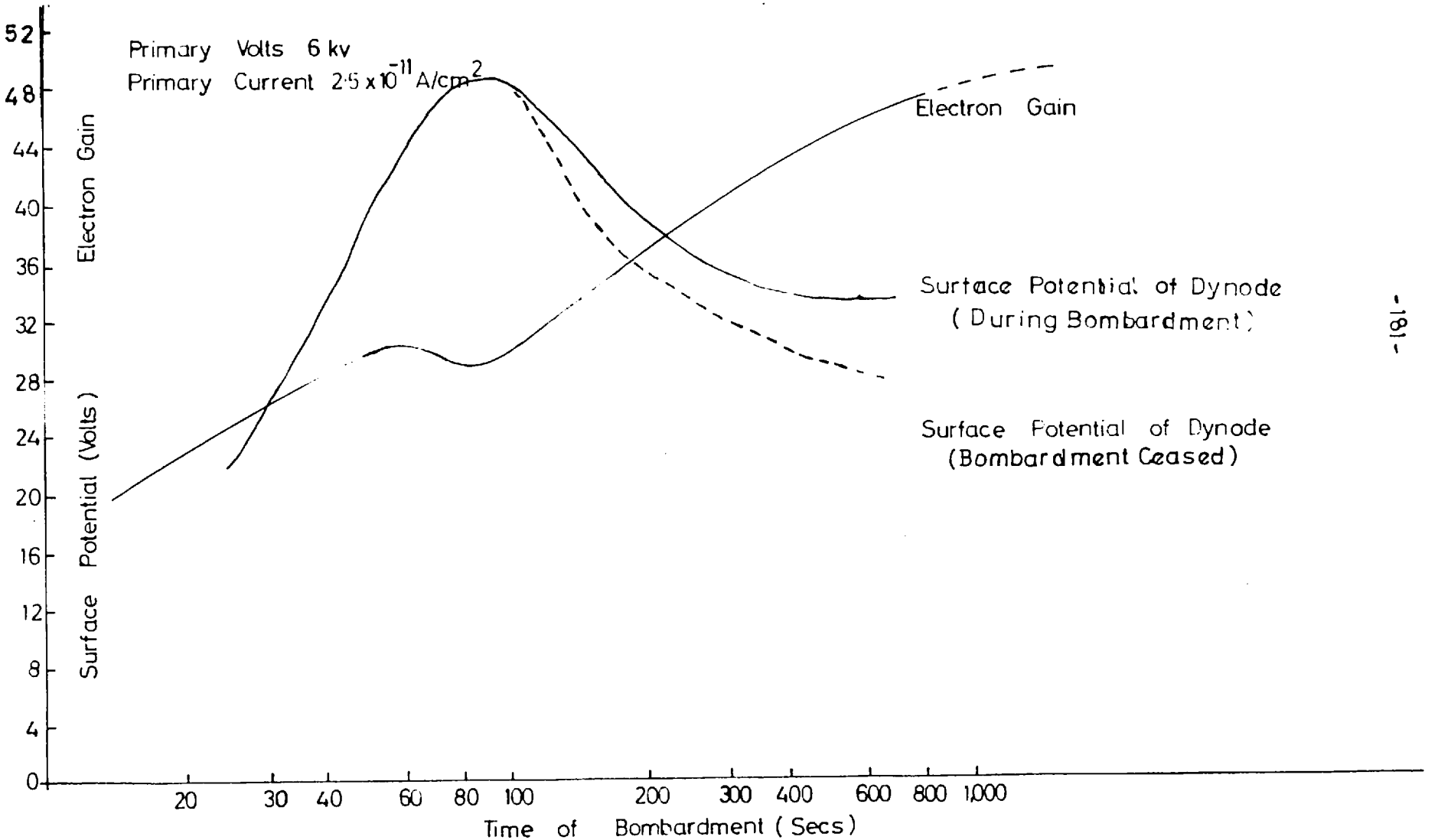

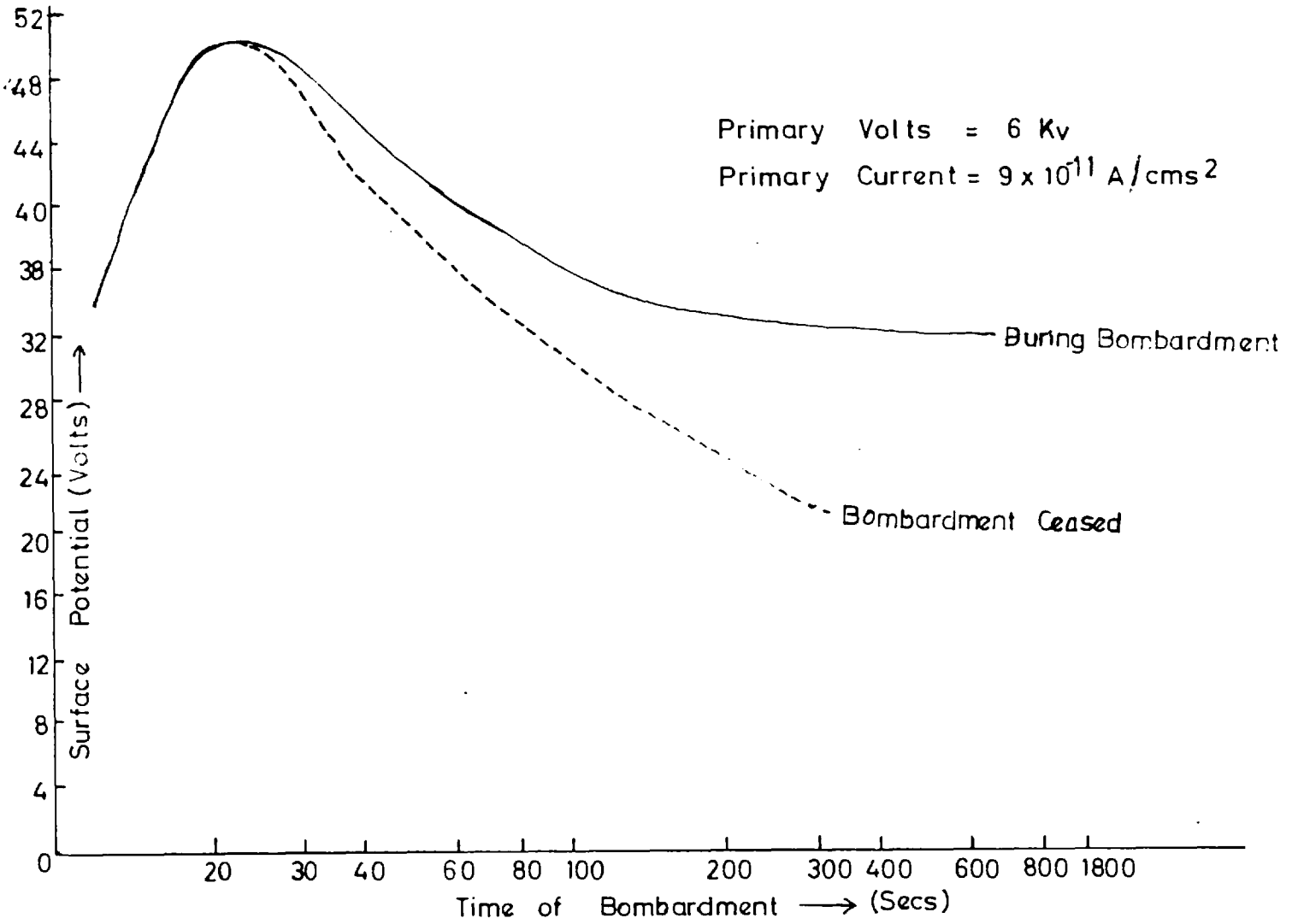

Fig. 8.2 Surface Potential as a Function of Time of Bombardment.

set up across the KCl layer. Further scanning at the same backing potential failed to produce a picture and the tube was left for twenty minutes after which the surface potential had dropped by less than 2 volts. Assuming that the target capacity was 500pf*., the minimum leakage resistance of the KCl layer was estimated at 5×10^{13} ohms. and the minimum resistivity as 2.5×10^{17} ohms/cm.

8.5 The Induced Conductivity and the Surface Potential

In order to account for the fall in surface potential of the KCl deposit on prolonged bombardment, it was necessary to assume that the conductivity of the deposit was increasing. It was not clear whether the increased conductivity resulted merely from the prolonged passage of primary electrons through the deposit or whether the conductivity increased only in the presence of a potential gradient.

The primary current was allowed to fall on the film for a period considerably longer than that in which the rise

---

* The mass per unit area of the film was known from conductimetric analysis on a simultaneously prepared film. Treating the film as a parallel plate capacitor and assuming its density to be 3.2%, its capacity was estimated at 500pf.

and fall in potential would have occurred. During this period the potential across the film was prevented from rising by scanning the surface of the film while the film backing was held at the potential of the gun cathode. The film backing was then made 40 volts negative with respect to the gun cathode without suppressing the electron beam. The picture on the monitor subsequently developed and then disappeared in the same manner as it would have done had the primary current not been incident for the period before the potential backing was reduced.

The fact that the potential was still able to rise to values well above the equilibrium value despite the prolonged bombardment, showed that the increased conductivity was not caused by the passage of the primary electrons alone and that a potential across the KCl deposit was essential for the conductivity to increase.

The continued fall in the surface potential after the primary current was interrupted indicated that the increased conductivity persisted for a short time in the absence of any primary current.

8.6 Relative Intensities in the Revived Image and the Sustained Emission in Intensifiers Using Low Density KCl Dynodes[+]

It has been demonstrated in section 8.3, that a drop in surface potential occurred soon after the bombardment of the dynode ceased. This drop in potential was found to increase with both the time of bombardment and the primary current density. It has also been shown that, apart from initial variations following a change in primary current density, the effect of prolonged secondary emission from the dynode was a rise in the electron gain[*]. Unless the drop in surface potential on ceasing bombardment was large, the local rise in surface potential was retained, and when the cathode was again illuminated, the area of the dynode which had previously been bombarded still exhibited a higher electron gain. As a result, the 'revived' image appeared bright against the flooding illumination. If, however, because of a heavy and sustained primary current, a large drop in surface potential occurred on interrupting the primary current, the field across the dynode was lowered to such an extent that the gain was reduced. As

---

[+] Section 4.10

[*] Chapter 6

a result, the 'revived' image appeared dark against the flooding illumination.

The comparative rapidity with which the sustained emission died in areas which had received heavy primary current densities, was also a result of a fall in surface potential when the primary current was interrupted. Areas which had received rather lower current densities did not experience such a large drop in surface potential and the sustained emission, although initially less intense, persisted for longer.

8.7 Enhanced Charge Gain of the Camera Tube Target

When a large positive potential was allowed to develop on the scanned surface of the target of the camera tube, it was found that the charge gain of the tube was considerably increased when the tube was again operated with lower backing potentials. This increase in gain died away as the tube was used, and the prolonged incidence of primary current when the backing potential was near that of the electron gun cathode removed all traces of previous operating conditions.

This increase in gain was found only after a large increase in surface potential and was not observed in normal camera tube operation unless the tube was overloaded

and secondary emission from the scanning beam caused a catastrophic rise in surface potential.

The cause of this enhanced charge gain was not established; the release of trapped charges may have been a contributary factor.

8.8 The Effect of Reducing the Incident Current Density

A surprising observation was that reducing the primary current density could lead to an increase in the surface potential. When an intense signal was applied and the film backing was held at such a potential that at equilibrium the surface was just negative with respect to the gun cathode, a reduction in intensity of the incident signal caused waves of light, which travelled outwards from the centre of the picture, to appear on the monitor screen. These died down in a few seconds and no further picture appeared on the screen. The appearance of the light areas on the monitor showed that the reduction in intensity of the input current had caused a temporary rise in the surface potential. A typical cause of this effect was a reduction in primary current of from 10×10^{-11} amps/cm^2 to 5×10^{-11} amps/cm^2 when a ripple was seen approximately 10 seconds after the reduction in intensity of the input signal.

A somewhat similar effect had been observed in image intensifiers when the primary current was suddenly reduced by the rapid introduction into the incident light beam of a ten times, or one hundred times, neutral density filter; the secondary current did not simply drop, but showed considerable oscillations before settling down to a steady value. It was believed that these effects were also caused by fluctuations in the film surface potential.

8.9 Uniformity of Surface Potential

The uniformity of the surface potential was investigated when the film was in an equilibrium state by noting the backing potentials at which various fractions of the film surface were accepting the scanning beam. The greater part of the film appeared to have potentials within a range of about 2 volts except at the edges where the film got thinner and the potential of the surrounding support plate, which was at backing potential, shielded the film from the effect of the control mesh.

8.10 The Mechanism of Enhanced Secondary Emission and Bombardment Induced Conductivity

The deposit of KCl was believed to consist of loosely packed crystallites with only vacuum in the spaces between

them. The primary electrons struck a large number of these crystallites, penetrating them or being reflected. At each crystal surface traversed or struck by the primary electrons, a number of secondary electrons were released into the vacuum interspace. In the absence of an electric field these electrons drifted about between the crystallites and were eventually recollected by crystal surfaces within the deposit which had themselves become positively charged by the liberation of secondary electrons. When a suitable potential gradient existed near the exit surface of the deposit, some of the secondary electrons liberated near the surface were able to escape. A positive charge accumulated on the surface and an electric field developed which caused electrons liberated further back to drift towards the surface. Many of these electrons were recollected before they reached the surface, but some reached the surface and were able to escape; it was these which appeared as the enhanced secondary emission current.

From figures 8.1 and 8.2 and an estimated value of the capacity of the film, it was possible to estimate the net charging current causing the initial rise in surface potential. Unless a negative charge existed on the surface this current was low, and ranged from approximately seven times the primary

current when no potential existed across the film to zero when the potential reached its maximum value. The very low value of the charging current compared with the enhanced secondary emission gain suggested that the positive charge formed at any point by secondary emission was to a large extent neutralised by the electron current across the film.

When the surface of the deposit nearer the electron gun was negatively charged, as in the use of the camera tube with the backing positive, the direction of the electron drift was reversed. The drift of electrons which had previously appeared as enhanced secondary emissions now constituted the 'bombardment induced current' described in section 7.6.

In many respects the mechanism so far proposed is inadequate to account for all the properties of the dynode. It offers no explanation for the peculiar response of the dynodes to changing primary currents, for the sustained emission and drop in surface potential when the primary current was interrupted, and for the instabilities and breakdown when high potentials were applied to the control mesh. The complicated time response of the enhanced emission implied that additional conduction mechanisms which grew and died very slowly were established within the dynode. These additional mechanisms may have resulted

from the generation of tertiary electrons and from field emission within the dynode. A contributary factor to their slow response may have been that they depended critically on the disposition of charges within the deposit, and that these charges and the fields between them took a long time to stabilise.

The fall in surface potential towards an equilibrium value discussed in section 8.3 was almost certainly accounted for by these conduction mechanisms; in the same section it was shown that the falling surface potential was accompanied by a rising electron gain. It is believed that the increased current across the dynode gave rise to a greater secondary current; at the same time more electrons were available to reduce the surface potential which then fell.

The failure of the additional conductivity to die rapidly probably accounted for the sustained emission, and for the drop in surface potential when the secondary current was interrupted.

CHAPTER 9

Summary and Conclusions

This thesis has described the development of dynodes showing high electron gains, their investigation in sealed off image intensifiers, and subsequently their use as targets in charge storage camera tubes. As a result of their poor imaging qualities, sustained emission and complicated response to changing primary currents, it was felt that the dynodes developed at Imperial College would not be very useful in image intensifiers, despite the high electron gains which could be achieved with single dynodes. Many of these adverse features were associated with the presence of high potential gradients which were developed across the dynodes and which were themselves essential for the mechanism of enhanced secondary emission.

In the application of the low density deposits where large potentials were not allowed to develop, i.e. as targets for television camera tubes, none of these complicated effects were observed. The very high resistivity of the deposits, the value of the target capacity and the charge gain available when only moderate potentials were allowed to develop across them, enabled charge storage targets with very promising properties to be developed.

It was noticed that when, whether by accident or by design, a high potential was allowed to develop across the targets, their properties were temporarily altered. In normal camera tube operation, such excessive potential gradients would be avoided however.

APPENDIX

A.1. Focussing in a Simple Tube

Suppose an electron is emitted with a velocity v at an angle θ to the direction of parallel magnetic and electric fields. Consider its motion in a plane perpendicular to the field direction.

Because the electron has a velocity $\sin\theta$ normal to the magnetic field it experiences a force of $Bev\sin\theta$ perpendicular to the direction in which it is travelling, and is constrained to move in a circle of radius r metres, where B is the magnetic induction in Webers/sq. metre, e is the charge of an electron in coulombs, m is its mass in Kg, and

$$\frac{mv^2\sin^2\theta}{r} = Bev\sin\theta$$

whence

$$r = \frac{mv\sin\theta}{Be} \qquad (A.1)$$

If τ is the time for the electron to complete one revolution

$$\tau = \frac{2\pi r}{v\sin\theta}$$

$$= \frac{2\pi m}{Be} \qquad (A.2)$$

The electron is also accelerated in the direction of the fields by the electric field along the tube; the resultant path is a helix about an axis parallel to the

direction of the fields. τ is independent of the direction and magnitude of the velocity with which the electron is emitted, and is thus the same for all electrons in a uniform magnetic field. Consider electrons emitted from a plane perpendicular to the field axis. Consider a second plane, also perpendicular to the field axis, but at a distance l from, and at a positive potential V with respect to, the former plane. In general, electrons travelling between the two planes will travel a distance s in a time t given by

$$s = vt\cos\theta + \tfrac{1}{2}\frac{Ve}{ml}t^2 \qquad (A.3)$$

In practice, the potential V is large and to a first approximation, the term $vt\cos\theta$ can be neglected, giving;

$$s = \tfrac{1}{2}\frac{Ve}{ml}t^2 \qquad (A.4)$$

The electrons undergo no net transverse displacement and are focussed between the two planes if

$$s = l, \quad \text{and} \quad t = n\tau$$

Substituting these values in equations (A.2) and (A.4.) and rearranging

$$l = \frac{\pi n}{B}\sqrt{\frac{2mV}{e}} \qquad (A.5)$$

A.2. Focussing in a Tube with One Mesh

The previous treatment of the focussing of a tube where

the electric field has only one value can be extended to the case where the electric field differs in two regions of the tube. Such a situation will be produced when a plane mesh is placed normal to the axis of the tube as in figure A.1. In addition to the symbols defined in the last section, let the distance of the mesh from the front end of the tube be Δl and its potential with respect to the emitting surface be ΔV ; also let B_n be the magnetic field to focus the tube when the potential gradients on both sides of the mesh are equal, and the electron executes n complete rotations. Let t_1 by the time for an electron to reach the mesh and t_2 be due time for the electron to travel from the mesh to the phosphor screen.

Substituting $s = \Delta l$, $t = t_1$, in equation (A.4)

$$\Delta l = \tfrac{1}{2} \frac{\Delta V}{\Delta l} \frac{e}{m} t_1^2 \text{ , whence } t_1 = \Delta l \sqrt{\frac{2m}{e\Delta V}} \qquad \text{(A.6)}$$

In the second section of the tube

$$l - \Delta l = \sqrt{\frac{2e\Delta V}{m}}\, t_2 + \tfrac{1}{2} \frac{V - \Delta V}{l - \Delta l} \frac{e}{m} t_2^2$$

whence

$$t_2 = \sqrt{\frac{2m}{e}} \frac{l - \Delta l}{\sqrt{V} + \sqrt{\Delta V}} \qquad \text{(A.7)}$$

Adding equations A.6 and A.7, and equating $t_1 + t_2 = k\tau$ where k is a small integer, the condition for electrons to be focussed becomes

$$l \sqrt{\frac{2m}{eV}} \left\{ \frac{1 + \frac{\Delta l}{l} \sqrt{\frac{V}{\Delta V}}}{1 + \sqrt{\frac{\Delta V}{V}}} \right\} = k\tau \qquad \text{(A.8)}$$

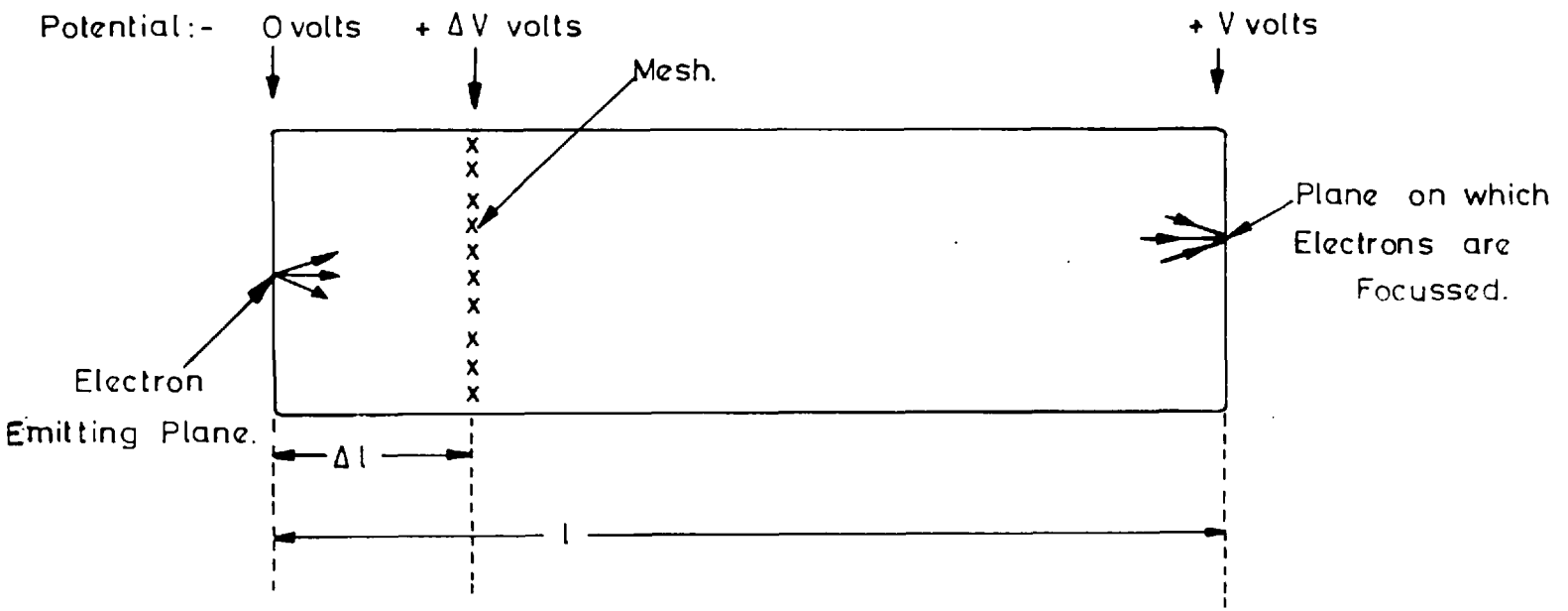

Fig. A. 1. Focussing Tube with One Mesh.

Substituting equations A.2 and A.5 in equation A.8 we have that the condition for focus is

$$B = \frac{k}{n} B_n \left\{ \frac{1 + \sqrt{\frac{\Delta V}{V}}}{1 + \frac{\Delta l}{l}\sqrt{\frac{V}{\Delta V}}} \right\} \qquad (A.9)$$

This relationship was confirmed in a tube which had a solid potassium chloride dynode. Figure A.2 shows magnetic field plotted against the function $\left(1 + \sqrt{\frac{\Delta V}{V}}\right)\left(1 + \frac{\Delta l}{l}\sqrt{\frac{V}{\Delta V}}\right)^{-1}$

Linear plots were obtained, and the gradients of the lines bore integral relationships to each other, showing that each line represented focussing with a different number of revolutions by the electrons. By dividing the gradients of these lines by small integers, and replotting, a single straight line could be obtained which represented the condition for single loop focussing. The value of B_n given by the gradient of the graph was within 5% of the value calculated from equation (A.5).

A.3. Phosphor Field Penetration

The following calculation is based on that used by Aldous and Appleton[90] in their treatment of the action of the grid in a triode valve.

It is assumed that the combined action of a mesh followed by a phosphor screen can be regarded as equivalent

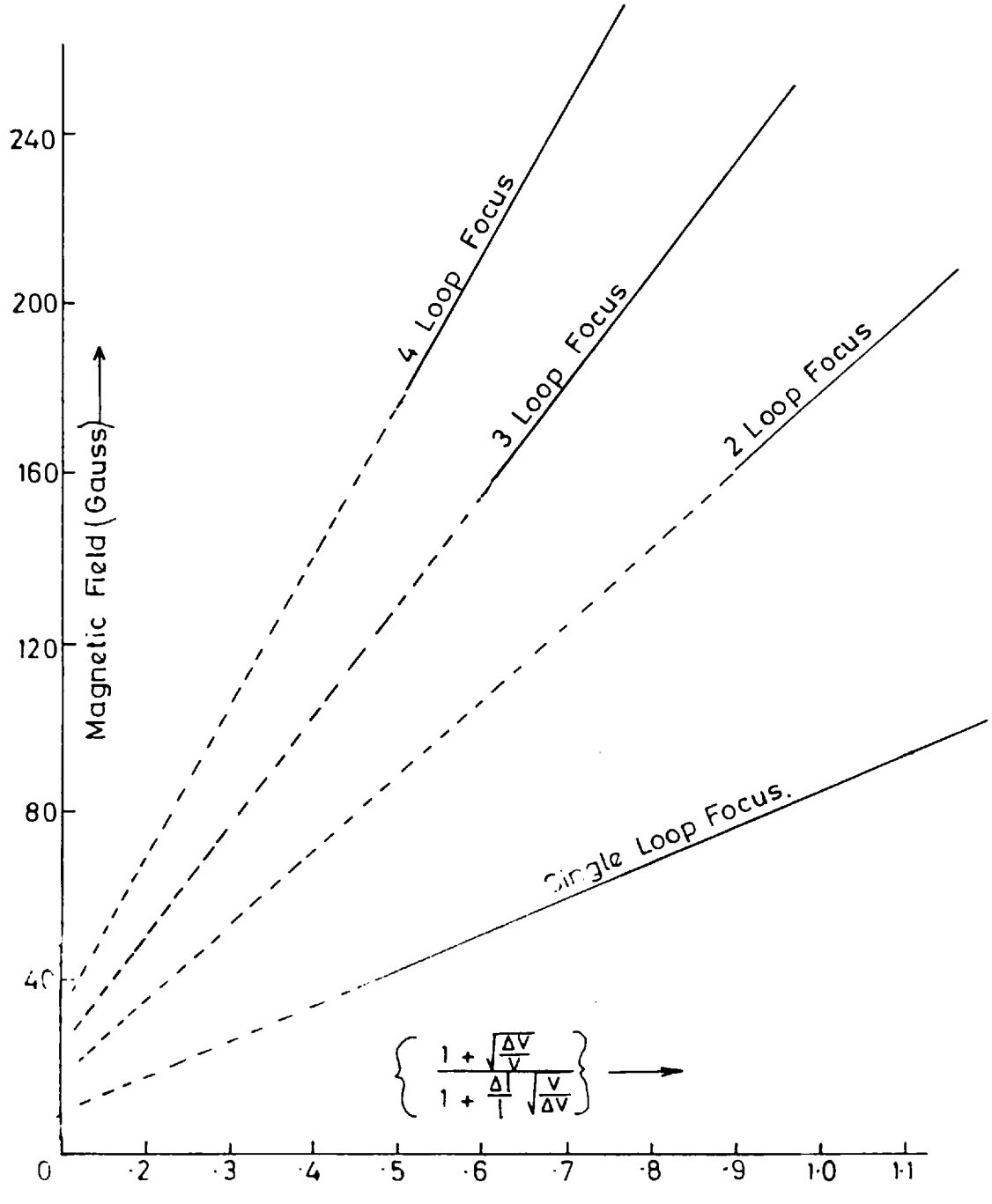

Fig. A·2. Focussing Tube with One Mesh, Empirical Curves.

to that of a single imaginary anode in the plane of the mesh, and at a potential which is a function of the mesh and phosphor potentials and the tube geometry. Let us first consider a single mesh tube, (figure A.3).

Let V_{ph} be the potential of the phosphor relative to the dynode surface,

V_g be the potential of the mesh relative to the dynode surface,

V_G be the potential of the imaginary anode relative to the dynode surface,

C_{Gg} be the capacity of the mesh to the imaginary anode,

C_{Ga} be the capacity of the phosphor to the imaginary anode,

and C_{Gk} be the capacity of the dynode to the imaginary anode.

Because the total charge on an imaginary anode must be zero;

$$V_G\, C_{Gk} + (V_G - V_g)\, C_{Gg} + (V_G - V_{ph})\, C_{Ga} = 0 \qquad (A.10)$$

whence
$$V_G = \frac{V_g + V_{ph}\,\frac{C_{Ga}}{C_{Gg}}}{1 + \frac{C_{Ga}}{C_{Gg}} + \frac{C_{Gk}}{C_{Gg}}} \qquad (A.11)$$

The term C_{Gg} represents the capacity of the mesh wires to the plane in which they lie. An expression is given by

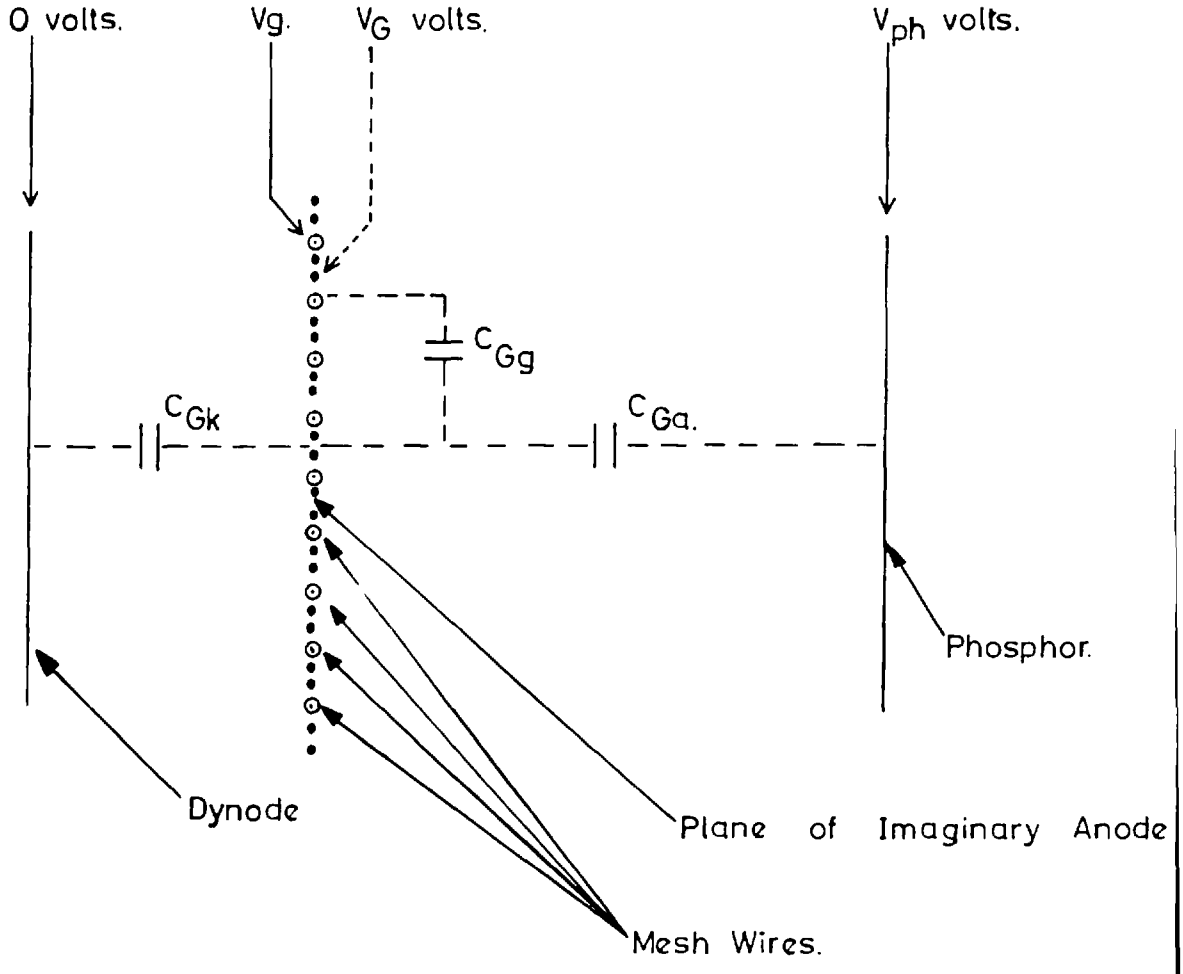

Fig. A.3. Phosphor Field Penetration.

Maxwell for the capacity of a grating of n parallel wires per cm. as

$$C = An\psi(nd)$$

where

$$\psi(nd) = \frac{1}{2 \log_e \frac{1}{2} \cos \frac{\pi nd}{2}}$$

where d is the diameter of the wire,

nd is the 'shadow ratio' of the grid,

and A is the area of the mesh considered.

The mesh can be regarded as two gratings, one of which has been turned through 90° from a position where its wires were parallel to, and half way between, the wires of the other grating. The capacity of the two gratings to the plane in which they lie will be only slightly changed by the rotation and to a first approximation will be given by

$$C_{Gg} = 2An\psi\ (2nd)$$

where 2nd is the total 'shadow ratio'.* This was measured optically and found to be 0.09 which is within the limits of applicability of Maxwell's formula.

The mesh used in most tubes had

$$n = 20 cm^{-1}$$

whence $\psi(2nd) = 0.395$

and $C_{Gg} = 15.8A$

C_{Ga} and C_{Gk} are capacities between parallel planes, whence

* n is the number of wires per cm of the mesh, hence the factor 2.

$$C_{Ga} = \frac{A}{4\pi l_{Ga}}$$

and

$$C_{Gk} = \frac{A}{4\pi l_{Gk}}$$

where l_{Ga} is the distance between the mesh and the phosphor screen, and l_{Gk} is the distance between the mesh and the dynode.

It can be seen that:

$$C_{Gg} >> C_{Ga}$$

and $$C_{Gg} >> C_{Gk}$$

and thus equation (A.11) can be written to a first order;

$$V_G = V_g + \frac{C_{Ga}}{C_{Gg}} V_{ph} \qquad (A.12)$$

This treatment for a tube with only one mesh is very easily extended to a tube with two meshes. The interposition of a control mesh between the dynode and the second mesh will affect only C_{Gk}; this quantity only appears as a second order term and the argument used in deriving an expression for the effective potential of the mesh will not be materially affected.

When numerical values are substituted for l_{Ga} and l_{Gk}, we get:

$$V_{G2} = V_{g2} + 5 \times 10^{-4} V_{ph}$$

where V_{G2} is the effective potential of the second mesh.

Whilst this treatment accounts satisfactorily for the effect of the phosphor potential on the secondary emission from the dynode, it does not account for the slow rise in electron gain with V_{G2}, where $V_{g2} > V_s$*.

If V_G is the effective potential of the control mesh when corrected for the penetration of the potential of the second mesh, then;

$$V_G = V_g + \frac{C_{Gg2}}{C_{Gg}} V_{g2}$$

where C_{Gg2} is the capacity of the plane of the control mesh to that of the second mesh, and C_{Gg} is the capacity of the control mesh to the plane in which it lies.

The two meshes were identical in construction and thus;

$$C_{Gg} = 15.8A$$

and

$$C_{Gg2} = \frac{1}{4\pi l_{Gg2}}$$

where l_{Gg2} is the distance between the two meshes.
Numerical substitution gives

$$V_G = V_g + \frac{1}{750} V_{g2}$$

The experimental results obtained would require that for

$$V_g = 100v. \quad \text{and} \quad V_c = 6.4Kv$$
$$V_G \simeq V_g + \frac{1}{7.5} V_{g2}$$

* Section 5.2.

This large discrepancy indicates that field penetration does not account for the rise in gain with increasing V_{g2}, when V_{g2} was greater than the surface potential.

A.4. Signal to Noise Ratio

Consider first a charge storage tube where the charge due to each photo-electron is discharged directly by the scanning beam. If $\bar{n}'$ photo-electrons are stored on average per picture element, the photo-electron shot noise will be $\sqrt{\bar{n}'}$ where

$$\bar{n}' = \bar{n}\sigma t,$$

$\bar{n}$ is the average rate of arrival of photons per picture point on the photo cathode, σ is the responsive quantum efficiency of the photo-cathode, and t is the integration time.

The noise due to the head amplifier can be regarded as a fluctuation of n_A electrons per picture element. The total noise per picture element is given by

$$(dn)^2 = \bar{n}' + n_A^2$$

If SN_1 is the signal to noise ratio, then;

$$SN_1 = \left\{ \frac{\bar{n}'}{1 + \frac{n_A^2}{\bar{n}'}} \right\}^{\frac{1}{2}}$$

As the signal to noise ratio in the incident light signal was $\sqrt{\frac{\bar{n}'}{\sigma}}$, it follows from section 1.2, that the detective quantum efficiency D.Q.E. is given by

$$D.Q.E. = \frac{\delta}{1 + \frac{n_A^2}{\bar{n}'}}$$

A typical value of n_A will be in the region of 1,000. It can be seen that the signal to noise ratio of the camera tube is limited at low light levels by the amplifier noise.

Consider now a camera tube where the charge due to the photo-current is multiplied before it is scanned by the electron beam. Let the electron multiplication have an average value of $\bar{m}$. If $\bar{S}$ is the signal per picture element, then;

$$\bar{S} = \bar{n}' \bar{m}$$

After Mandel[91] we have

$$\overline{\Delta^2 S} = \bar{m}^2 \overline{\Delta^2 n'} + \bar{n}' \overline{\Delta^2 m}$$

where the symbol $\overline{\Delta^2}$ represents the mean square fluctuation.

For electrons obeying a Poissonian distribution

$$\overline{\Delta^2 S} = \bar{n}' \{ \bar{m}^2 + \overline{\Delta^2 m} \}.$$

The total noise is given by

$$(dn)^2 = \bar{n}' (\bar{m}^2 + \overline{\Delta^2 m}) + n_A^2$$

The signal to noise ratio, SN_2 of this tube is given by

$$SN_2 = \left[\frac{\bar{n}'}{1 + \frac{\overline{\Delta^2 m}}{\bar{m}^2} + \frac{n_A^2}{\bar{n}' \bar{m}^2}} \right]^{\frac{1}{2}}$$

The detective quantum efficiency D.Q.E' is given by

$$D.Q.E.' = \frac{\delta}{1 + \frac{\overline{\Delta^2 m}}{\bar{m}^2} + \frac{n_A^2}{\bar{n}' \bar{m}^2}} \qquad (A.14)$$

Under some conditions a considerable increase in the detective quantum efficiency is effected by the reduction of the effect of the amplifier noise. In table 1, the detective quantum efficiency D.Q.E.' of a tube with an electron multiplying target has been calculated for various values of $\bar{m}$ and $\bar{n}'$; for comparison, the detective quantum efficiency D.Q.E., of a tube without charge gain has also been calculated. The amplifier noise term n_A has been taken as 1,000. In the absence of experimental evidence it was necessary to anticipate a value of $\frac{\overline{\Delta^2 m}}{\bar{m}^2}$ The value unity has been used in table 1 as this is the value obtained for an exponential variation of $\bar{m}$. Exponential variations are sometimes observed for multiplication by secondary emission and may not be inappropriate here.

It can be seen that a very considerable increase in low light level performance is to be expected when the target shows a high charge gain. Although the term $\frac{\overline{\Delta^2 m}}{\bar{m}^2}$ can reduce the detective quantum efficiency by a factor

Table I

The Effect of Charge Gain

	$\frac{DGE}{\sigma}$	$\frac{DQE'}{\sigma}$				
$\bar{n}'$		m = 1	m = 3.16	m = 10	m = 31.6	m = 100
10^3	.001	.001	.010	.08	.333	.487
$10^{3.5}$	.003	.003	.030	.198	.432	.492
10^4	.010	.010	.080	.333	.487	.498
$10^{4.5}$	.031	.030	.198	.432	.493	.500
10^5	091	080	333	487	498	500
$10^{5.5}$	.241	.198	.432	.432	.500	.500

Symbols as defined in text.

The dashed line represents a limit set by the capacity of the target. It has been assumed that a signal in excess of $10^{5.5}$ electrons per picture point will cause overloading.

of up to $\frac{1}{1 + \frac{\Delta^2 m}{m^2}}$

this is in general greatly offset by the increase arising from the reduction in the effect of amplifier noise.

A.5. 'Electron Skipping' in a Long Tube

The following analysis, which is an extension of the treatment of the focussing of electrons in axial magnetic and electrostatic fields, derives the resonance condition discussed in section 7.7 . A comparison of the radii of the wall of the tube and the circular path into which the magnetic field constrains the electrons shows that it is possible to treat the wall as a plane surface, the radii being three centimetres and approximately one millimetre respectively.

The electrons will be emitted from the tube wall at an angle ψ to the wall (figure A.4) and will subsequently be constrained in a helical path until they are returned to the tube wall after travelling a distance f_ψ in the direction of the electric field. The projection of the path of the electron in a plane normal to the field is part of a circle and the electron will strike the wall after turning through an angle of 2ψ . Because it has constant angular

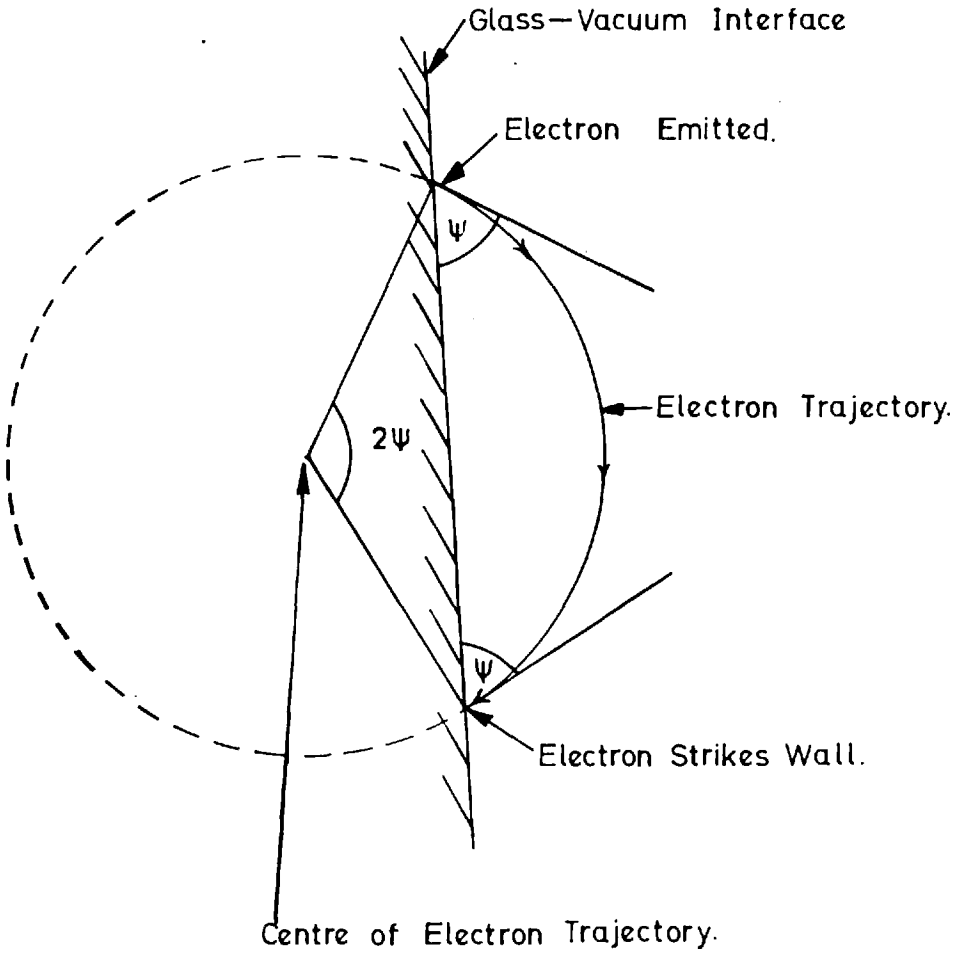

Fig. A 4. Projection of Electron Trajectory into a Plane Normal to the Field Axis.

velocity the electron will strike the wall after a time τ_ψ given by:

$$\tau_\psi = \frac{2\psi}{2\pi} \tau$$

where τ is the time of gyration of the electron in the magnetic field. It follows that

$$f_\psi = \tfrac{1}{2}\frac{eV}{ml} \tau_\psi^2 = \tfrac{1}{2}\frac{eV}{ml} \left(\frac{\psi}{\pi}\right)^2 \tau^2 \qquad (A.20)$$

where the symbols have the values assigned in section A.1. Let f_π be the distance that an electron describing a full circle will travel, then:

$$f_\pi = \tfrac{1}{2}\frac{eV}{ml} \tau^2$$

and

$$f_\psi = \left(\frac{\psi}{\pi}\right)^2 f_\pi$$

Let $\bar{f}$ be the average distance all electrons travel before striking the wall, then;

$$\bar{f} = \frac{\int_0^\pi p(\psi) f_\psi d\psi}{\int_0^\pi p(\psi)\, d\psi} \qquad (A.21)$$

where $p(\psi)d\psi$ is the probability that an electron is emitted at an angle in the range $\psi \rightarrow \psi + d\psi$.

We can discuss two likely angle distributions;

1) Lambertian, i.e. $p(\psi)d\psi = \frac{1}{2}\sin\psi d\psi$

In this case, $\bar{f} = \int_0^\pi \left(\frac{\psi}{\pi}\right)^2 f_\pi \sin\psi d\psi$

$= 0.298\, f\pi$

2) That where $P(\psi)\ dd\psi = \frac{\psi}{\pi}\ d\psi$
i.e. all angles are equally likely.

In this case

$$\overline{f} = \frac{1}{\pi} \int_0^{\pi} \left(\frac{\psi}{\pi}\right)^2 f_\pi\ d\psi$$

$$= 0.333 f_\pi$$

now, from (A.2) and (A.4)

$$f_\pi = \tfrac{1}{2} \frac{eV}{ml}\ \tau^2$$

and

$$\tau = \frac{2\pi m}{Be}$$

re-arrangement and substitution gives,

$$B = \frac{\pi}{\sqrt{f_\pi l}} \sqrt{\frac{2mV}{e}}$$

$$= \frac{334}{\sqrt{f_\pi l}} \sqrt{V}$$

where B is in gauss, l in centimetres and V in kilovolts.
The result obtained experimentally was

$$B = 27\sqrt{V}$$

whence direct comparison gives;

$$f_\pi = 7.4 \text{ cm.}$$

By substituting in the equations obtained for $\overline{f}$ for the two types of angular distribution we find

$$\overline{f} = 2.2 \text{ cm, and } \overline{f} = 2.45 \text{ cm respectively.}$$

The first of these figures is within 10% of the inter-electrode

spacing; closer agreement is not to be expected due to the fact that the limits of integration were 0 to π, whilst it can be seen that electrons near the limits will probably strike the platinum paint and not contribute to the cascade process. It is unlikely however that the errors introduced by this approximation will be sufficient to affect the argument substantially, especially considering that in the Lambertian distribution which gives the better result, few electrons are emitted near the limiting values of $\psi = 0$ and $\psi = \pi$.

References

1. C. E. Catchpole, Ph.D. Thesis, Imperial College, 1963.
2. M. E. Haine, P. A. Einsteine, Proc. I.E.E. pt. B, 109, 185, 1962.
3. D. G. Brandon, S. Ranganathan, D. S. Whitwell, Brit. J.A.P., 15, 55, 1964.
4. G. W. Goetze, A. Taylor, Adv. Elect., 16, 557, 1962.
5. P. Schagen, D. G. Taylor, A. W. Woodhead, Adv. Elect. 16, 75, 1962.
6. A. Bouwers, Adv. Elect., 16, 85, 1962.
7. W. B. Lewis, Proc. Phys. Soc. 59, 34, 1947.
8. A. Rose, Adv. Elect., 1, 131, 1949.
9. R. Clark Jones, Adv. Elect. 11, 87, 1959.
10. S. Hecht, Journ. Opt. Soc. Amer., 32, 42, 1942.
11. A. Sommer, Rev. Sci. Inst., 26, 725, 1955.
12. P. Fellgett, R.A.S. Monthly Notices, 118, 224, 1958.
13. W. A. Baum, Adv. Elect., 12, 1, 1960.
14. C. E. K. Mees, 'The Theory of the Photographic Process', Macmillan Co. (New York), 1942.
15. W. L. Wilcock, W. A. Baum, Adv. Elect., 16, 383, 1962.
16. G. Reynolds, Trans. I.R.E. NS 7, 115, 1960.
17. D. M. Binnie, M. Jane, J. A. Newth, D. C. Potter, J. Walters, Nuclear Inst. & Methods, 20, 221, 1963.

18. D. M. Binnie, M. Jane, J. A. Newth, D. C. Potter, J. Walters, Nuclear Inst. & Methods, 21, 81, 1963.

19. K. R. Coleman, Rep. Prog. Phys., 26, 270, 1963.

20. A. Lallemand, M. Duchesne, G. Wlerick, Adv. Elect., 12, 5, 1960.

21. W. A. Hiltner, W. F. Niklas, Adv. Elect., 12, 37, 1960.

22. J. D. McGee, B. E. Wheeler, Adv. Elect., 12, 47, 1960.

23. B. E. Wheeler, Ph.D. Thesis, Imperial College, 1961.

24. A. Khogali, Ph.D. Thesis, Imperial College, 1964.

25. L. Mandel, Journ. Sci. Inst., 32, 405, 1955.

26. B. O. Zacharov, Ph.D. Thesis, Imperial College, 1960.

27. P. H. Foreman, R. F. Thumwood, Adv. Elect., 16, 163, 1962.

28. J. Burns, M. J. Neumann, Adv. Elect., 12, 97, 1960.

29. E. A. Flinn, Ph.D. Thesis, Imperial College, 1963.

30. D. Theodoru, Ph.D. Thesis, Imperial College, 1963.

31. W. C. Wiley, C. F. Hendee, Trans. I.R.E., NS9, 103,1962.

32. E. J. Sternglass, M. M. Wachtel, Phys. Rev. 99, 646, 1955.

33. E. J. Sternglass, M. M. Wachtel, Rev. Sci. Inst., 26 1202, 1955.

34. M. Wachtel, D. D. Doughty, G. Goertze, A. E. Anderson, F. J. Sternglass, Rev. Sci. Inst., 31, 576, 1960.

35. P. C. Ruggles, N. A. Slark, Elect. Comp. 5, 208, 1964. Elect. Comp. 5, 294, 1964.

36. W. L. Wilcock, D. L. Emberson, B. Weekley, Trans. I.R.E., NS7, 126, 1960.

37. D. J. Blattner, H. C. Johnson, F. Sterzer, App. Phys. Letters, 4, 46, 1964.

38. D. L. Imberson, Ph.D. Thesis, Imperial College, 1960.

39. D. L. Imberson, A. Todkill, W. L. Wilcock, Adv. Elect. 16, 127, 1962.

40. W. L. Wilcock, Private Communication.

41. J. R. Waters, G. T. Reynolds, P. B. Scarl, R. A. Zdanis, Trans. I.R.E., NS9, 239, 1962.

42. G. W. Goetze , Adv. Elect., 16, 145, 1962.

43. G. W. Goetze, Trans. I.R.E., NS9, 97, 1962.

44. K. G. McKay, Adv. Elect., 1, 65, 1948.

45. H. J. Bruining, 'The Physics and Applications of Secondary Electron Emission', McGraw Hill, 1954.

46. L. Malter, Phys. Rev. 49, 478, 1936.
Phys. Rev. 50, 48, 1936

47. E. R. Piore, Phys. Rev. 51, 1111, 1937.

48. L. R. Koller, R. P. Johnson, Phys. Rev. 52, 519, 1938.

49. H. Mahl, Z. Tech. Phys. 18, 559, 1937.
Z. Tech. Phys. 19, 313, 1938.

50. H. Nelson, Phys. Rev. 55, 985, 1939.
Phys. Rev. 57, 560, 1940.

51. H. Jacobs, Phys. Rev. 84, 877, 1951.

52. R. M. Arronovitch, Bull. Acad. USSR, 8, 346, 1944.

54. L. A. Serebrov, S. A. Fridrikhov, Rad. Tech. i. Elect. 7, 1536, 1962.

55. V. G. Butkevich, M. M. Butslov, Rad. Tech. i. Elect. 3, 355, 1958.

56. B. A. Krasovsky, M. M. Butslov, Rad. Tech. i. Elect. 7, 1261, 1962.

57. A. L. Yasnopol'skiy, V. S. Malysheva, Rad. Tech. i. Elect. 7, 1543, 1962.
A. L. Yasnopol'skiy, V. S. Malysheva, N. A. Kardina, Rad. Tech. i. Elect. 6, 129, 1961.

58. L. Harris, Journ. Opt. Soc. Amer. 45, 27, 1955.

59. G. P. Harnwell, Principles of Electricity and Electromagnetism, McGraw Hill, New York, 1949.

61. S. Tolansky, 'Multiple Beam Interferometry', Oxford University Press, 1948.

62. C. Feldman, Phys. Rev. 117, 455, 1960.

63. F. Ansbacher, W. Ehrenberg, Proc. Phys. Soc., 64A, 362, 1951.

64. F. Seitz, 'Modern Theory of Solids', McGraw Hill, New York, 1940.

65. B. J. Todd, Journ. App. Phys. 26, 1238, 1955.

66. A. Sommer, Proc. Phys. Soc. 55, 145, 1943.

67. J. D. McGee, 'The Present and Future of the Telescope of Moderate Size', University of Pennsylvania Press, 1958.

68. A. Bril, H. A. Klasens, Philips Res. Rep. 7, 401, 1952.

69. E. J. Davis, Journ. Sci. Inst. 35, 308, 1958.

70. W. A. Baum, Adv. Elect. 16, 391, 1962.

71. A. Khan, Ph.D. Thesis, Imperial College, 1961.

72. A. Todkill, Private Communication.

73. J. B. Johnson, Phys. Rev. 73, 1058, 1948.

74. N. A. Slark, Ph.D. Thesis, Imperial College, 1958.

75. R. P. Randall, Adv. Elect. 12, 219, 1960.

76. W. Heimann, Adv. Elect. 12, 235, 1960.

77. R. L. Beurle, N. A. Slark, Adv. Elect. 12, 247, 1960.

78. B. Meltzer, P. L. Holmes, Brit. Journ. App. Phys. 9 139, 1958.

79. W. Heimann, Adv. Elect. 12, 238, 1960.

80. R. L. Beurle, Proc. I.E.E. 110, 1735, 1963.

81. J. D. McGee, Proc. I.E.E. 97, pt. C, 377, 1950.

82. L. Pensak, Phys. Rev. 75, 472, 1949.

83. W. E. Spear, Proc. Phys. Soc. B. 69, 1139.

84. J. W. Alexander, R. B. Durtt, Adv. Elect. 16, 247, 1962.

85. R. J. Schneeberger, G. Skorinko, D. D. Doughty, W. A. Feibleman, Adv. Elect. 16, 235, 1962.

86. P. R. Collings, J. Hirsch, Brit. Journ. App. Phys. 15 797, 1964.

87. G. W. Goetze, A. H. Boerio, Conference reported in Trans. I.E.E.E. (Electron Devices) Jan. 1964.

88. G. W. Goetze, A. H. Boerio, Proc. I.E.E.E., 52, 1007, 1964.

89. S. Mende, R. Filby, Private Communication.

90. W. H. Aldous, E. A. Appleton, 'Thermionic Vacuum Tubes and their Applications', Methuen, 1958.

91. L. Mandel, Brit. J.A.P., 10, 233, 1959.

(*Reprinted from Nature, Vol.* 201, *No.* 4921, *pp.* 801–802, *February* 22, 1964)

A NEW TELEVISION CAMERA, INTENDED FOR SCIENTIFIC APPLICATIONS, HAVING A VERY HIGH SENSITIVITY AND GOOD STORAGE PROPERTIES

By R. S. FILBY, S. B. MENDE, M. E. ROSENBLOOM and DR. N. D. TWIDDY

Department of Physics, Imperial College of Science and Technology, London, S.W.7

THERE are considerable advantages to be obtained by using a specially designed television camera for the detection of faint optical images. These advantages arise from the greater quantum sensitivity and the absence of reciprocity failure in the photoelectric effect compared with photography, and because the output is in the form of an electric signal, ideally suited for transmission or computer applications.

The obvious fields of application are astronomy, space research and medical physics and, in the astronomical field, the use of the technique to extend the range of existing astronomical telescopes was first proposed by McGee[1]. Several attempts have been made to use television cameras in astronomy[2], but these have not been sufficiently successful so far to merit wide use of the technique.

In space research a suitable electronic camera would permit long exposures to visible or other radiation to be made, the picture being stored until it is convenient to transmit it to base by slow read out.

Existing television camera tubes are unsuitable because of their inability to store for periods longer than a few seconds. What is required is a television camera of high sensitivity capable of integrating a weak light input over a long period, of storing this integrated picture for an appreciable time without deterioration and finally the picture should be read out in a single television frame period.

A tube which seems to offer all the required features has been developed; it has sensitivity which compares very favourably with the best television camera tubes at present available, it is capable of storing a charge image for several hours without deterioration, its charge storage

capacity can be adjusted in manufacture to suit the proposed application, and it does not exhibit appreciable persistence of image or 'lag' which is an undesirable feature of television camera tubes having too large a target capacity or using photoconductive layers.

The construction of the tube is shown in Fig. 1. The light input is focused on to a transparent photocathode (1). The photoelectron image so produced is then accelerated and focused by means of a uniform electric field provided by the metallic rings (2), and a uniform magnetic field produced by the long solenoid (3). These photoelectrons are accelerated to energies of the order of 5–7 keV and strike a special target (4).

The novel feature of the tube is the use of a target consisting of a thin conducting signal plate on which is deposited, on the side away from the photocathode, a spongy layer of highly insulating material. A cross-section through this target is shown in Fig. 2. It consists of a layer of aluminium oxide about 500 Å thick which serves as a support membrane for a signal plate of aluminium of similar thickness. On this signal plate is deposited a spongy layer of potassium chloride. The spongy layer is produced by evaporating the insulator in the presence of an inert gas so that atoms aggregate before reaching the target and form a spongy layer of much lower density and lower dielectric constant than the solid material. In a typical tube the spongy layer density may be of the order of 3 per cent of the solid and the layer thickness 5–10μ. The technique is similar to that developed by Goetze[3] for the preparation of films for transmission secondary emission image intensifiers.

Since the density of this layer is very low, electrons with energies of the order of 5 kV are able to penetrate it and build up a positive charge by transmission secondary emission. The secondary electrons are collected by the positive mesh (5).

In view of the relatively large thickness of the spongy layer, the capacitance between the surface of the layer

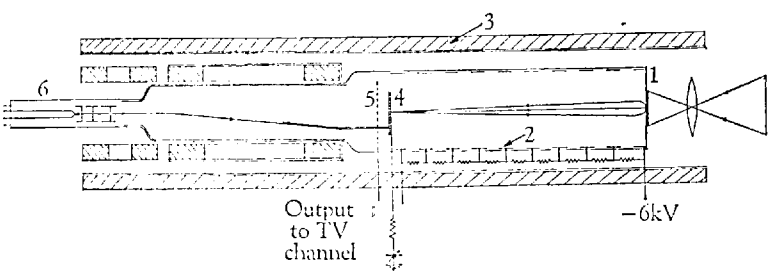

Fig. 1. New television signal generating tube. The optical input is imaged at the photocathode (1). The photoelectrons are imaged at the target (4) which is scanned on its reverse side by a low-velocity electron beam from the electron gun (6)

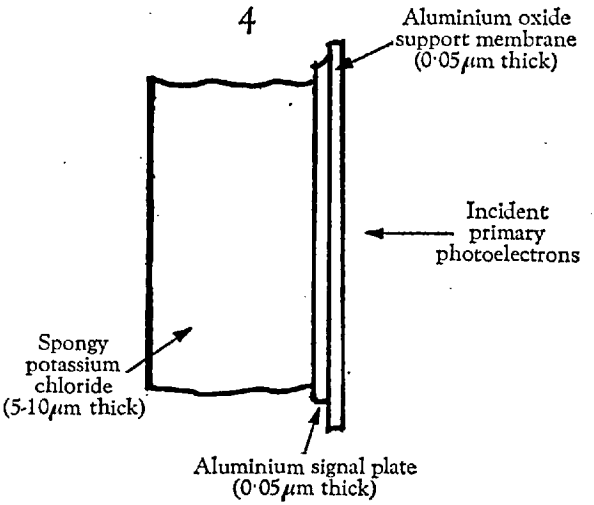

Fig. 2. Section through target (4)

and the conducting signal plate will be low compared with a tube using a solid layer. Therefore the undesirable capacitative 'lag' occurring in such tubes is avoided.

The capacity could be controlled during the formation of the layer by varying either, or both, the density and the thickness to achieve the ideal charge storage capacity for a given tube application.

The positive charge image can be retained on such layers for hours without deterioration and can be read out by scanning the layer surface orthogonally with a low-velocity electron beam from the gun (6). In the present tube the signal is obtained from the conducting signal plate. It could, however, also be obtained by collecting the return beam after it has scanned the insulating side of the target, in which case it would be advantageous to multiply the return beam by means of an electron multiplier as in the image orthicon. This amplification would result in a signal-to-noise ratio which would be determined mainly by the shot noise of the scanning beam and be independent of amplifier noise. The signal-to-noise ratio would, however, be better than that of an image orthicon because, unlike the image orthicon, there is no mesh in front of the target to intercept the primary electrons. Also the charge gain in the spongy layer is 7 compared with the image orthicon's gain of 5. However, the major improvement arises from the much larger charge storage capacity of the new tube. It is convenient to make this about 1,000–2,000 pF, that is, at least ten times the capacity of the image orthicon target[4].

However, even without this refinement, the performance of the tube is impressive. The experimental tube has a target capacity and signal extraction arrangement similar to a C.P.S. Emitron camera tube so that it was convenient to compare these cameras using identical head amplifiers. It was found that the new tube produced an output peak white signal seven times larger than the C.P.S. Emitron for the same light input and photocathode sensitivity. The experimental tube was operated to give a secondary emission gain of about 7 in this test and thus this result was to be expected since the C.P.S. Emitron has no secondary emission multiplication.

The tube has a limiting resolution of 13 line pairs/mm. The resolution is at present limited partly because the present reading section is identical to that of the C.P.S. Emitron and was designed to scan a larger target than that in the present tube, and partly due to the interaction between the primary electrons in the image section and the scanning fields, due to inadequate screening. In later versions it is proposed to use a scanning system designed for a vidicon camera which should improve the resolution.

In the image orthicon, the unavoidable penetration of the scanning field into the image section results in a loss of resolution, but this effect should be much smaller in our tube since the image-electron energies in the image section will be at least an order of magnitude larger.

If a potential difference is maintained across the spongy dielectric layer, then use may be made of electron bombardment induced conductivity to supplement the multi-

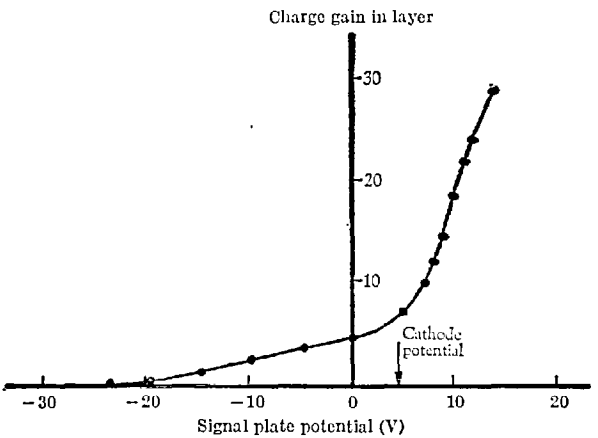

Fig. 3. The variation of the charge gain in the spongy target layer, with signal plate potential. The gain is 7 for zero volts across the layer (signal plate potential = cathode potential)

plication in the layer. The insulating surface of the layer is cathode potential stabilized and thus the potential difference across the layer may be conveniently varied by changing the signal plate potential. The variation of multiplication with signal plate potential is shown in Fig. 3. Satisfactory performance is obtained with relatively low voltages giving a multiplication of about seven, but, with the present layers, increasing the voltage across the layer to obtain gains of 20 or more results in the appearance of white spots due to pinholes in the layer. Under these conditions the tube is not suitable for television pictures or star fields, but would still be usable for scientific applications involving the detection of objects much larger than picture point size.

The output signal current is proportional to the input illumination, that is, the gamma (γ) is unity. When operated as a television camera, the tube is capable of withstanding light input overloads of 8 times the input corresponding to peak white signal before the target tends to anode potential stabilize. This may not be adequate for some television work. In a scientific application involving a long exposure to detect faint objects in the presence of bright ones, the rise of potential on the layer due to the bright sources can be limited by keeping the mesh at a potential below the first secondary emission crossover potential.

The device may, of course, be used for the detection of infra-red, ultra-violet, and X-radiation by replacing the existing photocathode by a photocathode or phosphor/photocathode sandwich sensitive to these radiations together with a suitable end-window.

[1] McGee, J. D., *J. Roy. Soc. Arts*, C, 329 (1952); *Astronomical Optics*, edit., by Kopal, Z., 205 (1956).

[2] Randall, R. P., *Adv. Electronics and Electron Phys.*, **12**, 219 (1960). Gebel, R. K. H., and Devol, Lee, *ibid.*, **12**, 195 (1960). Hynek, J. A., Barton, G., Aikens, R., and Powers, W., *ibid.*, **16**, 409 (1962). De Witt, jun., J. H., *ibid.*, **16**, 419 (1962). Livingston, W. C., *ibid.*, **16**, 431 (1962). Dennison, E. W., *ibid.*, **16**, 447 (1962). Gebel, R. K. H., *ibid.*, **16**, 451 (1962).

[3] Goetze, G. W., *Adv. Electronics and Electron Phys.*, **16**, 145 (1962).

[4] McGee, J. D., *I.E.E. Intern. Television Conf.*, 36 (1962).

Printed in Great Britain by Fisher, Knight & Co., Ltd., St. Albans.